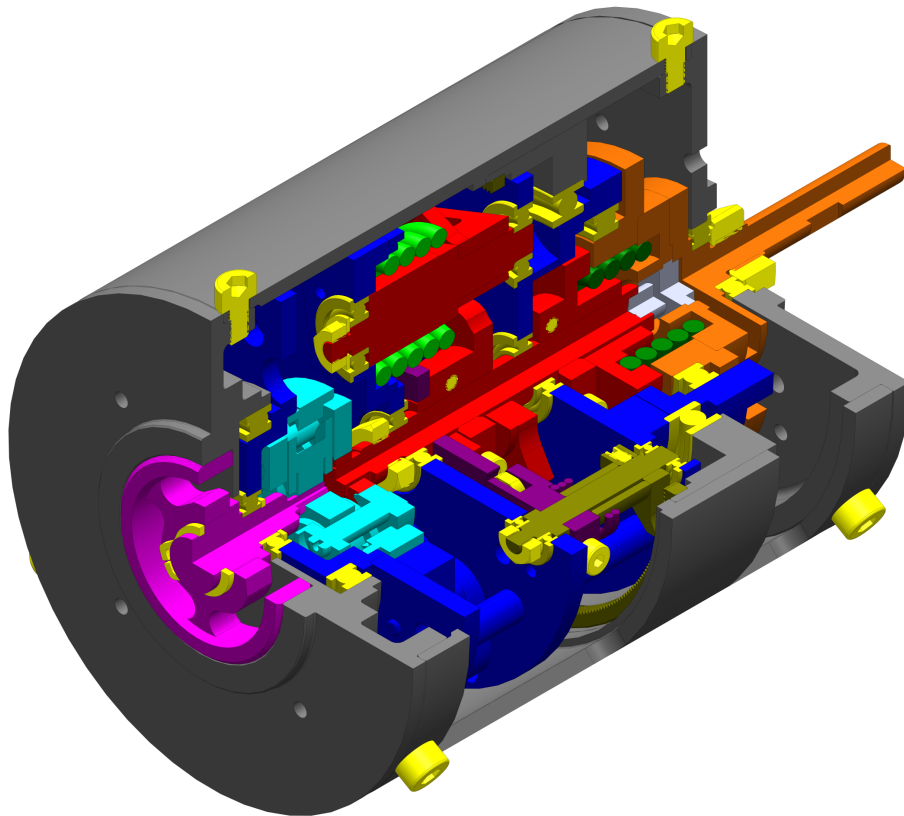


Design and Evaluation of an Energy-Saving Drive for a Versatile Robotic Gripper

Master Thesis

J.J. Neven (4089138)
Delft University of Technology
Mechanical Engineering, BioMechanical Design

August 22, 2017



Abstract

Nowadays, the number of robotic systems grows enormously. In order to execute their task, many of these robots need a *fixturing gripper* to grasp and hold objects. To reduce the environmental impact, the operational costs, the size of actuators and to improve the uptime of mobile robots, it becomes increasingly important to design robots for a minimum energy consumption. Therefore this thesis is dedicated to developing an energy saving robotic gripper.

The gripper's drive has to enable the gripper to perform *sizing*, the adjustment to the object size, and *forcing*, exerting retaining forces on the object. As drive strategy an actuator in combination with an internal force mechanism was selected, because this allows for autonomous grasping and passive retention in any orientation.

Based on a newly proposed performance metric, which normalizes the product of the minimum dislodging force in any direction and the average closing speed with the rated actuator power, a *Statically Balanced Force Amplifier* (SBFA) was selected as internal force mechanism. In addition to current state-of-the-art drives, which are able to switch between two transmission branches for either *high-speed* or *high-force* and overpower the motor because of static-load cancellation with dedicated locking mechanisms, an SBFA realizes a force reduction of approximately 95%.

A concept for a drive is developed based on this strategy. By analyzing the three subfunctions of the drive: 1) *sizing*, 2) *forcing* and 3) *switching between sizing and forcing* five design principles are derived. The SBFA is analyzed under the non-ideal conditions as occur in a gripper drive: a finite object stiffness and a position error in the size adjustment.

A topology selection is conducted, which resulted in a concept for a drive consisting of an SBFA with a movable frame and a differential that resolves the motor input in a forcing and sizing branch. The timing of the switching is controlled by an additional non-linear threshold spring and an endstop is implemented to bypass the main spring during switching.

An actual prototype for the implementation in the Delft Hand 3 is designed and realized.

The mechanism has a cylindrical housing with a diameter of 64 mm and a length of 78.5 mm and weights approximately 460 grams. Experiments are conducted which validate the working principle, i.e. the ability to perform sizing, forcing and switching, of the developed prototype. The maximum output torque is 1.073 Nm. For 5 emulated object sizes, an average torque reduction of 91.5% is measured. This prototype validates the feasibility to combine an SBFA, NBDM and two different transmission branches. Future work is required to further improve the functionality and assess the performance of the drive.

Contents

1	Introduction	8
I	Strategy	11
2	Selection of Drive Strategy	12
2.1	Introduction	12
2.2	Task of Robotic Gripper	12
2.3	Selection of Actuation Method	13
2.3.1	Selection Criteria	13
2.3.2	Description of Actuation Methods	14
2.3.3	Comparison	15
2.4	Selection of Internal Force Mechanism	16
2.4.1	Selection Criteria	16
2.4.2	Description of Mechanisms	16
2.4.3	Comparison	18
2.5	Discussion	18
2.6	Conclusion	19
3	Verification of Drive Strategy Selection	20
3.1	Introduction	20
3.2	Performance Metric	20
3.2.1	Performance Metrics in Literature	20
3.2.2	Novel Performance Metric	21
3.2.3	Application of Performance Metric	21
3.3	Description of Drives	24
3.3.1	Energy-demanding Strategies	24
3.3.2	Energy-neutral Strategies	29
3.4	Comparison	31
3.5	Discussion	32
3.6	Conclusion	34
II	Conceptual Design	35
4	Preliminary Design Considerations	36
4.1	Introduction	36
4.2	Subfunction 1: Effortless Position Adaptation	36
4.2.1	Fixed Frame SBFA	37
4.2.2	Moving Frame SBFA	37
4.3	Subfunction 2: Effortless Force Adaptation	37
4.3.1	Energy Storage	37
4.3.2	Transmission	38
4.4	Subfunction 3: Switch Between Force and Position Adaptation	41
4.4.1	Active Switching	42
4.4.2	Passive Switching	42
4.5	Imperfect Conditions	43

4.5.1	Description of Errors	43
4.5.2	Required Actuation Force	44
4.5.3	Required Work	44
4.5.4	Design Metrics	44
4.6	Discussion	46
4.7	Conclusion	47
5	Topology Selection	48
5.1	Introduction	48
5.2	Topology Representation	48
5.3	Subtopologies	49
5.3.1	Generation of subtopologies	49
5.3.2	Description of Subtopologies	50
5.3.3	Labeling of Subtopologies	52
5.4	Topology Selection	53
5.4.1	Step 1: SBFA Mounting and Splitters	53
5.4.2	Step 2: Threshold Implementation	57
5.4.3	Step 3: Threshold Loading	60
5.5	Explanation of Selected Topology	62
5.5.1	Sizing	62
5.5.2	Switching	62
5.5.3	Forcing	63
5.6	Discussion	63
5.7	Conclusion	64
III	Prototype Design	65
6	Design Requirements	66
6.1	Introduction	66
6.2	Environment of the Drive	66
6.2.1	Manipulator: The Plugless Arm	66
6.2.2	Gripper: Delft Hand 3	67
6.3	Design Requirements	67
6.3.1	Implementation	68
6.3.2	Grasp Force	69
6.3.3	Object Stiffness	71
6.3.4	Disturbance Force	72
6.4	Discussion	74
6.5	Conclusion	74
7	Typology Selection	75
7.1	Introduction	75
7.2	SBFA	75
7.3	Carriage Locking Mechanism	76
7.3.1	Selection Criteria	76
7.3.2	Locking Mechanisms	76
7.3.3	Comparison	77
7.4	Non-Backdrivable Mechanism	77
7.4.1	Selection Criteria	77
7.4.2	Possible Locking Mechanisms	78
7.4.3	Comparison	79
7.5	Differential	79
7.5.1	Selection criteria	79
7.5.2	Description of Differentials	79
7.5.3	Comparison	80
7.6	Discussion	81
7.7	Conclusion	81

8 Detailed Design	82
8.1 Introduction	82
8.2 Global Description	82
8.2.1 Working Principle	82
8.2.2 Specifications	83
8.3 Design of Subsystems	84
8.3.1 Carriage Locking Mechanism	84
8.3.2 SBFA	84
8.3.3 Differential	89
8.3.4 Threshold Mechanism	91
8.3.5 Nonbackdrivable Mechanism	95
8.3.6 Feedback	96
8.4 Realization of Prototype	96
8.5 Discussion	96
8.6 Conclusion	97
IV Experimental Validation	98
9 Experimental Validation of Working Principle	99
9.1 Introduction	99
9.2 Main Spring Characteristic	99
9.2.1 Methods	99
9.2.2 Results	100
9.2.3 Discussion	101
9.3 Input Characteristic	102
9.3.1 Methods	102
9.3.2 Results	103
9.3.3 Discussion	105
9.4 Discussion	107
9.5 Conclusion	107
10 Discussion	108
11 Conclusion	110
A Additions to Chapter 2	112
A.1 W.E.N-Principle	112
B Additions to Chapter 3	114
B.1 Alternative Performance Metric Visualization	114
C Additions to Chapter 4	115
C.1 Concept with Intermittent Transmission	115
D Additions to Chapter 5	116
D.1 Derivation of SBFA forces	116
D.2 Topology Generation using Graph Theory	116
D.2.1 Conventional Mechanism Representation using Graphs	116
D.2.2 Representation of CEAs using Bipartite Graphs	117
D.2.3 Analysis of Possibilities	118
D.2.4 Discussion	120
D.3 Mathematical Description Threshold Loading	120
D.3.1 Without Anticipation	120
D.3.2 With Anticipation	120

E	Additions to Chapter 6	122
E.1	Non-Linear Transmission in Fingers	122
E.2	Hand configurations	122
E.3	Apparent Stiffness of Finger	123
E.4	Mechanical Strength of Hand	123
F	Additions to Chapter 7	125
F.1	Outdated Typology Selection of the SBFA	125
F.1.1	Outdated Design Principle	125
F.1.2	Outdated Typology Selection	126
F.2	SBFA with a cylindrical CAM	129
G	Additions to Chapter 8	130
G.1	Carriage Locking Mechanism	130
G.2	SBFA	131
G.2.1	Cam Geometry	131
G.2.2	Static Analysis	132
G.3	Differential	132
G.3.1	Derivation of Equilibrium Condition	132
G.3.2	Selection of Connection Permutation	133
G.4	Threshold Mechanism	134
G.4.1	Spring Selection	134
G.5	Tension Tool	135
H	Additions to Chapter 9	136
H.1	Forcing Data Set	136
H.2	Spring Extension versus Input Torque	136

Chapter 1

Introduction

Since their introduction half a century ago [1], the number of robotic systems experienced an enormous growth, which is nowadays still continuing. For instance, in 2015 the stock of operational industrial robots increased with 11 % [2], which is a tenfold of the current growth rate [3] of the number of people worldwide. The reason for this is their ability to execute tasks in dangerous environments, to perform repetitive movements in a fast and accurate way without getting bored or distracted and to compensate (partially) for the function loss of impaired and elderly.

Many of these robots are equipped with grippers, because the ability to grasp and hold objects in order to reposition or reorient them, is essential in many tasks, such as in pick-and-place tasks, space missions [4], search-and-rescue operations [5], assisted living [6] and many more. These grippers can be divided in two categories [7]: The first category, *fixturing grippers*, are designed to fixture the object with respect to the wrist. The position of the object is manipulated by the robotic system the gripper is attached to. The second category, *dexterous hands*, are able to manipulate the object with respect to the wrist. These hands have typically more controlled Degrees of Freedom (DoF) and therefore their mechanical structure and the control tends to be more complex. For many tasks such complexity is unwarranted, as it is simply desired to grasp and hold objects. For these tasks, fixturing grippers are the better choice.

However, there is a challenge in the design of the gripper drives: Nowadays, the energy consumption of robots and their subsystems is becoming increasingly important. This is especially the case for mobile robots, because their energy consumption is one of the bottlenecks for successful task accomplishment [8], but also for stationary robots this is becoming increasingly important. In the first place this is because of the emerging awareness of the environmental impact. In the second place, because of the price of wasting energy, which not only consists of the consumed energy, but also the necessity for larger and heavier designs, because the power of an actuator is related to its mass. For instance, for electric motors the power-to-weight ratio is ~ 0.5 kW/kg [9].

The design of drives of robotic grippers for a minimum energy consumption is challenging. To explain this, two types of drives need to be distinguished: Those that rely on an actuator and those that don't. Both categories have particular drawbacks.

For the first category, energy is dissipated in the actuator and therefore the consumed energy is much higher than the theoretical amount of required energy. Kruit and Cool [10] realized that both operation modes of a fixturing gripper consume no energy at all. During the first mode, *sizing*, the gripper adjusts to the object size. This requires theoretically no force. During the second mode, *forcing*, the gripper exerts a force on the object. This requires theoretically no displacement. Because:

$$\text{Mechanical Work} = \text{Force} \times \text{Displacement} \tag{1.1}$$

both modes require theoretically no work. This means that all the energy supplied to the actuator is actually wasted energy.

Grippers from the alternative category, without an actuator, also have disadvantages. In the first place they are not fully autonomous, as they rely on external systems to open or close. This contradicts to the very nature of reprogrammable robotic systems. Second, these external systems are often required to perform dedicated actions or movements to control the gripper, which also involves an energy consumption, which is strongly dependent on those external systems. In the third place, they are typically not able to reorient the object, as they rely on external forces to open or close, which have to act in a specific direction. These aspects strongly compromise the applicability of these actuator-less grippers.

This became especially clear for the *PluglessArm* we¹ are developing. This particular robotic arm is a case to push the development of novel technologies to reduce the energy consumption of robots. The aim of this robot is to be extremely energy efficient, to such an extent that it should be able to execute pick-and-place operations solely driven by the downwards displacement of the package. In preliminary research [11] it is shown that existing grippers, such as the *Robotiq's 2-Finger 85* [12], are not suitable, because its energy consumption exceeds alone already the difference in potential energy from the package along the downwards displacement of the object. This case stresses the importance of reducing the energy consumption of all subsystems in the process towards energy efficient robots.

Therefore, this thesis is dedicated to the development of an *energy saving* drive for a robotic gripper. This drive will be implemented in a versatile robotic gripper. In a preliminary literature survey [11] I identified *static friction grasping* and *Van der Waals Adhesion* as feasible grasping principles, because they are passive (i.e. no energy consumption is required to retain the object) and are able to grasp a wide variety of objects (regarding their materials, surface conditions and geometries) in many environments. Although the developed drive might also be applied with Van der Waals adhesion, in this thesis the drive will be implemented in a static friction gripper, because static friction grippers are already widely known and employed. The goal of this thesis is formulated as:

Develop and evaluate an energy saving drive system for a versatile robotic gripper.

The subgoals to realize this are:

1. Identify a feasible strategy to improve the energetic performance.
2. Make a conceptual design based on this strategy.
3. Implement this concept in a prototype robotic gripper for the Plugless Arm.
4. Experimentally evaluate the performance of the drive.

During the design process the following requirements are taken into account:

- *Energy saving*: The energy dissipation in the complete gripper should be minimized as much as possible.
- *Reorientable*: The gripper should be able to operate in any orientation, as it is desired for many tasks to reorient the object.
- *Autonomous*: The gripper should be able to open and close as an autonomous system, independent of external systems. This ensures the reprogrammable nature of robotic systems is maintained. Moreover, it ensures there is no “hidden” energy consumption, i.e. a required energy consumption in external system for opening or closing of the gripper.
- *Adjustable Output Force*: The required force to hold objects varies for different tasks and objects. Because excessive forces may damage the object, it is desired to adjust the level of the forces accordingly to the task and objects, this requires the output force of the drive to be adjustable.

In addition to this, the gripper should be *lightweight* and *fast*. A lightweight gripper ensures a minimum reduction of the payload and a minimum energy demand for the manipulator to move the gripper. A fast opening and closing gripper minimizes the energetic costs due to the task independent power consumption (overhead) of the overall system. The effects of design choices, especially during the conceptual phase, on the speed and mass are not always clear. Therefore the *simplicity* of the gripper, evaluated using the required number of components, is taken as measure. Less components require less fasteners, bearings and supporting structures, hence simple mechanisms are likely to have a better performance in terms of speed and mass. Moreover, less (moving) components imply less friction losses, this improves the energetic performance.

Although the aim of this thesis is the design of an energy efficient robotic gripper, the developed knowledge might be applied in grippers and clamps in other areas as well, to name a few: prostheses, machine clamps, construction clamps and lifting clamps. Moreover it could be applied to other machines that have to maintain a force level at an initially unknown distance, but without doing work, such as for stamping-machines.

The core of this thesis is divided in four parts, related to the four subgoals mentioned earlier. In the first part, consisting of Chapters 2 and 3, the strategy selection is covered. In Chapter 2 a strategy

¹The team working on the *PluglessArm* consists of: Wouter Wolfsdag, Ralph Vosse, Linda v.d. Spaa and author

is selected based on a qualitative analysis. Chapter 3 verifies the selection with a quantitative approach. The second part, consisting of Chapter 4 and 5, covers the development of the concept. Chapter 4 addresses the theoretical aspects of the selected mechanism: a *Static Balanced Force Amplifier* (SBFA). This results in several design principles. Chapter 5 reasons about the topology, how the required components should be connected. Up to this chapter, the problem is covered from a general perspective.

The third part consists of Chapter 6 to 8 and describes the design of a prototype drive for the implementation in the Delft Hand 3. Chapter 6 derives the design requirements for this drive. Chapter 7 covers the typologies, i.e. the embodiments, of the various subsystems. Chapter 8 describes the detailed design of the prototype and its subsystems. The last part, Chapter 9, describes an experimental evaluation of the designed prototype.

The obtained results of this thesis are discussed in Chapter 10 and a conclusion is drawn in Chapter 11.

Part I

Strategy

Chapter 2

Selection of Drive Strategy

2.1 Introduction

As already briefly discussed in Chapter 1, various drive strategies exist for grippers. Arguably, the energy consumption of a gripper is strongly related to the drive strategy. For instance, a different energy consumption is expected for a gripper that is driven by a geared DC-motor, than for a gripper driven by a spring mechanism. It is important to realize a single gripper might exploit multiple drive strategies. An example is the *Spring Clamp* [13], depicted in Fig. 2.1. This spring retains the object using spring, but to grasp an object, this clamp needs to be opened by a human operator. Whereas the former strategy relies on an internal mechanism, the latter relies on an external system.

This chapter gives an overview on the existing drive strategies reported in literature and aims to select the best drive strategy for an energy-saving robotic gripper. To ensure the strategy is general applicable for various tasks, the versatility is highly valued. The drive has to enable the gripper to execute its main task, therefore this chapter starts in Section 2.2 with a description of this task. Then the first selection step is taken by comparing various actuation methods in Section 2.3. As this first step result in an actuation method based on an internal force mechanism that supports the actuator, various internal force mechanisms are compared in Section 2.4. This chapter will conclude with a discussion in Section 2.5 and conclusion in Section 2.6.

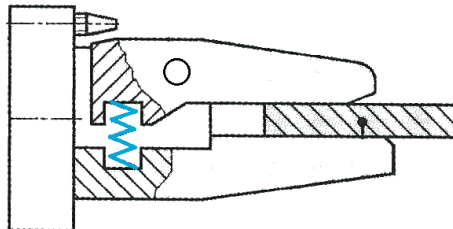


Figure 2.1: *Spring Clamp*. This gripper exploits two different drive strategies. It holds the object using a spring, but is opened by a human operator. Image adapted from [13].

2.2 Task of Robotic Gripper

The drive has to enable the gripper to execute its main task, therefore it is important to describe this main task before the performances of the different drive strategies are assessed.

Recall from Chapter 1 that robotic grippers can be categorized in *dexterous hands* and *fixturing grippers*. The scope of this thesis will be fixturing grippers, because their function is sufficient for many tasks and they are mechanically less complex. For these hands theoretically no work is done when an object is grasped, in contrast to dexterous hands for which it is certainly possible that work is done during object manipulations.

The following definition of the main function of a fixturing gripper is used: “... *grasp the object of manipulation, hold it during manipulation and release it at its destination.*” [14] This definition is closely

related to the different phases of a grasping cycle. Although the various descriptions [13, 15, 16] of these phases are not completely uniform, the following four phases are more or less distinguished:

1. *Approach*: The gripper approaches the object. It is positioned nearby the object. In some cases also the object is positioned or oriented, e.g. by a conveyor belt. Typically, the gripper itself performs no action during this phase.
2. *Prehension*: The gripper grasps the object. For static friction grasping this means that the fingers adjust to the size of the object. Once the fingers make contact, the contact forces are raised to a desired level.
3. *Retention*: The object is held by the gripper during manipulation. The gripper has to maintain the contact forces. The object and gripper can move as whole.
4. *Release*: The object is released at its destination. Basically, this phase is the inverse of prehension, as first the level of the forces is lowered, and then the fingers retract from the object.

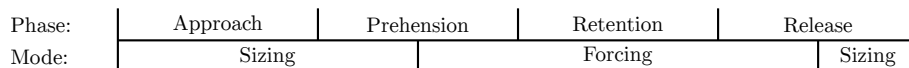


Figure 2.2: Timeline of grasping cycle and modes.

As briefly discussed in Chapter 1, a fixturing gripper has two operation modes:

1. *Sizing*: In this mode the gripper is able to adjust its configuration, for example when the fingers adjust to or retract from the object.
2. *Forcing*: In this mode the gripper is able to exert and vary forces on an object.

During prehension the mechanism is initially in the sizing mode. Once its configuration is adjusted to the object, it starts to exert forces on the object and its mode shifts to forcing. This forcing mode is continued during retention, where the gripper needs to exert forces to retain the object. Once the object reaches its goal, the gripper lowers the forces to zero and opens the hand. The gripper is switched back to the sizing mode. Once the hand is fully opened, the gripper is ready to approach the next object. Although the gripper is at rest, the gripper is still in the sizing mode, because it needs to be ready to adapt its configuration to the object once the mechanism enters the prehension phase again. A timeline of a single grasping cycle and the mechanism modes is depicted in Fig. 2.2.

During these two modes, the gripper behaves differently. As such, different requirements are applicable for these two modes. This is relevant for the next section in which various actuation methods are compared.

2.3 Selection of Actuation Method

There exist various methods to drive a robotic gripper. The current section provides an overview on these methods and aims to select the best one. To do so, selection criteria are formulated in Section 2.3.1. Then the various methods are described in Section 2.3.2, followed by a comparison in Section 2.3.3.

2.3.1 Selection Criteria

This subsection formulates the criteria, which will be used to compare the different drive strategies and select the best one. For the selection method, sizing and forcing mode are considered separately, as different behaviors of the gripper are desired during these phases. First the criteria related to prehension are presented, followed by the criteria related to grasping.

2.3.1.1 Criteria Related to Sizing

The following two criteria are identified for sizing:

1. *Autonomous*: The gripper should be able to open and close as autonomous system, independent of external systems. This ensures the reprogrammable nature of robotic systems. Moreover, it ensures there is no “hidden” energy consumption, i.e. a required energy consumption in external system for opening or closing of the gripper.
2. *Reorientable*: The gripper should be able to perform sizing in any orientation, because for many tasks it is desired to reorient objects.

2.3.1.2 Criteria Related to Forcing

The following two criteria are identified for forcing:

1. *Passive Retention*: Forcing during retention should not require any energy. During retention the drive has only to *preserve* the magnitude of the contact forces. Moreover, retention takes much longer than prehension for most tasks.
2. *Reorientable*: Also in the forcing the gripper should be reorientable, to be able to reorient the object.

Note that forcing during prehension and release ideally also requires no energy, but as these phases involve an adjustment in the force level, in practice some energy dissipation is likely to occur. Based on these selection criteria, in Section 2.3.3 the various drive strategies, which will be described in the next subsection, Section 2.3.2.

2.3.2 Description of Actuation Methods

This subsection will provide an overview on the various drive strategies and identify their advantages and drawbacks. The various drive strategies can be divided in two groups: Those that rely on an actuator and those that don't. These two categories are discussed in Sections 2.3.2.1 and 2.3.2.2 respectively.

2.3.2.1 With Actuator

The grippers in the first class rely on an actuator to open and close the hand or exert forces on the object. Monkman et al. [13] report the use of various types of actuators in grippers, such as electric, pneumatic and electric. An example of this drive strategy is the Delft Hand 3 [17], depicted in Fig. 2.3a. This hand uses a DC-motor and gearbox to drive the gripper.

Using an actuator to drive the gripper during sizing has two advantages. First, this ensures the gripper is autonomous, as the opening and closing is controlled using the motor input. Second, the actuator works independent of its orientation, hence this strategy allows the gripper to reorient.

If an actuator is used to drive the gripper during retention, the strategy has an important drawback: Energy is consumed. An advantage is that this strategy is reorientable.

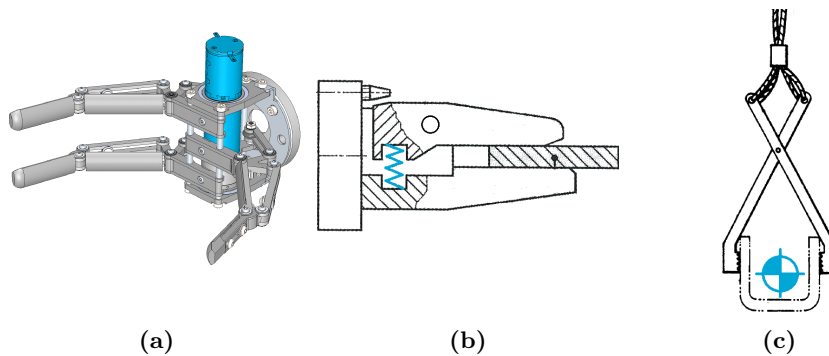


Figure 2.3: Examples of grippers. **a:** The *Delft Hand 3* [17] exploits the highlighted actuator for sizing and forcing. **b:** The *Spring Clamp* relies on a human operator for sizing and an internal force, delivered by the highlighted spring, for forcing. Image adapted from [13]. **c:** The *Conventional Clamp* relies on gravity for forcing and a human operator or dedicated movements of the manipulator for sizing. Image adapted from [13]

2.3.2.2 Without Actuator

The second category of drive strategies does not rely on an actuator for sizing or forcing. This strategy is subcategorized based on the alternative origins of the force: *External* or *Internal*. These two categories are discussed subsequently.

External Force This drive strategy relies on an external force to drive the gripper. These forces can act on the object or on the gripper. The external forces can be subdivided in *contact* and *remote* forces.

Contact forces arise from contact between the gripper or object and the environment. These forces can be used achieve sizing or forcing. Examples of such grippers are the spring *Spring Clamp* [13], depicted in Fig. 2.3b, which relies on a human operator for sizing and the gripper patented in [18], which relies on friction between an external guide rail to achieve both sizing and forcing.

The advantage of a contact force is that it enables passive retention. The drawback is that the gripper is dependent on external systems and non-reorientable during forcing and sizing, because the orientation is constrained to ensure the contact forces act in the required direction.

External forces arise from different phenomena than contact, but for instance from gravity. An example of a gripper that exploits gravity during retention is the *Conventional Clamp* [19] depicted in Fig. 2.3c. This gripper redirects the gravity acting on the object to achieve forcing. In [19] is also described how gravity could be used to achieve sizing, by counteracting the gravity on the gripper itself with a locking mechanism. Once the locking mechanism disengages, the center of mass of the gripper undergoes a downwards displacement which closes the gripper. Yet, to open the gripper again, work is required to move the center of mass upwards, which implies it is dependent on external systems.

The advantage of this strategy is again that passive retention is possible. The disadvantages are that the sizing is dependent on external systems and that the gripper orientation is constrained by the direction of the external force.

Internal Force The last drive strategy relies on components (other than actuators) that generate an internal force. These internal forces arise from buffers of potential energy, such as springs and permanent magnets. An example is the *Spring Clamp* [13] from Fig. 2.3b, which relies on a spring during forcing.

A drive based on an internal force is not able to perform sizing autonomously, as the energy buffers are passive components and don't have a control input. However, as the force is generated internally, the gripper is able to function in any orientation.

During retention this strategy does not consume energy to maintain the contact forces. Again, this strategy allows the gripper to reorient, as the force acts internally.

2.3.3 Comparison

The various actuation methods listed in will be compared based on the selection criteria formulated in Section 2.3.1. A good score, denoted by a “+”, is awarded if the criteria is met. A bad score, denoted by “-” is awarded if not. Table 2.1 provides an overview of the scores and a brief explanation.

Table 2.1: Comparison of Drive Strategies

Criteria	With Actuator	Without Actuator			
		External Force		Internal Force	
		Contact	Remote		
Sizing					
1 Autonomous	+ Control using actuator input	- Sizing dependent on external systems	- Sizing dependent on external systems	- Passive components without control input	
2 Reorientable	+ Actuator functions independent of orientation	- Orientation constrained to maintain contact with environment	- Orientation constrained by force direction	+ Internal force independent of gripper orientation	
Forcing					
3 Passive Retention	- Actuator requires energy consumption	+ No energy consumption required	+ No energy consumption required	+ No Energy consumption required	
4 Reorientable	+ Actuator functions independent of orientation	- Orientation constrained to maintain contact with environment	- Orientation constrained by force direction	+ Internal force independent of gripper orientation	

From Table 2.1 follows that no single drive strategy satisfies all criteria. However, when sizing and forcing

are considered separately, it follows that for sizing an actuator is the only satisfactory strategy, because this strategy is autonomous and reorientable. During forcing, only an internal force mechanism satisfies the criteria, as it allows for passive retention and reorientation of the gripper. This leads to the conclusion that an actuator should be used for sizing and an internal force mechanism should be used for forcing. In the next section a closer look will be taken how to execute this internal force mechanism.

2.4 Selection of Internal Force Mechanism

In Section 2.3 a combination of an internal force mechanism and an actuator was selected as best actuation method. The challenge is to combine these two subsystems such that they are indeed *supporting* each other, rather than counteracting. Therefore, this section explores and compares the various possibilities. The criteria for the comparison are formulated in Section 2.4.1. An overview on the various options for internal force mechanisms is provided in Section 2.4.2. The comparison itself is conducted in Section 2.4.3.

2.4.1 Selection Criteria

The following selection criteria are formulated to compare the various internal force mechanisms:

- *Low energy consumption* The *actuation* of the spring mechanism should have a low energy consumption. This energy consumption can be evaluated based on whether work is required to adjust the force level. This work has to be supplied by the actuator and is therefore accompanied with losses, as even for high-end robots the efficiency of the energy conversion from the battery to mechanical work is $\sim 63\%$ [20].
- *Manufacturable* In order to be viable, the mechanism should be manufacturable. This will be evaluated based on literature and practical considerations.

2.4.2 Description of Mechanisms

The internal force mechanisms deliver a force using a buffer of potential energy, such as springs or magnets. An important requirement for these mechanisms is that they are able to vary the output force: During forcing it is desired to adjust the force level, during sizing the force needs to be disengaged completely. The internal force mechanisms are divided in two categories, those that require work to adjust the output force and those that don't.

2.4.2.1 Work Non-neutral

Many mechanisms exist that require work to adjust the force level, but not all relieve the actuator during forcing. For instance, a spring in between the motor and the output is not work neutral, but does not relieve the motor from the static load during retention. The most basic mechanism that allows passive retention with an adjustable output force is the combination of a spring with a non-backdrivable mechanism (NBDM), as successfully realized by [21, 22].

This mechanism, depicted in Fig. 2.4a, consists of a spring connected to the NBDM, which is a dedicated locking mechanism that allows the motor to drive the load, but prevents the motor from being driven by the load. Consequently, the spring force can be adjusted using an input. When no input is provided, the spring is automatically locked and its force is preserved. Clearly, work is done when the output force is adjusted, as the potential energy in the mechanism is affected. This basic mechanism, as well as all other drives within this work non-neutral category, violates the first selection criteria. Therefore it is interesting to look at the alternative: work-neutral mechanisms.

2.4.2.2 Work Neutral

As work is force times displacement, no work is done when either the resultant force or displacement equals zero. This provides two categories for work neutral mechanisms, which will be discussed subsequently.

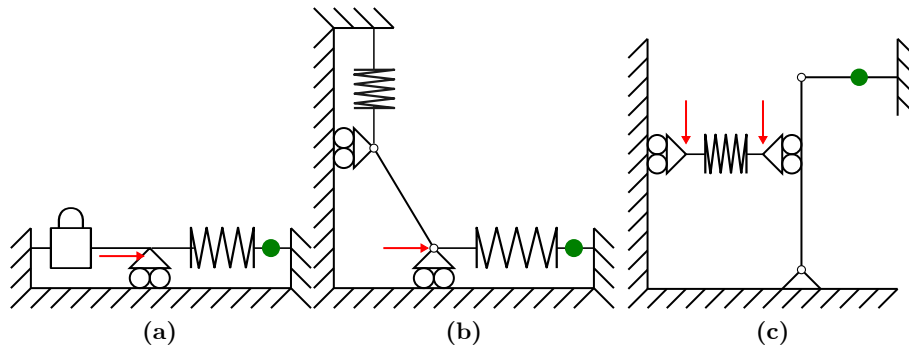


Figure 2.4: Various Actuation Methods. Using the input at the red arrow the output force at the green dot is varied. **a:** Non-backdrivable Spring **b:** Statically Balanced Force Amplifier (SBFA). **c:** Spring with Continuous Variable Transmission (CVT).

No Force The first strategy to obtain a work-neutral internal force mechanism is to eliminate the resultant force at the control input of the internal force mechanism. This is exactly what *Statically Balanced Force Amplifiers* (SBFAs) are designed for.

Fig. 2.4b shows a basic example [23] of a statically balanced mechanism amplifier. It consists of a main spring, which is compensated by a buffer spring. This is achieved by means of a dedicated non-linear transmission which ensures the potential energy is a constant, independent of the mechanisms configuration. Consequently, no force and work is required to adjust the elongation of the springs. For the depicted example, this means that the spring force, measured at the green dot, can be effortlessly varied using the input indicated by the red arrow. When the spring force, for instance occurring at the green dot in Fig. 2.4b, is rerouted, these force amplifiers provide a viable solution to deliver a high stationary force with a low energy consumption. In practice a small input force is required, as some balancing imperfections arise due to friction, hysteresis or manufacturing deficiencies. Input forces of 3%-5% of the maximum output force are reported for state-of-the art SBFAs [24, 25]. As the work is proportional force, the amount of work required at the input is drastically decreased by the buffer spring. The reported successful implementations substantiate the manufacturability of this strategy.

No Displacement The second strategy to obtain an energy-neutral force mechanism is to eliminate the displacement of the energy buffer. In literature one solution was found that employed this principle, the *W.E.N.-hand* [26]. A description of this hand is incorporated in appendix A.1.

The abstracted working principle of this hand is that the spring elongation is kept constant while the transmission ratio to the contact point with the object changes. In other words, it is a spring combined with a continuous variable transmission (CVT). To explain this, an example is depicted in Fig. 2.4c. The compression spring is mounted under pretension and ideally its length does not change. The lever with a moving pivot point forms a CVT. When the pivot point is shifted upwards or downwards the transmission ratio between the spring force and output, indicated by the green dot, changes as the moment arms of the lever changes. Consequently, the force in the green can be varied by varying the ratio of the CVT. An alternative description of this principle is a Variable Stiffness Actuator (VSA), as the transmission ratios affects the apparent stiffness “felt” at the output.

This principle requires theoretically no work to vary the output force because the elongation of the spring is constant, but manufacturing is challenging. In the first place, all components have to be very accurate to avoid any length change in the spring. A small deviation from the pretension length causes a large energetic error, because the the potential energy scales quadratically with the elongation.

In the second place, the spring needs to maintain its length, even when no object is present at the output. This means that the spring needs to be locked while under tension. The realization of locking mechanisms that are able to lock under tension is possible, but more challenging [27], especially when a high accuracy is desired.

In the third place it is challenging to realize a suitable CVT: A first category of CVTs are *friction CVTs*. These CVTs and rely on traction, i.e. a motion transmitted via rolling friction. As consequence high

normal forces are required to transfer high forces through the CVT, which limits the lifetime and efficiency [28] and are hard to downscale to a size suitable for robotic grippers [29]. A second and third category are CVTs based on non-linear mechanical interlinks and varying the lever length [30], for which the challenge remains to vary its ratio without affecting the spring elongation length.

2.4.3 Comparison

To make an informed decision for a viable strategy for an internal-force mechanism, the performance on the selection criteria of the various strategies is summarized in Table 2.2.

Table 2.2: Comparison of Internal Force Mechanisms

Criteria	Work Non-Neutral	Work Neutral	
		No Force SBFA	No Displacement Spring + CVT
1 Low Energy Consumption	– Inherent, as always work required	+ Theoretical no work required	+ Theoretical no work required.
2 Manufacturable	+ Successful implementation reported in [21, 22]	+ Successful implementation reported [24, 25]	– Conservation of pretension critical but challenging, realization of CVT challenging.

Although the two work-neutral alternatives have both a low energy consumption, the SBFA outperforms the spring with CVT based on manufacturability. As such, the SBFA is preferred over the CVT.

2.5 Discussion

In this chapter various drive strategies are compared in two steps with the aim to select a viable drive-strategy for an energy saving gripper. It is logical that a work-neutral internal force mechanisms seems the best solution. Theoretically, no work is required for grasping and it makes sense that the drive does neither. Yet, before this conclusion is drawn, the obtained overview and selection procedure is critically reflected.

Regarding the overview, it is important to realize that it is hard to prove that *all* drive strategies are listed. A first method to prove this is to assess all existing grippers. This is very hard to do, as in a preliminary literature survey [11] was found that only the search term “robotic gripper” in *Google Scholar* results in >45000 hits. More grippers exist in other fields, such as prosthetics or construction equipment. A second method is to look whether the categories are complete. I am convinced this is the case, as to the best of my knowledge there exist no alternatives to the categories. For instance, there is no third alternative to with or without actuator.

Yet, it should be noted that in the selection the assumption is made that a gripper employs at most two drive strategies. This assumption is justified since fixturing grippers have two operation modes. More redundant actuation methods would complicate the design unnecessarily. Another point of attention is that although the categorization of work-neutral mechanisms in “no-force” or “no-displacement” is complete, it is impossible to say whether additional solutions exist within these two categories, other than a SBFA or spring with CVT. I think this is not likely, as it are both rather particular mechanisms. Moreover, I did not encounter additional work-neutral drive strategies in a preliminary elaborate literature survey [11].

The selection is based on *qualitative* criteria. Likely, different results would be obtained with different selection criteria. The selection criteria are compiled with an eye on a low energy consumption and versatility, to meet the main goal of this thesis while it is applicable for many tasks. Deliberately, the selection is made traceable by detailed explanations on the criteria and rating. This allows others to reproduce the results or adapt the procedure to their own needs.

For the selection of the internal force mechanism, the low energy consumption is the decisive criteria. Unfortunately, this criteria is nested on the assumption that the exchange of work, arising from a change in potential energy, should be minimized. This neglects the dissipative work. This creates a gap between

theory and practice, as in practice always dissipation will occur, due to e.g. friction or hysteresis. Moreover, inherent to the *qualitative* approach it is not possible to say *how much* better one strategy is with respect to another. To gain more insight, a *quantitative* approach is needed. This is addressed in the next chapter.

2.6 Conclusion

The drive has to enable the gripper to execute its main task, which can be subdivided in four phases: 1) *Approach*, 2) *Prehension*, 3) *Retention* and 4) *Release*. During these phases, the gripper employs two modes, *forcing* and *sizing*. Various actuator-based and actuator-less drive strategies exist, of which an actuator combined with an internal force mechanism, for instance a spring, is preferred for an energy saving and versatile drive.

As internal force mechanisms work-neutral mechanisms are particularly interesting, as they theoretically require no energy conversion to adapt the output force, thereby preventing dissipation in the actuator. Two work-neutral solutions are found, of which the *Statically Balanced Force Amplifier* (SBFA) is preferred as it outperforms on manufacturability.

To verify the *quantitative* selection of this chapter, in the next chapter a *qualitative* estimation of the performance is made.

Chapter 3

Verification of Drive Strategy Selection using a Quantitative Performance Metric

3.1 Introduction

In the previous chapter a comparison of actuation methods was conducted. Based on a qualitative comparison the conclusion was drawn that the internal force mechanism should be work-neutral mechanism. Within this category the SBFA was the preferred type. It is not yet possible to determine *how much* better a SBFA is.

Therefore, this chapter will take a closer look at state-of-the art drives and quantify the performance. This will not be done from the perspective of exchanged potential energy, as done in the previous chapter, but the actuator properties are taken as base. The global idea is that the performance of various state-of-the-art and novel drives are compared based on a performance metric for the situation where they are implemented in the same gripper, a simple clamp, and driven by the same DC motor. This results in more insight and allows for an informed decision whether the SBFA is indeed a viable strategy. For the sake of thoroughness, also the CVT will be analyzed.

To do so, an adequate performance metric will be proposed in Section 3.2. This performance metric will serve to quantify the performance of various drives in Section 3.3 and conduct a comparison in Section 3.4. The obtained results will be discussed in Section 3.5 and a conclusion is drawn in Section 3.6

3.2 Performance Metric

This section will elaborate on a performance metric which enables the comparison of various drives. The main aspect of this comparison is the estimated performance in terms of energy consumption. Secondary aspects are, as described in Chapter 1, the complexity, closing speed and mass. Ideally these aspects are compared using a single performance metric.

The quest for an appropriate metric will start with a brief discussion of metrics in literature in Section 3.2.1. Unfortunately, the existing metrics do not relate to energy consumption. Hence, a novel performance metric is proposed in Section 3.2.2. To ease the comparison, the proposed metric is applied on a simple case, namely the drive of a simple clamp, and normalized. This is both described in Section 3.2.3.

3.2.1 Performance Metrics in Literature

Roa and Suárez [31] and Kragten and Herder [32] provide two extensive reviews on performance metrics for grasping.

The first review, the one of Roa and Suárez [31], focuses on performance metrics to determine the *quality of the grasp*, mainly of *dexterous hands*. These performance metrics are implemented in algorithms which have to calculate the optimal finger configuration and are therefore not very useful to compare grippers. Moreover, no performance metrics are mentioned with respect to the energy consumption of the grasps. The second review, the one of Kragten and Herder [32], focuses on performance metrics used in the

design and evaluation of *underactuated* robotic grippers. Underactuated grippers have less actuators than degrees of freedom [32] and are therefore able to *passively adapt* to the object's geometry. The ability to adapt is integrated in the mechanical structure, instead of using electronics. As in both reviews no performance metric was reported that relates to the energy consumption, a new metric need to be proposed.

3.2.2 Novel Performance Metric

Because no existing performance metric is reported in literature that quantifies the energy consumption, I propose a novel performance metric. This section describes the general form of this metric. In the next section, Section 3.2.3, this performance metric will be simplified to make it applicable to compare the various mechanisms.

The novel performance metric I propose is inspired by the *Cost of Transport*, which describes the energetic cost of locomotion by the normalization of the power consumption with the weight and speed. Likewise, I propose the the *Cost of Grip* (COG), which relates the nominal installed power P_A of the actuator(s) to the closing speed and dislodging force, which respectively characterize the performance during sizing and forcing:

$$COG = \frac{P_A}{\min_{\phi} (F_D(\phi)) v_m} \quad (3.1)$$

Where v_m is the mean closing speed of the hand and F_D is the minimum dislodging force with direction ϕ . The term $\min_{\phi} (F_D(\phi))$ results in the minimum dislodging force in any direction.

During prehension the average closing speed v_m is responsible for a good performance. A higher speed means faster closure of the gripper. During the retention the minimum dislodging force F_D acting on any direction ϕ is critical. Intuitively, the installed power relates to the energy consumption, but it also relates to the actuator mass M_A . For electric motors the power to weight ratio is typically ~ 0.5 kW/kg [9]. The advantage of this proposed performance metric is that it relates (albeit indirectly) to three aspects, namely 1) energy effectiveness, 2) mass and 3) closing time. Only the complexity is not quantified by this performance metric, but as this aspect does not directly relate to functionality, it is less important and might be simply evaluated by counting the number of required components.

However, the *COG* decreases when the performance increases. Therefore, it is convenient to express the performance metric as the inverse of the COG:

$$Q_{COG} = \frac{\min_{\phi} (F_D(\phi)) v_m}{P_A} \quad (3.2)$$

3.2.3 Application of Performance Metric

Eq. (3.2) provides a performance metric to evaluate the performance in terms of energy, mass and closing speed, of a *complete* robotic hand. Hence, it cannot be directly applied to compare various drives, as these are just a *subsystem* of the hand. To enable a fair comparison, the following assumptions are made:

- All drives are applied using the same layout for the contact with the object: A clamp. Section 3.2.3.1 elaborates on this.
- All drives are actuated by the same motor, this is described in Section 3.2.3.2

The application of these assumptions will result in a simplified performance metric Q'_{COG} , suitable to compare the drives. As example, the most simple drive, the *vanilla drive*, will be explained. This drive consists only of a geared DC-motor, directly connected to the gripper. The performance of the vanilla drive will serve as base to normalize the performance of other drives, as described in Section 3.2.3.3. This will ease the comparison, as it eliminates the motor properties, and avoids thereby the need to quantify these properties.

3.2.3.1 Implementation Contact Layout

To allow for an easy and fair comparison, all drives are assumed to transmit the forces using the same layout for the contact. For this purpose a simple clamp is selected.

The model of the vanilla drive is depicted in Fig. 3.1. For this case solely a geared DC motor is used to

drive the hand, as is for instance the case in the *Delft Hand 3* [17], as discussed in Section 2.3.2.1. The minimum dislodging force is proportional to the force F_C that the clamp exerts on the object, hence the simplified performance is:

$$Q'_{COG} = \frac{F_C v_m}{P_{A,N}} \quad (3.3)$$

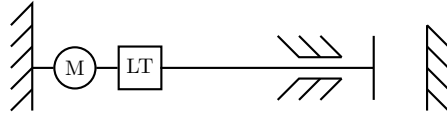


Figure 3.1: A clamp actuated by a Vanilla Drive. This drive consists of a motor (M) and linear transmission (LT_1) with ratio i .

3.2.3.2 Implementation of Motor Model

In addition to the assumption that the drives are connected to the same contact layout, it is assumed they are driven by the same motor. As actuator a (rotational) electric DC motors is selected. These are very common in robotics, because they perform good in terms of controllability, energy transmission, and environmental influences and modest in terms of maintenance, construction size and insensitivity to dirt [13], but most important: They allow for easy integration with the electronic microprocessors which are nowadays de facto standard to control robotic systems.

To describe the performance of the drive, the characteristics of the motor have to be known. These are described using a *motor model*. Based on this motor model, two important properties for the performance estimation can be estimated. For sizing this is the *adaptation speed*, for forcing this is the *maximum torque*.

Motor Model The motor speed is a function of the torque on the motor. The following relation [33] relates the motor speed ω_A to the applied voltage U_A and torque T_A :

$$\omega_A(T_A, U_A) = k_\omega U_A - \frac{\Delta\omega}{\Delta T_A} T_A \quad (3.4)$$

Where k_ω is the speed constant and $\frac{\Delta\omega}{\Delta T_A}$ the speed-torque gradient¹. This speed-torque curve is shown in Fig. 3.2. This equation shows that the voltage can be used to control the motor speed when it is loaded with a certain torque. The actuator current is proportional to the actuator torque:

$$T_A = k_m I_A \quad (3.5)$$

Where k_m is the motor constant. The speed and torque are limited to respectively $\omega_{A,max}$ and $T_{A,max}$ to ensure the mechanical integrity of the motor and its bearings.

¹Note that in [33] the motor speed is defined in RPM.

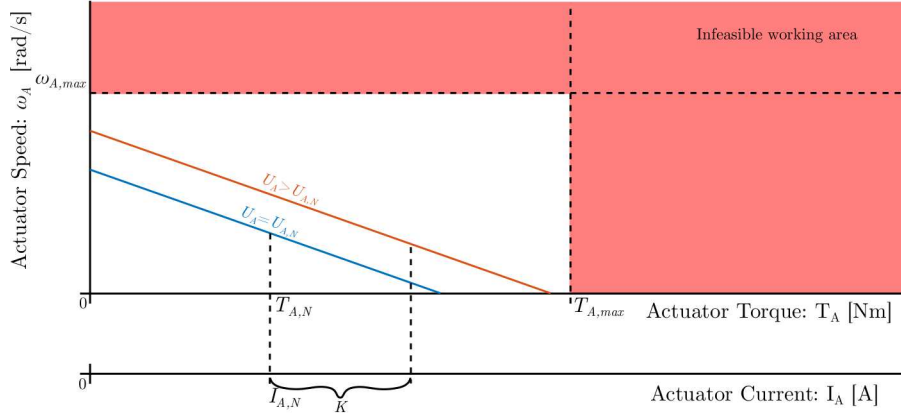


Figure 3.2: Speed-torque curve of DC motor [33]. The motor current I_A depends on the applied torque. The speed depends on the motor torque and applied voltage U_A . $T_{A,N}$ and $I_{A,N}$ are the nominal torque and current. A work point in the red area is infeasible, as the maximum speed or torque rating is exceeded.

Maximum Torque The nominal torque rating prevents overheating for the situation where the actuator is continuously energized, since the gripper does not need to hold the object all the time. When an actuator is intermittently energized, it is possible to *overpower* the actuator, i.e. exceeding temporarily the nominal current and torque [33] for short durations. For most grasping task the actuator is indeed intermittently energized. This is especially true when dedicated measures are taken to relieve the motor from the continuous static torques during retention. Hence, overpowering is taken into account in the motor model.

The ratio between the time the actuator is energized, t_{en} , and the total cycle time, t_{cycle} , is called the *Duty Cycle*, defined as:

$$D = t_{en}/t_{cycle} \text{ where } D \in [0, 1] \quad (3.6)$$

The basic guideline for overpowering [33] yields that the root mean square of the current does not exceed the nominal current. This ensures the average power does not exceed the nominal rated power. For a single workpoint this yields:

$$I_A \sqrt{D} \leq I_{A,N} \quad (3.7)$$

Where I_A is the applied current during intermittent energizing and $I_{A,N}$ denotes the rated nominal current of the actuator. According to Eq. (3.5) the current is proportional to the torque, hence the maximum torque scales with a factor K :

$$K = \frac{T_A}{T_{A,N}} = \frac{I_A}{I_{A,N}} \leq \frac{1}{\sqrt{D}} \quad (3.8)$$

The maximum force of the actuator is evaluated, while this overpowering effect is taken into account.

For the example of the vanilla drive this implies that the maximum clamp force is:

$$F_C = \frac{T_{A,N} i}{\sqrt{D_{PRR}}} \quad (3.9)$$

Where i is the gearbox ratio and D_{PRR} is the duty cycle of the prehension, retention and release with respect to the complete cycle, because the motor is energized during all these three phases. This is a conservative estimate, as the motor is not necessarily fully loaded all the time it is energized. Note that the actuation torque should never exceed its mechanical limit $T_{A,max}$.

Adaptation Speed Ideally no forces act during sizing, but in practice forces will arise due to e.g. friction or gravity. Yet, these forces are typically small compared to the maximum output forces. This means that the actuator is moving relatively fast. The maximum speed $\omega_{A,max}$ can be easily achieved with the proper applied voltage U_A . Therefore, this maximum speed is used to evaluate the performance during sizing.

For the vanilla drive, this means that the average adaptation speed can be approximated by:

$$v_m = \frac{\omega_{A,max}}{i} \quad (3.10)$$

3.2.3.3 Normalization

The gained knowledge on the motor model will now be applied on the vanilla drive. This will serve as example, but also as base for the normalization.

The performance of the Vanilla Drive and clamp follows from substituting Eqs. (3.9) and (3.10) in Eq. (3.3), this results in:

$$Q'_{COG,VD} = \frac{iT_{A,N}\omega_{A,max}}{i\sqrt{D_{PRR}}P_{A,N}} = \frac{T_{A,N}\omega_{A,max}}{\sqrt{D_{PRR}}P_{A,N}} \quad (3.11)$$

Remarkably, the transmission ratio does not affect the performance. This is because of the following “waterbed effect”: Increasing the transmission ratio to obtain a higher clamp force reduces the closing speed and vice versa.

The last step towards an easy comparison of the performance, is the normalization of the performance metrics. The performance of the vanilla drive, quantified by Eq. (3.11), is taken as base. The normalized performance is then expressed as:

$$\overline{Q'_{COG}} = \frac{Q'_{COG}}{Q'_{COG,VD}} = Q'_{COG} \frac{P_{A,N}\sqrt{D_{PRR}}}{T_{A,N}\omega_{A,max}} \quad (3.12)$$

As consequence, the normalized performance of the vanilla drive yields: $\overline{Q'_{COG,VD}} = 1$. As will be shown, this normalization will cancel out the motor properties. This allows the comparison to focus on the performance of the drive, without the need to quantify the motor properties.

3.3 Description of Drives

In this section the performance will be estimated and compared for a selection of state-of-the-art drives. Likewise as in Chapter 2, the drives are categorized in *work neutral* and *work non-neutral*, although the exchanged work is not further considered in the current chapter. The drives of both categories are described in respectively Sections 3.3.1 and 3.3.2. For each drive the performance metric will be expressed. In Section 3.4 a numerical evaluation is conducted in order to compare the different drives.

3.3.1 Energy-demanding Strategies

The first category contains the work-demanding strategies. The resemblance between the drives of this category is that the potential energy changes when the output force is adjusted. A numerical evaluation of the derived expressions for the performance is conducted in Section 3.4

3.3.1.1 Non-Backdrivable Drive (VD+L)

This solution relieves the actuator from the continuous static torque using a *Non-Backdrivable Mechanism* (NBDM), as is depicted in Fig. 3.1. This drive is very similar to a vanilla drive, except for the addition of a dedicate locking mechanism that allows the motor to drive the load, but prevents the motor from being driven by the load. A commonly known example of a NBDM is a wormwheel, but this mechanism has a poor efficiency due to the high friction forces within this gearing [27]. More sophisticated and efficient NBDMs, using rollers and springs to block automatically the motion, are reported in [21, 22, 34]. Efficiencies for these NBDM's can be as high as $\eta_L = 0.95$. [21]. In addition, the backlash might occur [21, 22] which also reduces the maximum output force. To be able to maintain an output force when locked, the drive needs to incorporate a stiffness, which is tensioned during prehension and is kept under tension by the NBDM. This stiffness can be an additional spring placed in the drive, but could also be the finite stiffness of the mechanism.

Taking the efficiency of the NBDM into account, the maximum clamp force is:

$$F_C = \frac{\eta_L T_{A,N} i}{\sqrt{D_{PR}}} \quad (3.13)$$

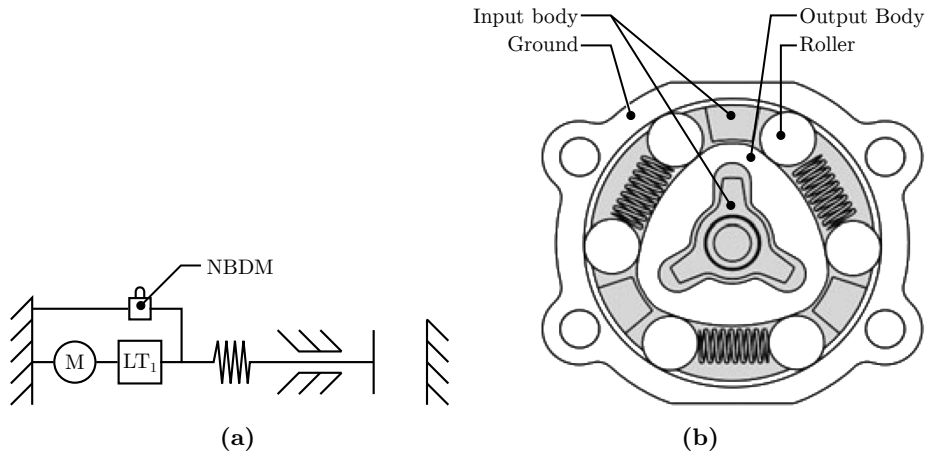


Figure 3.3: Non-Backdrivable Drive. **a:** Schematic representation A motor (M) with gearbox (LT_1) is connected parallel with a NBDM. Together they are in series with a spring. The NBDM cancels the static load, such that the motor does not need to be continuously energized during retention. **b:** Example of a Non-Backdrivable Mechanism (NBDM) [22]. The output body is automatically locked to the ground by the rollers as long as no torque is applied on the input body. Image adapted from [22].

Where D_{PR} is the duty cycle of the prehension and retention together with respect to the total cycle time, because the motor is only energized during these two phases. This is again a conservative assumption, as the motor is not necessarily fully loaded all this time. The resulting performance is:

$$Q'_{COG,VD+L} = \frac{\left(\frac{\eta_L T_{A,Si}}{\sqrt{D_{PR}}}\right) \left(\frac{\omega_{A,max}}{i}\right)}{P_{A,N}} = \frac{T_{A,S}\omega_{A,0}}{P_{A,N}} \cdot \frac{\eta_L}{\sqrt{D_{PR}}} \quad (3.14)$$

Normalizing according Eq. (3.12) yields:

$$\overline{Q'_{COG,VD+L}} = \eta_L \sqrt{\frac{D_{PRR}}{D_{PR}}} \quad (3.15)$$

Note that the normalized duty cycle $D_{PRR}/D_{PR} > 1$, because D_{PRR} incorporates in addition to D_{PR} the duty cycle of the retention. This reveals that a non-backdrivable locking mechanism indeed improves the performance as soon as $\sqrt{D_{PRR}/D_{PR}} > \eta_L^{-1}$. In Section 3.4 this equation will be numerically evaluated based on estimated values.

3.3.1.2 Automatic Clutch (AC)

A single transmission ratio, like the vanilla drive, implies a compromise between the adaptation speed during sizing and maximum output force during forcing. When the transmission ratio varies, this compromise is circumvented. A first way to do so is to switch between two different ratios using an *automatic clutch* [35], as is done in some prostheses. This results in a *high-speed-low-force* characteristic for sizing and a *low-speed-high-force* characteristic for forcing.

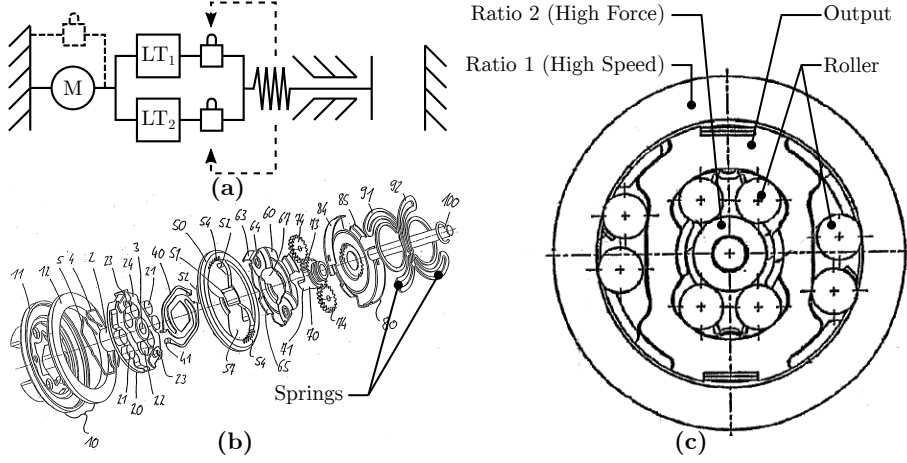


Figure 3.4: Automatic Clutch **a:** A motor (M) connected to two different linear transmissions (LT_1 and LT_2). Depending on the engagement of the clutches, either the first or second clutch is engaged, while the other is disengaged. This engagement is dependent on the extension of the pretensioned spring, as is represented by the dotted lines. The dotted clutch indicates the optional NBDM. **b:** Exploded view of an automatic clutch [35]. Image adapted from [35]. **c:** Cross-sectional view of an automatic clutch [35]. Two sets of rollers either connect the output of the first or second transmission to the output. The engagement of the rollers is determined by a pretensioned spring (not shown). Image adapted from [35].

The automatic clutch, depicted in Fig. 3.4, consists of two clutches connect the clamp to either the first or second transmission. This engagement is depending on the load that is “sensed” by a pretensioned spring, placed in series in the drive. As soon as the pretension is exceeded, the mechanism switches between from *high-speed* branch to the *high-force* branch. Images Fig. 3.4b shows an exploded view on an automatic clutch and Fig. 3.4c a cross-sectional view. In this mechanism the clutches are realized as two different sets of rollers. The pretensioned spring is shown in Fig. 3.4b.

The adaptation speed is depending on the transmission ratio i_1 for the *high-speed-low-force* mode. The maximum clamp force depends on the ratio i_2 for the *low-speed-high-force* mode. The ratio between these transmission ratios is $\iota = \frac{i_2}{i_1} > 1$.

When no NBDM is integrated, both the adaptation speed and stall force depend on $\sqrt{D_{PRR}}$. In this case the performance is:

$$Q'_{COG,AC} = \frac{\left(\frac{T_{A,S}i_2}{\sqrt{D_{PRR}}}\right) \left(\frac{\omega_{A,0}}{i_1}\right)}{P_{A,N}} = \frac{T_{A,S}\omega_{A,0}}{P_{A,N}} \cdot \frac{\iota}{\sqrt{D_{PRR}}} \quad (3.16)$$

Normalization yields:

$$\overline{Q'_{COG,AC}} = \iota \quad (3.17)$$

This equation shows that the performance increases with the difference in transmission ratios. This will be incorporated in the numerical analysis in Section 3.4.

When a NBDM is integrated, the maximum force scales with $1/\sqrt{D_{PR}}$ and η_L . As such, the normalized performance yields

$$\overline{Q'_{COG,AC+L}} = \eta_L \sqrt{\frac{D_{PRR}}{D_{PR}}} \quad (3.18)$$

3.3.1.3 Continuous Variable Transmission (CVT)

Quite similar to the automatic clutch is the employment of a *Continuous Variable Transmission* (CVT). Instead of switching between two discrete gear ratios, the ratio changes seamlessly throughout a certain range, depending on the external load.

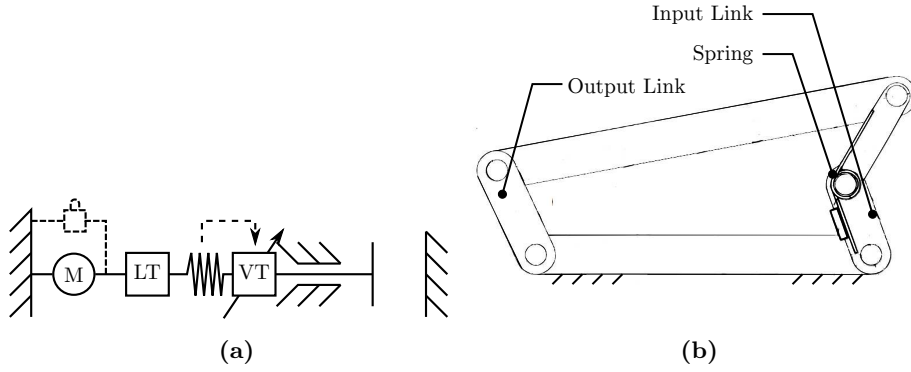


Figure 3.5: Continuous Variable Transmission (CVT) **a:** A geared motor (M and LT) connected with a CVT (VT). The transmission ratio is depending on the load, measured by the elongation of a spring in series with the drive. The dotted clutch indicates the optional NBDM. **b:** Example of a CVT [36], based on a five bar mechanism. The ratio is depending on the extension of the torsion spring.

Takaki and Omata [36] proposed a finger with a five bar mechanism as CVT. This mechanism, shown in shown in Fig. 3.5b, has two DoFs, of which one is constrained by a torsion spring. Consequently the transmission ratio between the input and output link of the mechanism varies with the load that is applied on the finger. In other words, the transmission ratio is depending on the extension of the spring, as is schematically indicated in Fig. 3.5a by the dotted line.

In the sizing mode, the mechanism has a ratio i_1 and fully loaded the mechanism has a ratio i_2 . The ratio ι between these ratios is dependent on the configuration of the output link. Consequently, the performance is exactly equal to the performance of the automatic clutch:

$$\overline{Q'_{COG,CVT}} = \overline{Q'_{COG,AC}} = \iota \quad (3.19)$$

And with NBDM:

$$\overline{Q'_{COG,CVT+L}} = \overline{Q'_{COG,AC+L}} = \iota \eta_L \sqrt{\frac{D_{PRR}}{D_{PR}}} \quad (3.20)$$

3.3.1.4 Synergetic Drive (SD)

An alternative to varying the transmission ratio is employ two separate motors to drive the same DoF. These motors are either placed in series or connected to a differential [37], as depicted in Fig. 3.6a. A differential is a mechanical device that resolves two inputs in a single output [38], or vice versa. For both cases the motor speeds adds up to the output speed² Another embodiment of the serial connection is when the two motors would drive two opposed fingers, as shown in Fig. 3.6b. In this case the relative closing speed of the two fingers is still proportional to the sum of the two motor speeds.

The first motors and gearbox operate at *high-speed-low-force*, while the other motor and gearbox operate at *low-speed-high-force*. As can be easily seen for the serial case, both gearbox outputs would be equally loaded in the case no locking is applied. The same holds for when the differential is used. Typically the *high-speed-low-force* is prevented from being backdriven by a NBDM, for instance using a wormwheel, as shown in 3.6b. When a second NBDM is integrated, also the *high-force-low-speed* motor is relieved from being continuously energized during retention.

For the quantification of the performance, it is assumed the motors are identical and controlled with the same input, such that they are energized simultaneously. More complex control strategies with two independently controlled motors might also be possible, although this complicates the software and

²In fact, for a differential the input velocities $v_{in,1}$ and $v_{in,2}$ adds up to an output velocity v_{out} according to the following relation:

$$v_{out} = a_1 v_{in,1} + a_2 v_{in,2}$$

Where a_1 and a_2 are two transfer ratios. For many differentials $a_1 = a_2 = 1/2$, but different values for a_1 and a_2 are also possible. For now it is for simplicity assumed $a_1 = a_2 = 1$ to comply with the serial connection. Consequently, the overall ratios i_1 and i_2 equate to the ratios of the linear transmissions. For the case that a_1 or a_2 do not equal unity, the gearbox ratios can be adjusted to obtain the same overall ratios.

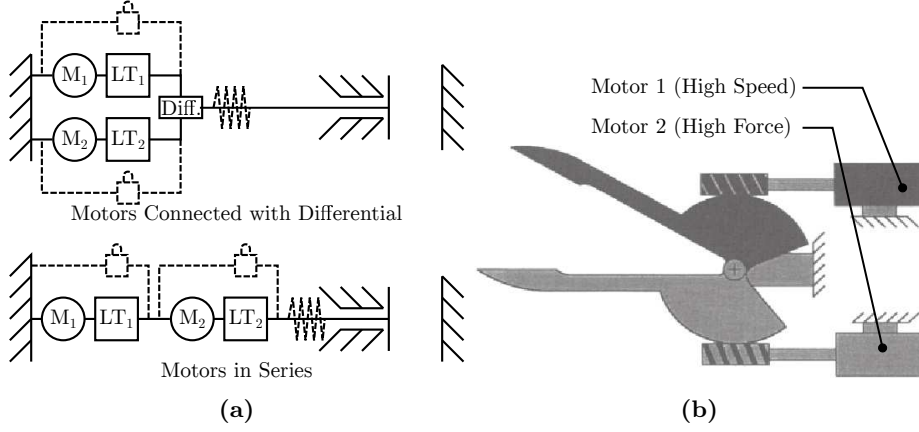


Figure 3.6: Synergetic Drive **a:** Two identical motors (M_1 and M_2) with different transmissions (LT_1 and LT_2) are connected with a differential or in series. The gearbox speeds adds up to the clamp speed. The dashed lines represent the optional NBDMs and stiffness to relieve the actuators during retention. **b:** An example of a synergetic drive, where the two motors are connected in series by driving two opposing fingers. Image taken from [37].

hardware design, as it requires additional algorithms, motor control boards, sensors etc.

For the case when two NBDMs are applied, the velocities add up as long as the clamp does not exceed the force at which the *high-speed-low-force* motor stalls:

$$v_c = \max(v_{c,1} + v_{c,2}, v_{c,2}) = \begin{cases} \frac{w_A}{i_1} + \frac{w_A}{i_2} & \text{if } F_C \leq F_T \\ \frac{w_A}{i_2} & \text{if } F_C > F_T \end{cases} \quad (3.21)$$

Where F_T is the clamp force for which the “low-force-high-speed” motor stalls. During sizing the motors are (nearly) unloaded, which means both motors run at maximum speed. The clamp adaptation speed equals: $v_m = w_{A,max}(i_1^{-1} + i_2^{-1})$.

The maximum clamp force equals the maximum output force of the *low-speed-high-force* motor, as both gearbox outputs are equally loaded. Note that the other motor is locked at this force to prevent it from backwards motion. The maximum force scales with $(\sqrt{D_{PR}})^{-1}$, as both motors are relieved during retention. The resulting maximum clamp force is: $F_C = \eta_L T_{A,N} i_2 / \sqrt{D_{PR}}$. The nominal installed power is $2P_{A,N}$ because two motors are installed. The resulting performance is:

$$Q'_{COG,SD+L} = \frac{\left(\frac{\eta_L T_{A,N} i_2}{\sqrt{D_{PR}}}\right) \left(\frac{\omega_{A,max}}{i_1} + \frac{\omega_{A,max}}{i_2}\right)}{2P_{A,N}} = \frac{\eta_L T_{A,N} \omega_{A,max}}{P_{A,N}} \cdot \frac{\iota + 1}{2\sqrt{D_{PR}}} \quad (3.22)$$

Normalization yields:

$$\overline{Q'_{COG,SD+L}} = \frac{\eta_L(\iota + 1)}{2} \sqrt{\frac{D_{PRR}}{D_{PR}}} \quad (3.23)$$

If the NBDMs are omitted, the main force is limited to the maximum force of the *high-speed-low-force* motor, as both gearbox are equally loaded. Moreover, a duty cycle of D_{PRR} applies. The maximum force of the clamp becomes: $F_C = i_1 T_{A,N} / \sqrt{D_{PRR}}$. The adaptation speed does not change. This results in the following performance:

$$Q'_{COG,SD} = \frac{\left(\frac{T_{A,N} i_1}{\sqrt{D_{PRR}}}\right) \left(\frac{\omega_{A,max}}{i_1} + \frac{\omega_{A,max}}{i_2}\right)}{2P_{A,N}} = \frac{T_{A,N} \omega_{A,max}}{P_{A,N}} \cdot \frac{1 + \iota^{-1}}{2\sqrt{D_{PRR}}} \quad (3.24)$$

Normalization yields:

$$\overline{Q'_{COG,SD}} = \frac{1}{2} \left(1 + \frac{1}{\iota}\right) \quad (3.25)$$

3.3.2 Energy-neutral Strategies

Recall from the previous chapter the two strategies to obtain a work-neutral drive: Eliminate the displacement using a *Spring with CVT* or eliminate the resultant force with a *Statically Balanced Force Amplifier* (SBFA). In Sections 3.3.2.1 and 3.3.2.2 the performance is quantified for these two solutions. To do so, it is assumed both solutions are driven by a single motor. This reduces the complexity of the control, the overhead energy consumption and costs, as less actuators and sensors need to be incorporated.

3.3.2.1 Spring with Continuous Variable Transmission (SCVT)

The first work-neutral drive strategy, inspired on the on the *W.E.N.-principle* [26], aims to eliminate the displacement of the main spring. It consists of a CVT connected to a spring.

Fig. 3.7b shows a mechanism, consisting of a lever based CVT. Other embodiments, with other CVTs, are also possible. The mechanism from Fig. 3.7b requires two inputs. This is true for all embodiments, as one input is required to adjust the position of the clamp during sizing and another to adjust the transmission ratio to adjust the force level.

Fig. 3.7a shows schematically how this mechanism is applied in a drive. Other possibilities are also possible, but the characteristics do not change. It consist of a geared motor, connected to a *drive splitter*, which is a dedicated mechanism that enables the motor to drive two different inputs subsequently. These splitters are discussed in more detail in Chapter 5. In the sizing mode the splitter controls the position of the clamp with its first output. The spring extension should not change and is therefore locked with a locking mechanism, C_2 . When the clamp is in contact with the object, the position of the clamp needs to be locked, this is done with the other clutch, C_1 . The *splitter* can now switch to its second output to alter the CVT's ratio.

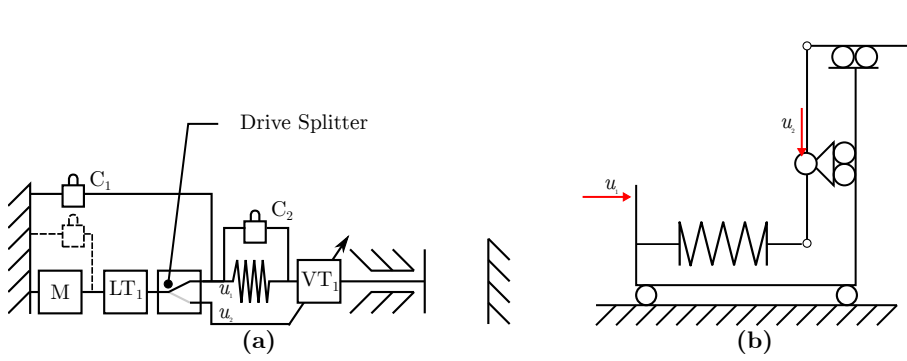


Figure 3.7: Spring with CVT. **a:** Example embodiment of a spring with CVT in a drive. Clutch C_1 locks the position of the clamp during forcing. Clutch C_2 maintains the elongation of the spring during forcing. A single motor is used to adjust the clamp position during forcing and the ratio during forcing. **b:** Lever based CVT with spring.

The CVT is able to vary the overall ratio ratio between i_{min} and i_{max} . The motor gearbox has a reduction of i_{GB} . When the mechanism is in the sizing mode, the ratio equals $i_{GB} \cdot i_{min}$, as such the adaptation speed of the clamp is: $v_m = \omega_{A,max} / (i_1 \cdot i_{min})$.

The maximum spring force is limited to the maximum motor force. This ensures the mechanism is able to recover from imperfect situations, such as position errors. For instance, when clutch C_1 locks while there is some play between the clamp and object, the spring will loose some tension as soon as clutch C_2 unlocks. To be able to restore the initial tension the spring, the motor should be able to deliver the maximum spring force. This spring force is increased by the CVT's maximum ratio i_{max} . Although theoretically no static loads acts on the motor during retention, in practice it is likely that the motor is loaded due to imperfections in the CVT, hence the maximum force depends on D_{PRR} . The maximum clamp force is: $F_C = T_{A,N} i_1 i_{max} / \sqrt{D_{PRR}}$. The performance equals:

$$Q'_{COG,SCVT} = \frac{\left(\frac{T_{A,N} i_1 i_{max}}{\sqrt{D_{PRR}}} \right) \left(\frac{\omega_{A,max}}{i_1 i_{min}} \right)}{P_{A,N}} = \frac{T_{A,S} \omega_{A,0}}{P_{A,N}} \cdot \frac{i_{max}}{i_{min} \sqrt{D_{PRR}}} \quad (3.26)$$

Normalization yields:

$$\overline{Q'_{COG,SCVT}} = \alpha \quad (3.27)$$

Where $\alpha = i_{max}/i_{min}$ describes the ratio range of the CVT.

If the motor is relieved from static loads during retention, the maximum force equals $F_C = \eta_L T_{A,N} i_1 i_{max} / \sqrt{D_{PR}}$, which results in a normalized performance of:

$$\overline{Q'_{COG,SCVT+L}} = \alpha \eta_L \sqrt{\frac{D_{PRR}}{D_{PR}}} \quad (3.28)$$

To obtain an estimation of the performance, an estimate of α is obtained based on several prototypes of CVTs applied in robotics. A common application of CVTs in robotics are *Variable Stiffness Actuators* (VSAs) [30]. In Table 3.1 an overview is given of some CVTs applied in robotics and its ratio α . This value is determined either by the reported transmission range, or based on the reported stiffness. Because the apparent stiffness relates quadratically to the transmission, the ratio follows from: $\alpha = \sqrt{k_{max}/k_{min}}$, where k_{max} and k_{min} are the minimum and maximum stiffness of the VSAs. The approximate maximum value of $\alpha = 7$ is used to estimate the performance of the spring with CVT.

Table 3.1: Reported values for α

	CVT-type ^a	i_{min} [-]	i_{max} [-]	k_{min} [Nm/rad]	k_{max} [Nm/rad]	α [-]
CVT Finger [29]	NLMI	0.5	3.3			6.6
DLR FSJ [39]	NLMI			826	52.4	3.97
AwaS [40]	LL			30	1300	6.6
HSVA [41]	LL			4.0	126	5.6
Prototype of Energy Efficient VSA [42]	LL	$\propto 26$ mm	$\propto 76$ mm			2.9

^a NLMI: Non-linear mechanical interlink. LL: Changing Lever Length [30].

3.3.2.2 Statically Balanced Force Amplifier (SBFA)

The second work neutral strategy eliminates the force using a *Statically Balanced Force Amplifier* (SBFA). An example of an applied SBFA is shown in Fig. 3.8b. It is based on the *sliding ladder balancer* [23], with the addition that the frame and output can move as whole to adjust to the object size. Chapter 4 and 5 will discuss other solutions, but this will not affect the performance.

Again, the mechanisms requires two separate inputs to perform sizing and forcing. Hence, a splitter is implemented in Fig. 3.8a. In the sizing mode, the motion of the buffer spring (S_B) is blocked, using clutch C_2 . Both springs move simultaneously without changing the elongation. In the forcing mode, the buffer spring is locked to the ground with engaged clutch C_1 . Using the second input, the configuration of the balancer is changed to adjust the output force.

Theoretically, an infinite force amplification could be achieved. However, in practice balancing imperfections and friction limit this amplification factor. In literature, various statically balanced mechanisms are reported that achieve a force reduction of $\zeta = 0.95 - 0.97$ [24, 25].

To performance of this strategy is determined based on the notion that the actuator has to compensate for the balancing imperfections, which equals at most a factor $(1 - \zeta)$ of the maximum spring force. As such, the maximum clamp force equals:

$$F_C = \frac{T_A i_2}{(1 - \zeta)} \quad (3.29)$$

Note that unlike for the *spring with CVT*, the motor is not required to deliver the maximum spring force, as the buffer spring assists the motor. In case of a position errors the motor has to compensate for the balancing imperfection, which is a fraction of the maximum spring force for small errors. Ideally, the motor is not subjected to any load during retention, but in practice imperfections arise, hence the motor is energized during prehension, retention and release.

$$Q'_{COG,SBFA} = \frac{\left(\frac{T_{A,N} i_2}{\sqrt{D_{PRR}(1-\zeta)}}\right) \left(\frac{\omega_{A,max}}{i_1}\right)}{P_{A,N}} = \frac{T_{A,N} \omega_{A,max}}{P_{A,N}} \cdot \frac{l}{\sqrt{D_{PRR}(1-\zeta)}} \quad (3.30)$$

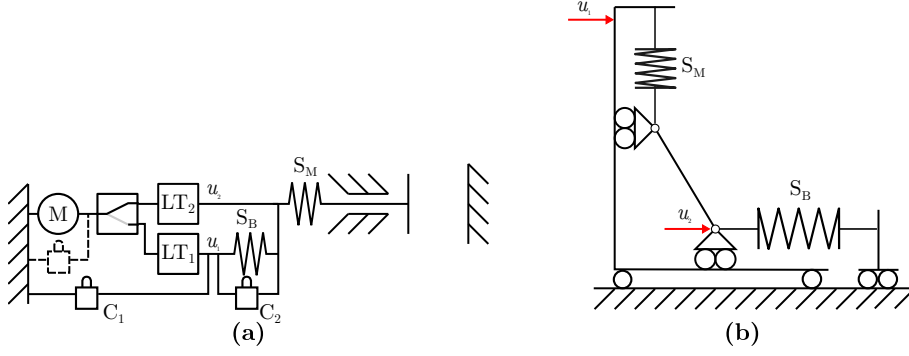


Figure 3.8: Statically Balanced Force Amplifier (SBFA). **a:** Possible embodiment of a SBFA in a drive. The main spring S_M and balancing spring S_B move together during sizing, with u_1 as input while and engaged clutch C_2 . During forcing, the buffer spring is locked to the ground with clutch C_1 and the output force is controlled with u_2 . **b:** Exemplary SBFA mechanism for grasping, based on the *sliding ladder mechanism* [23]. The two inputs are shown as red arrows.

Normalization yields:

$$\overline{Q'_{COG,SBFA}} = \frac{\iota}{1 - \zeta} \quad (3.31)$$

With the application of a NBDM the normalized performance resolves to:

$$\overline{Q'_{COG,SBFA+L}} = \frac{\eta_L \iota}{1 - \zeta} \sqrt{\frac{D_{PRR}}{D_{PR}}} \quad (3.32)$$

3.4 Comparison

The discussed strategies will be compared based on their normalized performance metric $\overline{Q'_{COG}}$. Table 3.2 provides an overview on the expressions for the normalized performances.

Table 3.2: Performance metrics of strategies

	Without NBDM	With NBDM (+L)
Vanilla Drive (DD)	1	$\eta_L \sqrt{\frac{D_{PRR}}{D_{PR}}}$
Automatic Clutch (AC)	ι	$\iota \cdot \eta_L \cdot \sqrt{\frac{D_{PRR}}{D_{PR}}}$
CVT (CVT)	ι	$\iota \cdot \eta_L \cdot \sqrt{\frac{D_{PRR}}{D_{PR}}}$
Synergetic Drive (SD)	$\frac{1}{2} (1 + \iota^{-1})$	$\frac{\eta_L (\iota + 1)}{2} \sqrt{\frac{D_{PRR}}{D_{PR}}}$
Lockable Spring with CVT (SCVT)	α	$\alpha \eta_L \sqrt{\frac{D_{PRR}}{D_{PR}}}$
Statically Balanced Force Amplifier (SBFA)	$\frac{\iota}{1 - \zeta}$	$\frac{\iota \eta_L}{1 - \zeta} \sqrt{\frac{D_{PRR}}{D_{PR}}}$

On beforehand it is difficult to predict the transmission ratios, because the determination is related to the dynamics and friction in the system. This requires detailed analyses. The duty cycles vary for different tasks. This becomes even more clear when the normalized duty cycle is rewritten to:

$$\frac{D_{PRR}}{D_{PR}} = 1 + \frac{t_{retention}}{t_{prehesion} + t_{release}} \quad (3.33)$$

Where $t_{retention}$, $t_{prehesion}$ and $t_{release}$ are the durations of respectively the retention, prehension and release phase. For instance, the retention takes much longer for an assisted living robot carrying objects from the kitchen to the living room than for a palatalizing pick-and-place robot. Therefore the performance is plotted as function of the normalized duty cycles for two different values of ι in Fig. 3.9. In appendix B.1 an alternative visualization is presented.

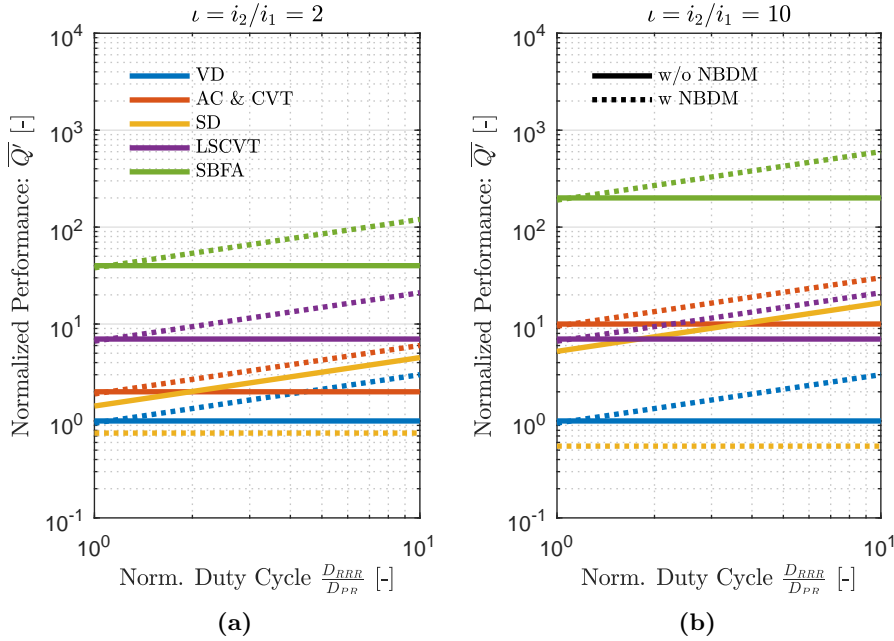


Figure 3.9: Normalized performance of the different strategies. The line color represent the strategy. The linestyle, solid or dotted, represent without NBDM or with NBDM respectively. For the LSCVT is assumed: $\alpha = 7$. For the SBFA is assumed: $\zeta = 0.95$. **a:** Typical pick and place task. **b:** Typical assisted living task.

The results of Table 3.2 and Fig. 3.9 lead to the following conclusions.

- Except for the *synergetic drive*, the application of a NBDM multiplies the performance without NBDM with a factor $\eta_L \sqrt{D_{PRR}/D_{PR}}$. This means the performance improves as soon as this factor is larger than unity, which is true when $D_{PRR}/D_{PR} > \eta_L^{-2}$. This condition is satisfied for both tasks, as Fig. 3.9 shows that the performance of the strategies with NBDMs is higher than without.
- For eight of the ten strategies the performance is a function of ν . In general, the performance increases with ν , except for the *Synergetic Drive without NBDM*. The reason is that for both the *high-speed* and *high-force* branch are subjected to the same load. Without locking, the maximum clamp force is limited to the maximum force of the *high-speed* branch, which is no improvement with respect to the *vanilla drive*. The installed power is twice as large as compared to the base, hence the normalized performance approaches half the performance of the *vanilla drive*.
- If all strategies are compared without NBDM, i.e. only the solid lines of Fig. 3.9 are taken into account, the SBFA outperforms them all. The same holds when all strategies are compared with NBDM.

3.5 Discussion

The results of Section 3.4 suggests the SBFA is a viable solution. But before this conclusion is drawn, the results obtained in this chapter are subjected to a critical reflection.

The first issue is regarding to the the definition of the performance metric. The newly proposed performance metric mainly relates to the closing speed, energetic performance and indirectly to the the mass of the actuator. However, the performance metric does not account for the mass of the additional required components, such as springs and clutches. Unfortunately, it is very difficult to estimate the mass of the systems beforehand, because the final mass is also strongly dependent on components not shown, such as bearings and fasteners. This would require a more detailed analysis, which is beyond the scope of this comparison. Using the mass reported in literature is also not likely to be a solution, because the mass is not always reborted. Moreover, the implementation of the drives is not uniform: the the *Delft Hand 3* [17] is a complete hand, the load sensitive CVT [29] is a single finger and the automatic clutch [35] is only the drive. Comparing those would be comparing cheese and chalk. Moreover, to quantify the

consideration between those two aspects is difficult: How much additional mass is allowed for lowering the energy consumption with one unit of energy? These difficulties on the incorporation of the mass justifies the use of the proposed performance metric for this rough comparison.

The second issue is regarding the simplifications done to express the performance. The simplification of the contact lay out to a clamp is necessary to allow for a fair comparison between the drives, because the geometry of the finger (i.e. one or more phalanges, curved) has significant influences on the minimum dislodging force [17].

In the analysis effects of friction and dynamics are neglected. In addition, rather than the complete force-stroke characteristics, only the two extreme workpoints are considered: maximum force and maximum speed. This leads to the neglect of the transient-times. Incorporating those aspects would require more complex models and procedures. However, more complex models require also assumptions. As such, this approach would shift the problem, while the increased complexity impedes a straightforward comparison.

The third issue is regarding the assumed cyclic task of the the gripper. Not all tasks are cyclic, for these tasks the absolute duration should be taken into account to prevent overheating of the actuators. In fact, the same holds for cyclic tasks, as the absolute duration is still relevant. If a motor would be energized for a day and be at rest for a day, the duty cycle $D_{PRR} = 0.5$. Yet, overpowering the motor with a factor $\sqrt{D_{PRR}^{-1}}$ would result in overheating because too much heat has accumulated. This absolute time constraint should also be taken into account in the detailed design. For a concise comparison this is less suitable, as it is dependent on the motor specifications and therefore less general. The static-load cancellation and overpowering are also relevant in case of non-cyclic tasks, as they potentially increase the up-time and maximum force, which further justifies the simpler cyclic approach.

The fourth issue is regarding that ι has practical limitations. A larger reduction involves typically multiple reductions involve typically multiple reduction stages, resulting in a larger transmissions with more internal friction.

The fourth issue is regarding the completeness of the overview. Although there is no guarantee that the overview is complete, the overview shows a significant difference between the state-of-the-art work non-neutral mechanisms and work-neutral mechanisms. This substantiates the conclusion of the previous chapter that work-neutral mechanisms, and especially SBFA are a viable strategy for energy saving gripper drive.

Combining the results of the previous and current chapter suggest a SBFA is a viable concept, as it outperforms the other strategies and is likely to be manufacturable. The performance of the SBFA falls apart in three factors:

- *The transmission ratio change ι .* Because the mechanism has two separate inputs, the transmission ratios of both branches can be easily optimized for either *high-speed* or *high-force*. This improves the performance with respect to the *vanilla drive* with a factor ι .
- *The force reduction ζ .* For SBFA a force reduction of ζ can be achieved, which means that a (geared) motor has to deliver just $1 - \zeta$ of the maximum clamp force. For a reported value of $\zeta = 0.95$ this means that the maximum output force increases a factor 20 with respect to the *vanilla drive*.
- *Static load cancellation $\eta_L \sqrt{\frac{D_{PRR}}{D_{FR}}}$.* When a NBDM is applied to cancel any balancing imperfections, this ensures the motor is relieved from any static torques during retention. This means the motor is only energized during prehension and release and can therefore deliver higher forces when it is overpowered. Yet, it should be taken into account that a NBDM has a non-unity efficiency. The actual improvement w.r.t. the *vanilla drive* depends on the duty cycles of the task.

It should be noted that the factor $1 - \zeta$ groups the effects of friction, hysteresis and balancing imperfections. Only balancing imperfections will actual results in static loads during retention, as it has a conservative nature. It might be the case that the friction counteracts this balancing imperfection and relieves the actuator from the static loads. Yet, to be sure of this it is better to implement a NBDM as both the balancing imperfection and friction are hard to predict exactly due to stochastic variations in the realization.

All in all, this sections confirms the conclusion of Chapter 2: also based on a numerical analysis the SBFA outperforms the competing state-of-the-art strategies. The next step is to analyze how a SBFA can be implemented effectively in a drive for a gripper. This is the subject of the next chapter.

3.6 Conclusion

Several state-of-the-art drive strategies for grippers are compared based on a novel performance metric, which relates to the nominal installed power of the actuators, average closing speed and minimum dislodging force. The SBFA outperforms all other listed strategies, as it is able to amplify the actuator output with a factor ~ 20 and allows for two different ratios during forcing and sizing, as the mechanism has two inputs. The additional implementation of NBDMs ensures the actuator is relieved from static loads during retention, which allows the motor to be overpowered, to obtain an even higher force for the same amount of installed power.

Part II

Conceptual Design

Chapter 4

Preliminary Design Considerations

4.1 Introduction

Although successful implementations of SBFAs have been reported [24, 25], in a preliminary survey no implementation of SBFAs in grippers was found [11]. This implementation is not straightforward: The existing SBFAs deliver an output force at a fixed output position. However, to be able to cope with various object sizes, the output position needs to vary, which is a novel addition. This chapter aims to derive a set of design principles, which will be used to in the conceptual and detailed design in the following chapters. These design principles are obtained by investigating the three subfunctions of the drive:

SF 1 *Effortless Sizing*

SF 2 *Effortless Forcing*

SF 3 *Switching between Sizing and Forcing*

These three subfunctions are subsequently discussed under the ideal conditions in Sections 4.2 to 4.4. In Section 4.5 the mechanism is analyzed while it is subjected to imperfect conditions. This chapter concludes with a discussion and conclusion in Sections 4.6 and 4.7

4.2 Subfunction 1: Effortless Position Adaptation

The first subfunction is *Effortless Sizing*: the SBFA has to deliver the output force at a range of output positions to be able to cope with different object sizes. The ability to do so is a novel addition to existing SBFAs, which are designed to deliver the output force at a fixed position.

Two different solutions are identified to achieve sizing, based on a *fixed frame* or *moving frame*. To understand the theoretical framework they are introduced in this section, but a comparison and selection will take place in the next chapter.

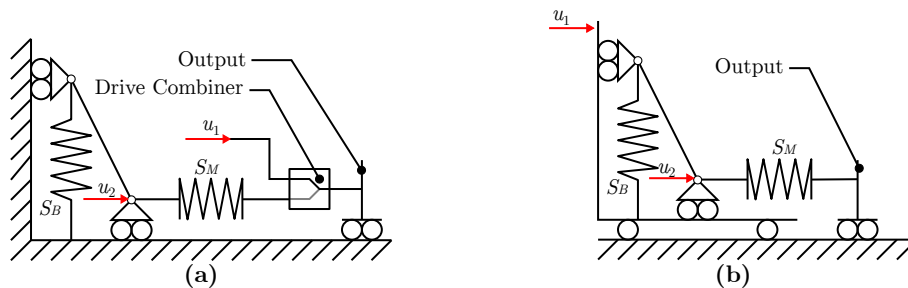


Figure 4.1: SBFA Mountings. **a:** Fixed Frame SBFA. The *drive combiner* connects either the sizing input (u_1) or the SBFA output to the output of the drive. **b:** Moving Frame SBFA, the frame is moved by the sizing input u_1 and the force level is varied by the difference between u_2 and u_1 .

4.2.1 Fixed Frame SBFA

A first solution to enhance the SBFA to deliver an output force at various positions is to *sum* the output of the output of the SBFA with an additional input. This is done using a *drive combiner*, which is the inverse of the *drive splitter* discussed in the previous chapter. This combiner is able to select one of the two inputs to drive one output. A combiner is realized using clutches, whether or not combined with a differential. The next chapter will compare the various combiners. Fig. 4.1a shows an example of the implementation of a *fixed frame SBFA* with splitter. The first input of the splitter is driven by an additional input, used to adjust the output position of the drive. The second input is connected to the output of the SBFA, when this input is engaged it is able to transmit the output forces of the SBFA. The overall mechanism has two inputs, the first input u_1 is used to alter the output position. The second input, u_2 is used to vary the output force.

4.2.2 Moving Frame SBFA

The second solution is to enable the frame of the SBFA to move with respect to the ground, an example is shown in Fig. 4.1b.

This mechanism requires also two inputs to function. A first one, u_1 , to adjust the position and a second one, u_2 , to adjust the force level of the SBFA. Note that this embodiment is a kind of *differential drive*. The output force level of the SBFA is depending on the difference $\Delta u = u_2 - u_1$ between the two inputs. Note that for force equilibrium, the SBFA requires a reaction force on the frame when it exerts an output force, this implies the need of a locking mechanism which blocks the motion during forcing.

The *moving frame SBFA* is the general case of the two, because a *fixed frame SBFA* can be obtained by fixing the frame to the ground by constraining the first input as stationary to the ground. Therefore, the *moving frame SBFA* will be used for the theoretical analysis of SBFAs in grippers.

4.3 Subfunction 2: Effortless Force Adaptation

The second subfunction of the SBFA based drive is *effortless forcing*. This means the ability to adjust the output force within a certain range without the need to exchange work at the input of the mechanism. As already discussed, this force originates from a potential energy stored in an internal force mechanism. Section 4.3.1 will consider two suitable energy buffers and select the best one. The key to static balancing is a dedicated transmission between the different energy buffers. This transmission will be considered in Section 4.3.2

4.3.1 Energy Storage

A statically balanced force amplifier is based on two mechanical energy buffers, with the transmission ratio such that they allow for perfect energy exchange. The use of springs [24, 23] and permanent magnets [25, 43] are reported as energy buffers of statically balanced mechanisms. Although counterweights are also used for statically balancing [23], they are not considered, because they belong to the category of *external forces*, which underperform compared to *internal forces*, as is described in Chapter 2. The selection between springs and permanent magnets is made based on whether they are simple and lightweight.

Whereas springs and masses might be balanced with the use of very simple mechanisms, consisting of a single lever [23], the highly non-linear behavior of permanent magnets require more complex mechanisms. In [25, 43] multiple springs are used for a piece-wise approximation of the force-characteristic of the magnet.

Nowadays, Neodymium magnets have a maximum energy density of 0.45 MJ/m^3 ($\sim 56 \text{ MGOe}$) [44], and a density of 7500 kg/m^3 . This results in an energy-to-mass ratio of 60 J/kg . The energy-to-mass ratio for a spring is evaluated based on the theoretical maximum of stored potential energy in a elastically deformed material:

$$\frac{V}{m} = \frac{\sigma_y^2}{2E\rho} \quad (4.1)$$

For RVS 301 spring steel, with a yield strength of $\sigma_y \approx 1000 \text{ MPa}$, a density of $\rho = 7.8 \cdot 10^3 \text{ kg/m}^3$ and a Young's Modulus of $E = 200 \text{ GPa}$ this results in an energy density of approximately 320 J/kg .

Table 4.1: Consideration on energy buffer

Criteria	Spring	Permanent Magnet
Lightweight	+ $\frac{V}{m} \approx 320 \text{ J/kg}$	– $\frac{V}{m} \approx 60 \text{ J/kg}$
Simple	+ Simple mechanisms reported [23]	– highly-non linear force characteristic results in complex designs.

In Table 4.1 the considerations on the energy buffer are depicted. From this table follows that springs are the best option as energy buffers, because they combine a high energy to mass ratio $\frac{V}{m}$ with a the potential to implement it in a simple mechanism. This results in the first design principle:

Design Principle 1: The Statically Balanced Force Amplifier should be constructed using springs as energy buffers.

4.3.2 Transmission

The key to static balancing is the transmission that ensures that the springs of the SBFA are statically balanced. The configuration of the SBFA is controlled with an input. This input can attach at various locations of the SBFA, although some locations are less suitable because they result in singular configurations, this is addressed in Section 4.3.2.1. Section 4.3.2.2 derives the the required transmission. Section 4.3.2.3 argues this transmission should be executed as non-intermittent mechanism, which allows for a simplified representation of SBFAs.

4.3.2.1 SBFA Input

Due to the non-linear transmission singular configurations may arise. When the input of the mechanism reaches a singularity, it means that an infinite high force is required to adjust the configuration. In practice this means the input is blocked and the mechanism is uncontrollable. This condition should be avoided, which can be achieved by selecting an appropriate location for the input.

Hoeven [45] made a thorough analysis of singularities in statically balanced linkage and cam mechanisms. Based on this work three possible locations for the input are identified: 1) At the main spring, 2) at the buffer spring or 3) at the transmission between the main and buffer spring. This section will compare and explain these three options and compare the *possible stroke* and *complexity* of the mechanisms.

The singularities will be visualized using the *sliding ladder mechanism*, as it is the most easy to depict. The depicted singularities will also arise for other embodiments, as the non-linear ratio needs to be the same for all embodiments.

The complexity is analyzed for both a linkage mechanism and a cam mechanism. The *sliding ladder* mechanism was the only linkage mechanism that was suitable for a compact implementation according to [45]. The properties of the cam mechanism are universal for all cam mechanisms, regardless of the nature of the DoFs.

Input at Main Spring The first input location is at the main spring, as depicted in Fig. 4.2a. This results in a singularity when the main spring is fully tensioned, as in shown Fig. 4.3a. To avoid singularities, the working range of the main spring is: $s_M \in [0, s_{M,max})$. This means the main spring can not be fully tensioned. This implies a slight reduction of the realized force compared to the theoretical maximum of this mechanism. Yet, this is not a real problem as the singular position can be nearly approached and the mechanism can be executed with slightly stiffer springs to achieve the required force.

When this mechanism is executed as cam mechanism, at least one cam and one follower are required to connect the main spring and buffer spring to. The linkage mechanism requires a translational input, which is also straightforward to realize, for instance using a spindle drive.

Input at Balancing Spring The second input location is at the buffer spring, as depicted in Fig. 4.2b. This mechanism is in a singular configuration when the main spring is at rest, this is depicted in Fig. 4.3b. The working range of the main spring becomes: $s_M \in \langle 0, s_{M,max}]$. This poses a problem, as the rest

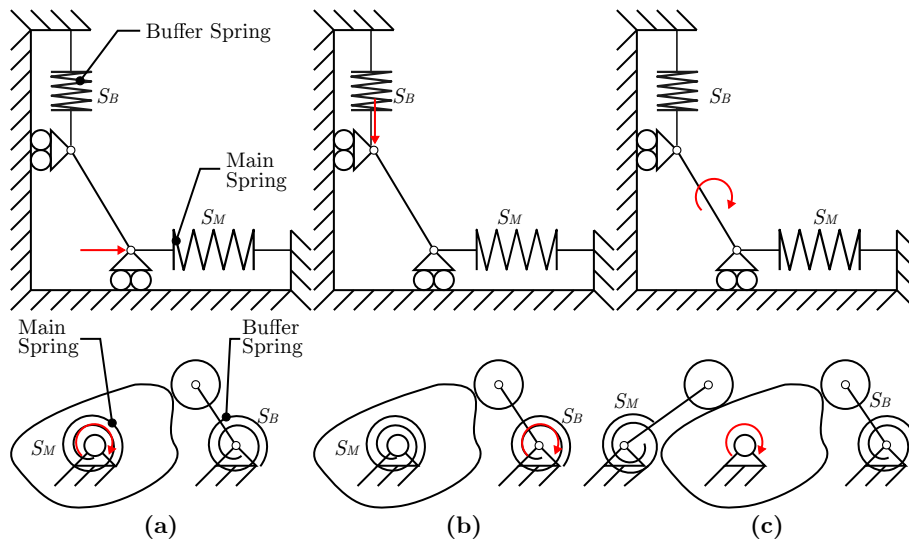


Figure 4.2: SBFA input locations. The arrow indicates the input. The main spring is labeled S_M and the buffer spring is labeled S_B . **a:** Input at Main Spring. **b:** Input at Buffer Spring. **c:** Input at Transmission.

position of the main spring can not be achieved, which means that some work is exchanged when the mechanism changes between the forcing and sizing mode. Except for the different input location, the execution of this mechanism is the same as for the connection at the main spring.

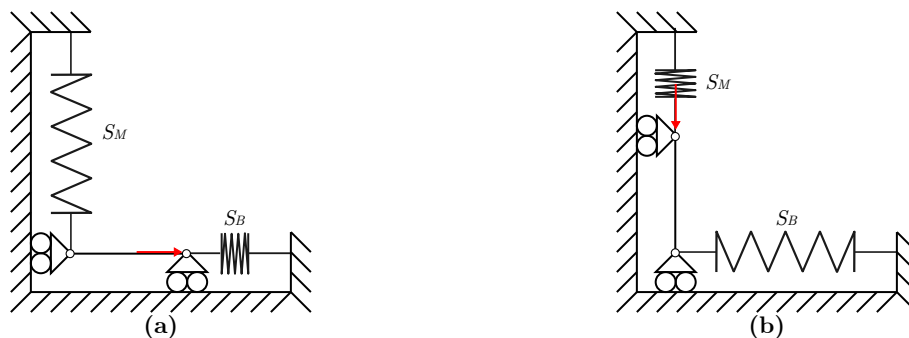


Figure 4.3: Singular Configurations of SBFA. **a:** Input at Main Spring. This mechanism reaches a singular condition for the input when the main spring S_M is fully tensioned: $s_M = s_{M,max}$. **b:** Input at Buffer Spring, this mechanism is in a singular position when the main spring S_M is at rest: $s_M = 0$.

Input at Transmission The third input location is at the transmission is shown in Fig. 4.2c. For the example linkage mechanism this means that the rotational DoF of the linkage is controlled. For the cam mechanisms this means that a cam between two followers is controlled. For this input location no singular configurations appear for the motor. The working range of the main spring is: $s_M \in [0, s_{M,max}]$. This mechanism is the most complex to realize. The cam mechanisms require two followers and an intermediate cam. The linkage mechanism requires the actuator to move with respect to the ground, as the linkage translates with respect to the ground, which also implies extra parts, such as bearings to guide this motion.

Comparison Table 4.2 summarizes the comparison of the input locations. Based on this table the input at the main spring is selected even although a singularity arises when the main spring is fully tensioned. This singularity can be avoided by slight reduction in the stroke, this has no severe consequences. This mechanisms is preferred over the input at the transmission as it is simpler for both the cam-mechanism

Table 4.2: Comparison of Input Locations

Criteria	At Main Spring	At Buffer Spring	At Transmission
Stroke	± Singularity for maximum elongation of main spring, which is easily avoided without severe consequences by limiting the stroke.	– Singularity for rest position of main spring, this implies exchange of work when switching between sizing and forcing	+ No singular configurations.
Simplicity	+	+	– Additional follower required for cam mechanism or moving actuator w.r.t. ground for linkage mechanism.

and linkage mechanism. This leads to the following design principles:

Design Principle 2: The input of the SBFA should attach to the main spring.

Design Principle 3: The singularity that occurs when the main spring is fully tensioned should be avoided by a slight reduction of the stroke.

4.3.2.2 Transmission Function

Static balancing requires a dedicated non-linear transmission between the two springs. This paragraph will derive the analytic expression for this transmission. This will be done for the general form, the *moving frame SBFA*, depicted in Fig. 4.4.

The basic idea of the procedure is inspired on [24] and is as follows: A static balanced mechanism has as property that its potential energy is constant for any configuration [23]. This can be used to derive the required transmission by rewriting the required extension of one of the springs as function of the extension of the other. Consequently, the configuration of the SBFA is defined by the extension of this spring. The extension of the main spring will be used for this purpose, because in Section 4.3.2.1 the main spring was selected as input. The actual non-linear transmission ratio between the two springs is evaluated using the partial derivative.

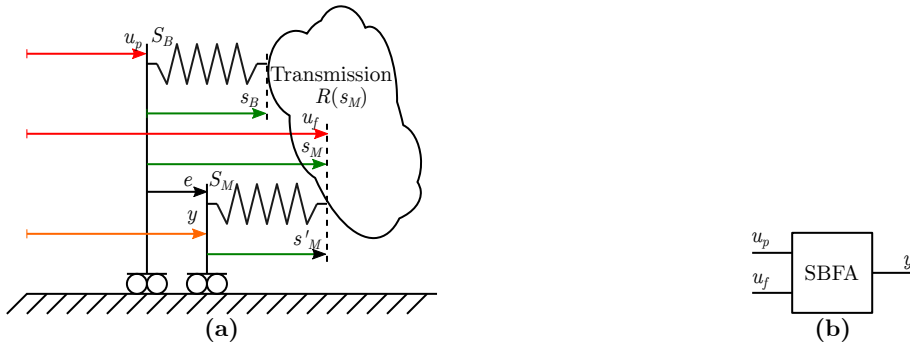


Figure 4.4: Models of SBFA. **a:**Inputs (red), output (orange) and spring extensions (green) of the *moving frame SBFA*. The effect of the error e will be discussed later in this chapter. **b:** Simplified block representation of SBFA.

Fig. 4.4a depicts the coordinates of the inputs and output of the *moving frame SBFA*, as well as the spring extensions. Ideally the output y and u_p are stationary w.r.t. to each other, i.e. the difference always equals a certain constant but arbitrary offset: $y - u_p = c$. For simplicity this offset is set to $y - u_p = 0$ in this analysis. Section 4.5 investigates the effect of the deviation e from this ideal condition.

The potential energy in the mechanism is the sum of the energy stored in the two springs:

$$V = \frac{1}{2}k_M s_M^2 + \frac{1}{2}k_B s_B^2 \tag{4.2}$$

Where k_M and k_B respectively denote the stiffness of the main and buffer spring, and $s_M \in [0, s_{M,max})$ and $s_B \in [0, s_{B,max}]$ the elongations of those springs. The required extension of the buffer spring as

function of the extension of the main spring is found by equating the potential energy to a constant: $V = C$. Using this condition, Eq. (4.2) is rearranged to:

$$s_B = \sqrt{\frac{2C - k_M s_M^2}{k_B}} \quad (4.3)$$

Later on, it will be convenient to use an expression of C , parameterized by the properties of the springs. Any configuration can be used to express C , because the potential energy is constant for any configuration. A convenient configuration is where one springs, in this case S_B is at rest: $s_B = 0$. As Eq. (4.3) is monotonically decreasing, this means that the main spring S_M is at its maximum extension, i.e. $s_M = s_{M,max}$. Substituting those conditions in Eq. (4.3) result in:

$$C = \frac{1}{2} k_M s_{M,max}^2 \quad (4.4)$$

The non-linear transmission ratio R between the two spring elongations follows from the partial derivative:

$$R(s_M) = \frac{\partial s_B}{\partial s_M} = -\frac{k_M s_M}{k_B \sqrt{\frac{2C - k_M s_M^2}{k_B}}} \quad (4.5)$$

Note that when main spring is fully elongated, i.e. $s_M = s_{M,max}$, the transmission ratio goes to infinity:

$$\lim_{s_M \rightarrow s_{M,max}} R(s_M) = \infty \quad (4.6)$$

This confirms that the position $s_M = s_{M,max}$ is a singular position of the mechanism, as is described in Section 4.3.2.1.

4.3.2.3 Intermittency

The transmission can be either intermittent or non-intermittent. Intermittent means that at a given moment the transmission between the two springs is decoupled using a locking mechanism. If required, additional locking mechanisms are used to maintain the tension in springs. Although allowing this intermittency may lead to interesting concepts (see for two examples appendix C.1), it has several major drawbacks:

- An intermittent locking mechanism violates the second subfunction, because once the transmission is the interrupted state, it no longer allows for force adaptation. As such, it is not able to vary the grasping force during time while the gripper is in the “forcing” mode.
- The non-linear transmission is the key to static balancing. An error in the transmission will result in imperfect balancing. Because an intermittent mechanism fixes and releases two parts repetitively, it is likely deficiencies will occur. Furthermore an intermittent mechanism requires additional moving components in the transmission, and is therefore likely to be more sensitive to wear. This both will result in imperfect balancing, which requires additional actuation power to correct for.

Because intermittency violates the second subfunction, this option is ruled out. This leads to the formulation of the following design principle:

Design Principle 4: The transmission between the energy buffers of the SBFA should be non-intermittent.

Because of this principle, the representation of a SBFA is simplified to a block, having two position inputs u_p and u_f and an output y , as depicted in Fig. 4.4 b. This is useful in the next chapter, where the implementation of a SBFA with the surrounding required components, such as clutches is considered.

4.4 Subfunction 3: Switch Between Force and Position Adaptation

The third subfunction states that the mechanism should switch between force and position adaptation. This timing of this switching should be resilient to perturbations, for instance due to accelerations. This

switching is always concerned with clutches changing their state, as the *fixed frame SBFA* requires a clutch between the frame and ground and a *moving frame SBFA* requires clutches in the *drive combiner*. Plooij et al [27] provided an elaborate review on locking mechanisms. They distinguish *active* and *passive* mechanism, based on whether an actuator is incorporated in the locking mechanism to change the timing of the locking, the locking position or the locking force. In line with this categorization, the timing of the locking will be categorized as active (electronic) or passive (mechanic) switching and a selection will be made based on the energetic performance. The focus of this comparison will be on the nature of the energy conversions, whether the energy is conserved as mechanical energy or dissipated.

4.4.1 Active Switching

The first method, active switching, relies on an electronic subsystem to time the locking. This subsystem requires a sensor to measure the contact with the object, actuators to control the locking mechanisms and a micro-controller or for the information processing. All these components will inherently dissipate energy due to Ohmic losses and the switching losses in active electronics. For an elaborate survey on this, the reader is referred to [46]

4.4.2 Passive Switching

To time the (dis)engagement of a passive locking mechanism, *information* need to be supplied to the locking mechanism. This signal has to be in the mechanical domain, because the electrical domain is excluded for passive mechanisms. Hence the information should be conveyed using *forces* or *motion*. Examples of *mechanical information* are the relative position between the input and output as in the *Geneva Wheel* [34], the magnitude and/or direction of the relative velocity as in an *overrunning clutch* [34] or the difference in the input and output load, for instance in NBDMs [21].

To be resilient to the disturbance forces, the switching mechanism should incorporate a force threshold. As such, the mechanism switches only when the input force is deliberately raised above this threshold, preventing unwanted switches. The method to realize this threshold is categorized based on the two types of mechanical forces: *conservative* and *non-conservative*.

4.4.2.1 Conservative Forces

For conservative forces the work affects the potential energy stored in the mechanism. Examples are forces in springs and permanent magnets. The advantage to the use of conservative forces is that theoretically no net work is required for a grasping cycle. In practice this is slightly more complicated, as the work needs to be supplied and regenerated using an actuator in which losses occur. Unlike the active locking mechanism, this actuator is not incorporated in the clutch itself, but is the main actuator of the drive. The work can not be supplied by another passive mechanical device, because only statically balanced mechanisms allow for a perfect exchange of potential energy [23], but these mechanisms are sensitive to disturbances. When a disturbance is applied it will leave the equilibrium configuration and once the disturbance is removed, return to the initial equilibrium configuration is not guaranteed. Yet, this energy consumption is presumably lower than for active switching, as no sensors are powered and there is less computational effort for the controller. In addition, instead of regeneration using the actuator, the released potential energy might be used in a useful way, for example by relieving the actuator temporarily.

To prevent the mechanism from switching “accidentally”, for instance due to dynamic loads the conservative force should have a stable equilibrium. This guarantees the clutch recovers its initial configuration after the mechanism is perturbed.

4.4.2.2 Non-Conservative Forces

Contrary to conservative forces, the work of non-conservative forces does not affect the potential energy. They are *path-dependent* and also called *dissipative* forces as they dissipate energy. Examples are friction and viscous damping. Presumably the energy consumption is still better than active mechanism as less electric energy is required to read out the sensors and process the information. Yet it performs less than passive switching using conservative forces, as all work is by definition dissipated, and can not be used to relieve the actuator for instance.

4.4.2.3 Comparison

Table 4.3 summarizes the energetic performances of the various switch methods. From this table follows that a passive mechanism based on a conservative scores performs best, as it does not require power consumption in electronic components and microprocessor and possibly some work might be used to relieve the actuator, instead of dissipating it. This leads to the following design principle:

Design Principle 5: The switch mechanism should be passive and based on a conservative force.

Table 4.3: Comparison of Switch Methods

Criteria	Active	Passive	
		Conservative	Non-Conservative
Energy Consumption	– Powering of sensor and micro-controller. Ohmic losses.	+ No powering of sensor and micro-controller. Work stored as potential energy and possibly used to temporarily relieve actuator.	± No powering of sensor and micro-controller but all work dissipated

4.5 Imperfect Conditions

Although statically balanced mechanisms theoretically allow for 100 % force reduction, in practice this is never achieved. Reductions of some reported prototypes vary between 95-97 % [24, 24]. This is caused among others by friction, parasitic stiffness, non-linearities in the spring characteristic and so forth. In this section two issues will be investigated which are particular for SBFAs in grippers. First of all, the object has a finite stiffness, which may result in unwanted displacements of the output. Second, position errors might occur during sizing, which results in a deviation from the output with respect to its ideal position. These effects will be quantified in Section 4.5.1 and their effect in terms of required actuation force and work in Sections 4.5.2 and 4.5.3. Because the error is dependent on the object, Section 4.5.4 will describe a method to average the characteristics over various objects, which can be used as metrics in the design procedure.

4.5.1 Description of Errors

This section will describe the finite stiffness and position error. This will be used in Sections 4.5.2 and 4.5.3 to quantify the required actuation force and work of the SBFA.

In the derivation for the transmission, a stationary output was assumed. Ideally, the movement of the output the output is fully obstructed by the object. However, when the object has a finite stiffness the output will slightly move due to the deformations of the object once the force level is adjusted. In [47] the stiffness of a standardized set of everyday life objects is measured. These values are in a range from $2.6 \cdot 10^3$ N/m for a cracker box to $67.2 \cdot 10^3$ N/m for a coffee can.

The object stiffness, denoted by k_O , acts in series with the main spring. The dimensionless variable $\kappa = k_O/k_M$ is introduced to relate the stiffness of the object to the main spring. The combined stiffness k'_M , which defines the actual behavior of the balancer is then:

$$k'_M = \left(\frac{1}{k_M} + \frac{1}{\kappa k_M} \right)^{-1} = \frac{\kappa k_M}{\kappa + 1} \quad (4.7)$$

When a transmission is present between the finger and the drive output, this will affect the *apparent* stiffness at the drive output.

During the adjustments to the object size, deviations with respect to the ideal position might occur, for instance due to the resolution or accuracy of the locking mechanism. Consequently to this error the ideal condition $y - u_p = 0$ is not met, but resolves to $y - u_p = e$, where e is the difference between the ideal and actual output position. This is depicted in Fig. 4.4 This results in a difference between the expected

main spring extension s_M and actual extension s'_M :

$$s_M - s'_M = e \quad (4.8)$$

4.5.2 Required Actuation Force

The effect of the parasitic stiffness and position error on the actuation force is derived from the expression for the potential energy. In addition, the actuation force will be normalized by the maximum output force.

The effect of the parasitic stiffness and position error are quantified by substituting Eq. (4.7) and Eq. (4.8) in the first term of Eq. (4.2), which describes the potential energy of the main spring. As the parasitic stiffness and position errors may deviate for each object, the transmission does not account for them. This results in the actual potential energy stored in the mechanism:

$$V' = \frac{1}{2} (k'_M s'^2_M + k_B s^2_B) = \frac{1}{2} \left(\frac{\kappa k_M (e - s_M)^2}{\kappa + 1} - k_M s^2_M + 2C \right) \quad (4.9)$$

The estimated expression for the main spring is rewritten as function of the two inputs:

$$s_M = u_f - u_p \quad (4.10)$$

This is substituted in Eq. (4.9), the expression for the actual potential energy. The input force follows from the partial derivative of this expression to the input u_f :

$$F'_f = -\frac{\partial V'}{\partial u_f} = \frac{k_M (u_f - u_p + \kappa e)}{\kappa + 1} = \frac{k_M (s_M + \kappa e)}{\kappa + 1} \quad (4.11)$$

Normalization of this force with respect to the maximum force results in:

$$\overline{F}'_f = \frac{F'_f}{k_M s_{M,max}} = \frac{\overline{s}_M}{\kappa + 1} + \frac{\kappa \bar{e}}{\kappa + 1} \quad (4.12)$$

where $\overline{s}_M = \frac{s_M}{s_{M,max}}$ is the normalized stroke and $\bar{e} = \frac{e}{s_{M,max}}$ the normalized error.

4.5.3 Required Work

As consequence of the balancing imperfection, exchange of work is required to control the configuration of the SBFA. In this subsection this work is quantified.

As the mechanism performs cyclic forcing and releasing, theoretically no net work is done for each cycle. If an amount of positive work is done during prehension, the same amount of negative work during release. Yet, as already described in Chapter 2, the exchange of work is accompanied with losses in the actuator and should therefore be minimized. To quantify the exchange of work, the absolute force is integrated over the extension:

$$W_{ex} = \int_0^{s_M} |F'_f| ds_M \quad (4.13)$$

4.5.4 Design Metrics

This section will describe two design metrics than can be used to evaluate the design. The basic idea is that although the equations for the input work and force of the previous subsections provide valuable insight in the design, they are only applicable for a single value of the object stiffness, error and force, whereas in practice these values will differ for various objects. To incorporate the range of these parameters, the input force and work is averaged using the *root-mean-square* (RMS). This results in two design metrics. First the range of the parameters will be briefly discussed. Second, the design metrics will be expressed and finally an example is given.

Before the two design metrics are introduced, it is important to identify a design variable which can be used by the designer to optimize the design. In a typical design procedure the drive is designed for a certain targeted maximum force $F_{M,max}$. The product of the stroke $s_{M,max}$ and stiffness k_M of the main spring should together result in this targeted force, which means that the designer can use one as free design variable and constrain the other to obtain the targeted force. Which one is used as design variable is an arbitrary choice. I find it convenient to use $s_{M,max}$ because of it can be directly measured in practice.

4.5.4.1 Range of Parameters

The range of the parameters varies for the object and task. First of all, the object stiffness k_O is a property of the object. The range of the object stiffness for a variety of objects is $k_O \in [k_{O,min}, k_{O,max}]$. When a transmission is present between the finger and the drive output, this will affect the *apparent* stiffness at the drive output.

Second, the position error is expected to lie in a certain range $e \in [e_{min}, e_{max}]$, of which the upper and lower limits e_{min} and e_{max} are defined by practical limitations, for instance the resolution or accuracy of the locking mechanism.

Third, the ability of the mechanism to adjust this output force to a desired level implies that the applied output force is in the range of $F_M \in [0, F_{M,max}]$. Because the force is proportional to the stroke, this range is equivalently described by $s_M \in [0, s_{M,max}]$.

The input force and work will be averaged over these ranges.

4.5.4.2 Design Metrics

The first metric relates to the average force reduction. Recall from Chapter 3 that one of the principles for the performance was “amplification” of the input force with a factor $1/\zeta$, where ζ is the force reduction of the mechanism. The normalized force expressed by Eq. (4.11) also expresses this force reduction, because it describes the ratio between the required input error and the maximum output force. Averaging using the RMS results in:

$$\overline{F'_{RMS}} = \sqrt{\frac{\int_{k_{O,min}}^{k_{O,max}} \int_{e_{min}}^{e_{max}} \int_0^1 \overline{F'}^2 ds_M de dk}{(k_{O,max} - k_{O,min})(e_{max} - e_{min})(1 - 0)}} \quad (4.14)$$

The inverse of this RMS input force describes the averaged amplification factor. This is the first design metric. This metric should be as large as possible to improve the performance of the drive.

The second metric relates to the required work to actuate the mechanism. The work is also averaged using the RMS:

$$W_{RMS} = \sqrt{\frac{\int_{k_{O,min}}^{k_{O,max}} \int_{e_{min}}^{e_{max}} \int_0^{s_{M,max}} W_{ex}^2 ds_M de dk}{(k_{O,max} - k_{O,min})(e_{max} - e_{min})(s_{M,max} - 0)}} \quad (4.15)$$

This is the second design metric. It describes the average work exchanged at the input. This metric should be minimized in order to improve the performance of the drive.

These metrics will be applied in Chapter 6, which describes the detailed design of a drive prototype.

4.5.4.3 Example

To illustrate the effect of the stroke on the two design metrics, an example is evaluated. The targeted force in this example is 45 N, the stiffness and error range are respectively $k_O \in [2.6, 67]$ kN/m and $e \in [0, 1]$ mm. Eqs. (4.14) and (4.15) are evaluated using the MATLAB command `integrate13`. The results are plotted in Fig. 4.5

This figure shows that to minimize the RMS work the stroke should be minimized, but this results in a small amplification factor. So clearly, there is a trade-off between the RMS work and the amplification factor.

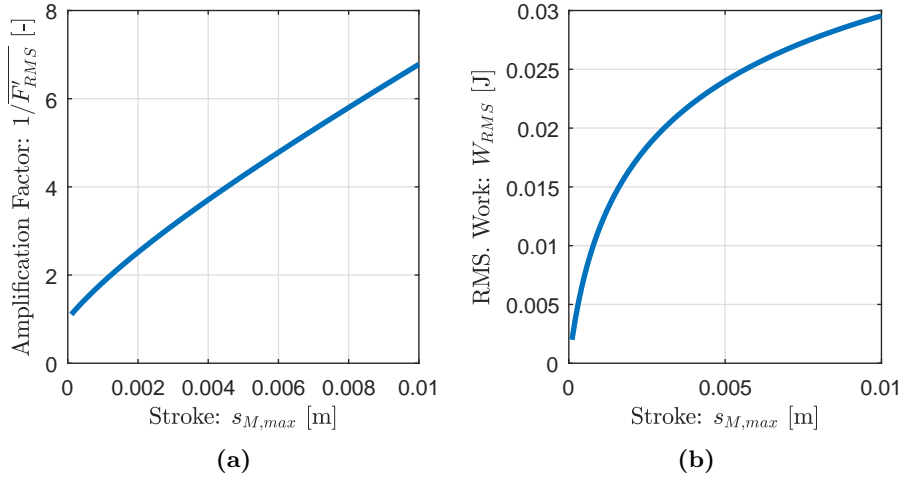


Figure 4.5: Input metrics for example. **a:** Amplification factor, which equals the inverse of the RMS actuation force. **b:** RMS work.

4.6 Discussion

In this chapter design principles are derived to ensure the functionality of a SBFA-based energy saving drive. This section critically reflects on the obtained results.

First of all it should be noted that in the comparison of the energy buffers the energy density is a theoretical maximum. In practice this is lower. For instance, springs subjected to bending or torsion do not have a uniform stress distribution. The stress in the core is lower than at the edge, which results in a lower energy density. Although the practical values are probably lower, the results show that the energy density is approximately an order of magnitude larger for the spring, which is enough for this concise comparison.

Regarding the design metrics, the effect of the variation in the values for the object stiffness and error is averaged out using the RMS. The underlying assumption to this is that the stochastic variation is a normal distribution. Arguably also other distributions could be used, for example a normal distribution. The corresponding probability density function could be used as weight factor along the range. For this thesis the uniform distribution is sufficient, as it allows for a versatile design. When more details about the task and the properties of the involved objects are known, it might be indeed useful to use other distributions. If the hand is designed to grasp a set of objects of which the parameters are known the discrete form of the RMS expression could be used, that sums the discrete points instead of integrating it over a continuous range.

Another interesting design metric that could be considered is the dispersion in the actuation force. The efficiency of the motor has an optimum for a certain torque. Deviations from this torque results in a reduced efficiency. This means that the larger the dispersion, the smaller the average efficiency. This force dispersion can be expressed using the *root-mean-square-error* (RMSE). The challenge is to relate this dispersion to the actual reduction in efficiency. The efficiency curve is strongly dependent on the specifications of the motor and is therefore less suitable for a general approach.

The selection of the switch mechanism is done based on a quantitative comparison, which regards whether the energy is directly dissipated or used. Yet, it does not consider the absolute amount of used energy. For instance, when an active mechanism would consume in total 100 times less energy to switch than its competitor it is still worth to consider this solution, even though this energy is dissipated. As already argued this is not likely the case, because active mechanisms require additional electronic components which consume energy. Moreover, the passive switching corresponds to state-of-the-art robotic fixturing grippers and biological hands, which rely on *underactuation*, i.e. a clever mechanical structure [17, 48], to adapt to the object rather than electronic control.

Several ideas for a more advanced drive, that could be followed up in future work are:

- Investigate whether the balancing imperfection can be reduced by anticipation on the average object stiffness, i.e. making the mechanism perfectly balanced while the average object stiffness is

incorporated, instead of an infinite stiffness as is currently done. It is expected that this is especially interesting when the gripper deals its whole lifetime with the same kind of objects. An even more advanced solution would be to incorporate a spring with adjustable stiffness, such that the stiffness can be tuned for a dedicated task.

- Investigate whether it is possible to eliminate the effect of the position error, for example by adding a third spring.

The next step is to investigate how the SBFA should be combined with the surrounding elements, such as clutches, and drive splitters. This will be done in the next chapter.

4.7 Conclusion

This chapter derived design principles which ensure the SBFA based gripper drive is able to perform its three subfunctions: Effortless sizing, effortless forcing and switching between those two. The following design principles are obtained:

1. The Statically Balanced Force Amplifier should be constructed using springs as energy buffers.
2. The input of the SBFA should attach to the main spring.
3. The singularity that occurs when the main spring is fully tensioned should be avoided by a slight reduction of the stroke.
4. The transmission between the energy buffers of the SBFA should be non-intermittent.
5. The switch mechanism should be passive and based on a conservative force.

Two possible deficiencies particular for grasping were considered, namely the finite object stiffness and position error that occur in sizing to for instance the resolution of the locking mechanism. Two metrics are proposed to average these effects over a variety of objects.

Chapter 5

Topology Selection

5.1 Introduction

In the previous chapter the statically balanced force amplifier was considered from a theoretical perspective. This resulted in several valuable design principles. Yet, this amplifier could be implemented in many ways. The design of the drive contains two aspects: a *topology* and *typology*. Topology refers to how the components, i.e. the bodies, bodies, springs, differentials are connected. Typology refers to how these components are realized, for instance whether the bodies form linkages or gears, and is addressed in the chapter 7.

The current chapter is dedicated to the generation and evaluation of various concepts for the topology of the mechanism. This will result in an abstract scheme that describes how the components should be interconnected. To do this in a structured way, the topology is subdivided in subtopologies in four categories. The combination of four subtopologies, from each category one, results in a topology for the mechanism.

This chapter starts with the introduction of a representation of the topologies in Section 5.2. The various subtopologies are described in Section 5.3. In Section 5.4 three steps are taken in which the subtopologies are combined and compared to select the best overall topology. The obtained topology will be applied on an example in Section 5.5 to explain the working principle of the selected topology. The results of this chapter are discussed in Section 5.6 and the chapter is concluded in Section 5.7.

5.2 Topology Representation




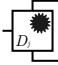


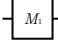

A uniform representation of the topologies is required to facilitate the description and comparison of the various (sub)topologies. In the current section, such a representation will be introduced.

The proposed representation is largely inspired of the representation of *Clutched Elastic Actuators* (CEAs) as proposed by Plooij et al. [28]. They define CEAs as: “*all mechanisms that consist of at least one spring and one clutch and possibly incorporating gears or differentials.*” [28] According to this definition, the drive which is developed in this thesis is definitely a CEA, because the SBFA consists of springs and the splitters and combiners require clutches. In addition to this representation, I added the SBFA as functioning element. The simplification of a SBFA to a single functioning element is justified in Section 4.3. Besides, I distinguish the ground from the other bodies.

The representation is based on bodies, represented by circles, being connected to functioning elements, represented by squares. In Table 5.1 two types of bodies and five types of functioning elements are introduced.

Rigid connections between bodies and functioning elements are indicated by lines. Functioning elements, depicted as squares, are always adjacent to two bodies, depicted as circles, and vice versa. In other words, two bodies (circles), are never directly connected. This is logic: Connecting two rigid bodies with a rigid connection would result in a single rigid body. Functioning elements (squares) can neither be directly connected, an additional intermediate body is required.

Table 5.1: Topology Representation

Name	Identifier	Symbol	Equation	Description
Bodies				
Moving Body	Number			Moving bodies have 1 DoF, which can be translational or rotational. x_n denotes the position and \dot{x}_n the velocity of the body.
Ground	0		$x_0 = 0, \dot{x}_0 = 0$	Body connected to the fixed world. Its position serves as reference.
Functioning Elements				
Clutch	C_j		$c_j(\dot{x}_m - \dot{x}_n) = 0$	$c_j \in \{0, 1\}$ A clutch, also called a locking mechanism, is able to block ($c_j = 1$) or allow ($c_j = 0$) relative motion between two bodies [27].
Differential	D_j		$\dot{x}_j = a_1 \dot{x}_m + a_2 \dot{x}_n$	Differential constrains multiple inputs and outputs. a_1 and a_2 describe the transmission ratios of the differentials. For most cases these ratios are constant, but for some differentials (e.g. the seesaw mechanism [38]) these parameters vary with the position of the in- or outputs.
Linear Transmission	LT_j		$\dot{x}_j = i \dot{x}_m$	A linear transmission is a special case of a differential: one of the inputs is connected to ground, resulting in a transmission between two bodies. Typically the ratio i is constant.
Spring	S_j		$F_j = f_j(x_m - x_n)$	Springs exert a force or torque F_j as a function of their relative position.
Motor	M_j			A motor is able to impose a force or displacement between two bodies. A gearbox is assumed to be incorporated in the motor.
SBFA	$SBFA_j$		$\begin{cases} F_{f,j} = k_M(y - u_p) \\ F_{p,j} = k_M(u_p - u_f) \\ F_{y,j} = k_M(u_f - y) \end{cases}$	The SBFA is able to exert an output force of which the magnitude is effortlessly controlled by the input u_f . The position of the frame is determined by input u_p . (The equations are derived in appendix D).

5.3 Subtopologies

In this subsection various subtopologies, categorized in four groups, are discussed. In Section 5.3.1 it is briefly discussed how the concepts for these subtopologies are generated. Then the subtopologies itself are described in Section 5.3.2, followed by a brief overview combined with a labeling system in Section 5.3.3.

5.3.1 Generation of subtopologies

In the past, concepts were typically generated by creative engineers. Intuition and experience dominated this approach [49]. Nowadays, it is acknowledged that this resulted in many “random” solutions, which span a small portion of the design space. Therefore, the “random” solutions are not necessarily the best. A better approach is to investigate the solution space in a structured way.

To do so, I explored two methods. The first one, based on *graph theory*, resulted in too many concepts for a thorough evaluation. The reader interested in this approach is referred to appendix D.2. The second method is called *ACCReX* [50], which stands for *Abstracting, Categorizing, Reflecting, Reformulating and Extending*. In this method brainstorming and categorizing is alternated. Although the procedure stays a manual process, for which the designers subjectivity can not be completely eliminated, it tends to explore a much larger portion of the design space due to its structure approach.

The next subsection describes the found concepts for the subtopologies. The process itself is not documented, because it involves many iterations and brainstorming. A description of this would fill many pages with irrelevant information.

5.3.2 Description of Subtopologies

Using the *ACCRES* method, subtopologies in four categories were found. Combining four subtopologies, from each category one, results in a topology for the mechanism. The four categories are:

- *Drive Splitters* The drive splitters enable the motor to drive one input in multiple outputs. They can also be inverted, resulting in combiners, which are used to add multiple inputs to a single output.
- *Frame Mounting* As discussed in chapter 4, the frame of the SBFA can be either moving or fixed w.r.t. the ground.
- *Implementation of Threshold* Multiple concepts are identified for the implementation location of the threshold.
- *Threshold loading* Several routes are identified for the flow of the threshold mechanism through the mechanism.

The exact meanings of these categories and the subtopologies they contain are described in Sections 5.3.2.1 to 5.3.2.4 respectively. For now only the focus is on the working principles of the subtopologies. The advantages and drawbacks will be taken into account in Section 5.4. To ease the descriptions, the components and bodies are labeled with arbitrary identifiers.

5.3.2.1 Drive Splitter and Combiners

The first category is regarding the nature of the *drive splitters* and *combiners*. Drive splitters are used to resolve a single input into multiple outputs. The use of a splitter enables actuation of multiple DoFs subsequently and independently of each other with a single motor. It is also possible to invert the inputs and outputs to obtain a “combiner”: Multiple inputs are resolved to a single output.

A distinction is made between *continuous* and *intermittent* splitters/combiners. They splitters explained in Table 5.2. The same description holds for the working principle for combiners, but the inputs and outputs are inverted. For now, all possible locations of clutches are incorporated. When the topologies are compared in Section 5.4 it will be determined which clutches are necessary and which are superfluous for a given topology.

Table 5.2: Subtopologies for Drive Splitter

Type	Representation	Description
C: Continuous		<p>For a continuous splitter the output bodies 2 and 3 of the splitter are always connected via a differential to the driving body 1. Which output is driven is determined by clutches. These clutches could be integrated on five different locations. Clutches C_1, C_1' and C_1'' all have the same result, they all lock the internal DoF of the differential. When one of these clutches is engaged, $\dot{x}_1 = \dot{x}_2 = \dot{x}_3$. Clutches C_2 and C_3 are able to lock respectively the motion of the second and third body w.r.t. the ground.</p>
I: Intermittent		<p>For intermittent splitters the output bodies 2 and 3 are decoupled from the driving body 1 using clutches C_1 and C_2. To prevent the undriven output bodies to move uncontrolled, they are connected to the ground with additional clutches C_3 and C_4.</p>

5.3.2.2 Mounting of Force Amplifier

The second distinction is regarding the fixturing of the force amplifier. Recall from Section 4.2 the two different methods for the SBFA to achieve sizing: using a SBFA with either a *moving* or a *fixed* frame.

To enable the fixed frame amplifier to adjust to various object sizes a second input needs to be added to the amplifier output. This is achieved using one of the two combiners of Section 5.3.2.1. The three resulting subtopologies are tabulated in Table 5.5.

Table 5.3: Subtopologies for Frame Mounting

Type	Representation/Example	Description
M: Moving Frame		The amplifier is able to move when both inputs of the SBFA element are connected to moving bodies. When body 1 and 2 move simultaneously, the position of the frame is adjusted. A difference in the motion of bodies 1 and 2 changes the tension in the springs. This resembles a differential drive.
FC: Fixed Frame w/ Continuous Combiner		This subtopology uses a differential to add the movement of body 1 to body 3, the output of the fixed frame amplifier. Hence, using body 1 the output body 4 is able to adjust to the object size and using body 2 the force level at the output is controlled. To work properly the motion of body 1 needs to be locked during forcing, as it is also loaded with the amplifier output force, this will be taken into account in Section 5.4.
FI: Fixed Frame w/ Intermittent Combiner		This subtopology uses a set of clutches as combiner. Initially, the clutches are engaged such that the output body 4 is solely driven by body 1. The movement of body 1 is used to adjust the position of body 4 and perform sizing. Once the sizing is completed, the engagement of the clutches is changed so that the output body 4 is connected to the amplifier output, body 3. Consequently, the movements of body 2 controls the output force level.

5.3.2.3 Threshold Implementation

As explained in Chapter 4 a force threshold should be imposed by a conservative force. This prevents unwanted motions with the least energy dissipation. A mechanical spring will be used as origin of this force. This spring, which is potentially non-linear, can be implemented in four ways. These four options are listed and described in Table 5.4. These solutions are not visualized as they are not self-containing but rather modifications of an existing topology.

Table 5.4: Subtopologies for Threshold Implementation

Type	Description
A: Additional spring	The first way to obtain a threshold is to incorporate an additional dedicated non-linear spring in the topology.
R: Replacement of Clutch	Remarkably, a pretensioned spring functions similar to a clutch, as it prohibits motion between bodies when the applied force on it is lower than the pretension. When the pretension is exceeded, relative motion is permitted. As such, those clutches that are subjected to a low load when engaged can be replaced by non-linear springs.
I: Incorporation in SBFA	A third way to obtain a threshold is to modify the non-linear transmission between the two springs. Consequently, the input force is no longer zero for every configuration. By dedicated modifications the desired input force characteristic is obtained, which functions as threshold.
RI:	A fourth option consists of the combination of two solutions. The transmission of the balancer is modified such that the input characteristics corresponds to the desired threshold. This functionality is also used to replace a clutch.

5.3.2.4 Threshold Loading

The fourth category is regarding the loading of the threshold. For every topology the threshold force follows a certain path within the mechanism from the contact point with the object to the sizing input. Based on whether the force flows through the amplifier’s output or spring, the subtopologies are distinguished.

Table 5.5: Subtopologies for Threshold Loading

Type	Representation/Example	Description
TT: Trough SBFA output and main spring		For this subtopology the force flows through the amplifier output and the main spring. The path of the force is indicated by a red arrow.
TB: Trough SBFA output, bypassing main spring		For this subtopology the force flows through the amplifier’s output, but bypasses its main spring. This is achieved by means of a limit stop, integrated in parallel to the SBFA between body 1 and 3. Due to the uni-directional locking of the limit stop, the main spring is relieved from the threshold force during switching, while the amplifier is still able to deliver an output force during forcing. The limit stop is depicted as a clutch as it blocks the relative motion under certain conditions.
B: Bypassing SBFA output		For this subtopology the force bypasses the output of the SBFA. In addition to the output body 3, body 1 makes simultaneously contact with the object. During switching, the threshold force flows through this second contact.

5.3.3 Labeling of Subtopologies

To be able to refer to all topologies, a labeling system is introduced. Each topology consists of a combination of subtopologies in four categories. Therefore, each topology is labeled with a sequence A-B-C-D, where A-D are substituted with values from Table 5.6 to indicate the subsolutions that form the topology. To refer to one subtopology, the other labels are denoted using a “•”-sign. For instance, the label •-M-•-• refers to the *moving amplifier frame* in the second category.

Table 5.6: Labeling of Topologies

A (Splitter)	B (SBFA Mounting)	C (Trigger Implementation)	D (Trigger Loading)
C Continuous	M Moving SBFA	A Additional Spring	TT Trough SBFA and its main spring
I Intermittent	FC Fixed SBFA + I continuous combiner	I Incorporation in SBFA	TB Trough SBFA bypassing its main spring
	FI Fixed SBFA + Intermittent Combiner	R Replacement of clutch	B Bypassing SBFA
		RI Replacement of clutch and incorporation in SBFA	

5.4 Topology Selection

Combining the subtopologies from the four categories results in 72 topologies. The aim of the current section is to compare the topologies and select the best.

This could be done by thoroughly comparing all 72 solutions, but this would be a cumbersome process. Although the actual selection took multiple iterations, the final selection is explained based on three subsequent steps. In the first step, the various drive splitters and SBFA mountings are combined and compared and the best combination is selected. This forms the base of the topology. In the next two steps, the trigger implementation and loading are respectively addressed. These second and third step modify the the base slightly. In the discussion of this chapter, Section 5.6, the consequences of this stepwise approach are discussed. The three steps are discussed in Sections 5.4.1 to 5.4.3 respectively.

5.4.1 Step 1: SBFA Mounting and Splitters

The first step is to combine the three subtopologies of splitters with the three subtopologies of SBFA mountings, this forms the base of the topology. First the selection procedure and criteria are introduced. Then the various concepts are described and rated, followed by a selection.

5.4.1.1 Selection Criteria and Procedure

The selection of the best combination of SBFA mountings and splitters is based on the *complexity*, which is evaluated based on the number of bodies and elements required for the concept to function. The complexity relates to whether the mechanism is lightweight and elegant. The less components, the better the solution. The mechanisms are not rated on whether they are fast or energy effective, because the former is hard to estimate and the latter is incorporated in the constraint that the mechanism has to be functional.

To determine the required number of components, the required motion constraints on the mechanism are taken as starting point. As described in Chapter 4, the mechanism has to switch between the forcing and sizing mode. These two modes are subject to a different set of constraints on the relative motion between the various bodies. The clutches and transmissions have to be positioned such that these motion constraints are satisfied. The procedure to do rate the complexity consists of the following stages:

1. Determine the required constraints during the two different operation modes of the mechanism.
2. Generate a topology based on the combination of a drive splitter and SBFA mounting. Where necessary additional clutches and transmissions are introduced to satisfy all constraints.
3. Determine the complexity by counting the number of bodies and elements.

5.4.1.2 Required Constraints

The first stage of the selection of the SBFA mounting is to investigate the motion constraints. In the next stage, these constraints are used to determine the locations of the required clutches and transmissions. The required motion of the SBFAs can be taken as starting point. The two inputs of the SBFA are subjected to two different sets of motion-constraints to ensure functioning during both sizing and forcing. Therefore clutches are required to engage and disengage these motion constraints. Furthermore, as is shown in Chapter 3, forcing and sizing should occur using different transmission ratios. For all the three SBFA mountings the required constraints are identified.

Rather than to express the constraints with equations, the constraints are visualized by colored lines in Table 5.7. The blue lines indicate the constraints during sizing and the red lines during forcing. Solid lines indicate a blocked relative motion, dashed lines indicate a relative motion constrained by a transmission ratio. The constraints are visualized for both the schematic topology and an example based on the *sliding ladder* mechanism. A brief description of the constraints is provided in Table 5.7 as well. Note that the numbering of the components is again arbitrary, but serves to ease the descriptions.

Table 5.7: Motion constraints for SBFA mountings

Type	Visualization ^a	Description
M: Moving frame		<p>The moving SBFA is in the <i>sizing mode</i> when the two input bodies, body 1 and 2, move synchronously while driven by the motor. This way, the frame of the amplifier moves simultaneously with the forcing input and is able to perform sizing. To achieve this, two of the three constraints depicted in red in are required. One of these constraints is redundant. For the <i>forcing mode</i> the frame of the amplifier needs to be locked to the ground in order to redirect the reaction forces on the frame to the ground. The forcing input should be driven by the other, preferably with a different transmission ratio than during sizing.</p>
FC: Fixed Frame with Continuous Combiner.		<p>This mechanism is able to perform <i>sizing</i> when body 1 is driven by the motor. The motion of body 1 is then transmitted through the differential to the output, body 4. Ideally the forcing input of the amplifier, body 2, is locked to the ground to prevent unwanted motions due to perturbations. For <i>forcing</i> the motor needs to drive the forcing input of the amplifier, body 2. As the differential distributes the output force of the amplifier among body 4 and 1, body 1 needs to be locked to the ground to withstand the resulting force.</p>
FI: Fixed Frame with Intermittent Combiner.		<p>This mechanism is in the <i>sizing mode</i> when the output body 4 is coupled to body 1, which is driven by the motor. The output body 4 needs to move independently of the SBFA output, body 3, hence these bodies need to be decoupled. To withstand external disturbances and balancing imperfections, the forcing input, body 2, is ideally fixed to the ground. The mechanism is able to perform <i>forcing</i> when the forcing input, body 2, is driven by the motor. The output of the amplifier, body 3, needs to be connected to the output of the mechanism, body 4 in order to prevent the SBFA output force. To prevent unwanted motions due to perturbations of the uncontrolled body 1, it is ideally locked to the ground.</p>

^a The red lines indicate the constraints during sizing, and the blue lines indicates the constraints during forcing. A solid line between two bodies indicates there is no relative motion between the bodies possible. Dashed lines indicate the relative motion between the bodies is constraint by a transmission ratio. u_m indicates the motor input.

5.4.1.3 Resulting Topologies

This section describes six different possibilities of the base topologies. These six combinations are obtained by the combination of the subtopologies from the first and second category, respectively the drive splitters and SBFA mountings. The clutches and transmissions are positioned such that they enable the mechanism to fulfill the identified motion constraints. This description allows for a comparison based on the required number of bodies and clutches that are required. The actual comparison is described in Section 5.4.1.4

Before the description is presented, two remarks are made on the method. First off all a NBDM clutch is incorporated to relieve the motor from a continuous static load. In Chapter 3 was shown that this improves the performance of the mechanism. In the second place, for some topologies, clutches could be placed at multiple bodies. For example, the internal DoF of a differential is blocked by a clutch between any of the two in- and outputs of the differential. Although this has no effect on the number of components it will be briefly addressed and indicated in the visualization. If the selected topology has such a redundancy, it will be considered later on.

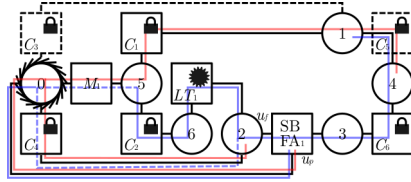
Table 5.8 provides an overview of the six possibilities. For each topology it contains a visualization and a

description. The numbering in the visualization is such that the motion of body 1 results in size adjustment and motion of body 2 results in adaptation of the force level. Body 5 is driven by the motor. The red lines indicate the mechanism's sizing mode, the blue lines its forcing mode. The NBDM is represented by the blue dotted lines, as its engagement alternates with the activation of the motor. The grey dotted clutches connected to dotted lines represent the omitted clutches from the drive splitters and combiners. The dotted clutches on solid lines represent the clutches replaced with a rigid connection, note that as consequence some bodies should merge to one body, but for clarification these bodies are depicted separately.

Table 5.8: Description of Base Topologies

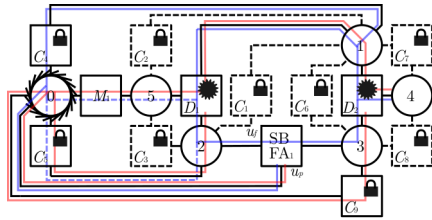
Topology	Visualization ^a	Description
C-M-●●		<p>During sizing, clutch C_1 locks the internal DoF of the differential and constrains the amplifier inputs, bodies 1 and 2, to move synchronously. Clutch C_1 is interchangeable with C_2 or C_3, because these clutches all lock the internal DoF of the differential. To relieve the actuator from delivering a continuous static torque, clutch C_2 engages when the motor is inactive. In the forcing mode, clutch C_4 locks the relative motion between body 1 and the ground, this redirects the forces on the amplifier frame to the ground. Body 2 is driven by the motor via the differential. To realize a reduction (quantified by the ratio i_2), the differential should be non-standard. This means the coefficients of the differential are subjected to: $a_1 \neq a_2$. Again clutch C_2 is used to relieve the motor from the continuous static torque. Alternatively the NBDM, depicted as clutch C_5, can be connected to body 2 as well. Although this would enable clutch C_5 to relieve the motor during forcing, it won't relieve the motor during sizing. As such, the mechanism is less resilient to disturbances. This base consists of 3 clutches and 1 differential.</p>
I-M-●●		<p>During sizing, clutch C_1 and C_3 are engaged. This ensures both inputs of the SBFA, bodies 1 and 2, are synchronously driven by the motor input. The other clutches have to be disengaged. During forcing, clutch C_4 is engaged to ensure the position input, body 1, of the SBFA is locked to the ground. This redirects the reaction forces on the amplifier frame. The forcing input, body 2, is driven by the motor via the linear transmission and engaged clutch C_2. This linear transmission improves the performance as it introduces the difference in transmission ratios during forcing and sizing. Clutch C_4 is able to relieve the motor from the continuous static torque. It could be connected to body 2 as well. This mechanism consists of 5 clutches and 1 linear transmission.</p>
C-FI-●●		<p>In the sizing mode, the C_5 blocks the motion of body 2, as such the position input body 1 is driven via the differential. Clutch C_6 is also engaged and transmits the input motion to the output, body 4. Clutch C_7 is disengaged to allow body 4 to move w.r.t. body 3, the output of the SBFA. During forcing, clutch C_4 is engaged, as such body 2 is driven via the differential. The differential is a non-standard one, i.e. $a_1 \neq a_2$, this provides the difference in the transmission ratios for forcing and sizing. Clutch C_5 is also able to relieve the motor from the continuous static torque. Clutches C_1, C_2 and C_3 are omitted, because the internal DoF of the differential should never be locked. Clutch C_5 has a double function. During sizing it is engaged all the time, and during forcing it is engaged when the motor is inactive. To account for the increased complexity of this clutch, it is counted double. This topology requires 5 clutches and 1 differential.</p>

I-FI-●●



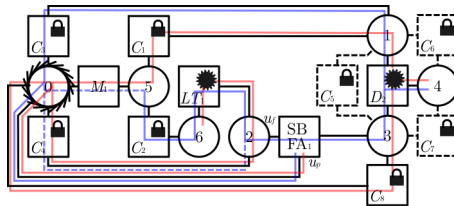
During sizing, clutch C_1 and C_5 are engaged. The motor drives the output body 4 as consequence. To prevent the force input, body 2, to “float” and thereby be sensitive to output disturbances, it is locked using clutch C_4 to the ground. Note that this clutch could also indirectly be attached, via body 6. During forcing the force input body 2 is driven via engaged clutch C_2 and the transmission LT_1 . Clutch C_4 is able to relieve the motor from the static continuous torque. To prevent body 1 from “floating”, it should be connected to another body, but not to body 5 to prevent overconstraints. Body 1 could be locked to the ground using clutch C_4 , but a more elegant solution is to merge body 1 and 4. This makes clutches C_4 and C_5 superfluous. A normal transmission, LT_1 , provides the required transmission ratio for forcing. Clutch C_4 is counted double as it has two functions. This topology consists of 5 clutches and 1 transmission.

C-FC-●●



In the sizing mode clutch C_5 and C_9 are engaged. C_5 blocks the motion of the force input body 2 of the SBFA. As consequence, body 1 is driven by the motor. C_9 blocks the motion of the SBFA output body 3, this is required to ensure the mechanism’s output body 4 is driven via body 1. During forcing clutch C_4 is engaged, this blocks the motion of body 1. As consequence the force input body 2 of the SBFA is driven by the motor. Moreover, this ensure the SBFA output body 3 drives the mechanism output via differential D_2 . Clutch C_5 is able to relieve the motor from the continuous static torque. In both modes the internal DoFs of the differentials should not be blocked, hence clutch $C_1 - C_3$ and $C_6 - C_8$ are omitted. Clutch C_5 has a double function. This mechanism requires 4 clutches and 2 differentials.

I-FC-●●



During sizing, C_1 and C_8 are engaged to ensure the motor drives the output body 4 via body 1 and 5. Clutch C_4 is engaged to prevent body 2 and 6 from “floating”. During forcing, the motor drives the SBFA force input body 2 via the engaged clutch C_2 . Clutch C_3 is engaged to ensure the output body 3 of the SBFA drives the mechanism’s output body 4 via differential D_1 . Clutch C_4 is able to relieve the motor from the continuous static torque. The internal DoF of D_1 should not be blocked, hence $C_5 - C_7$ are superfluous. The clutch C_4 has two functions. This mechanism consists of 6 clutches 1 differential and 1 linear transmission.

^a Motion of body 1 results in size adjustment, motion of body 2 results in adaptation of the force level. Body 5 is driven by the motor. The red lines indicate the mechanism’s sizing mode, the blue lines its forcing mode. During forcing balancing errors and external disturbances need to be counteracted by either the motor or the engagement of a clutch to the ground. This is represented by the blue dotted lines. The dotted clutches connected to dotted lines represent the omitted clutches. The dotted clutches on solid lines represent the clutches replaced with a rigid connection, note that as consequence some bodies should merge to one body, but for clarification these bodies are depicted separately.

5.4.1.4 Comparison

The six bases for the topologies are rated based on their complexity, which is done by counting the number functioning elements: Differentials, transmissions and clutches. The SBFAs and motors are not counted, because each topology incorporates one of them. The bodies are also not counted, because rigid bodies are relatively simple components compared to clutches and transmissions.

The results of this counting are listed in Table 5.9. The base with a continuous splitter and moving SBFA (C-M-●●) has the least counted components, namely 4. The reason that this mechanism is simple is the that no additional combiner is required. Moreover, the employment of a differential as splitter also realizes the desired difference in transmission ratio for forcing and sizing.

A first point of attention is that the differential should be executed as non-standard differential, i.e. its coefficients are subjected to $a_1 \neq a_2$. Furthermore it should be noted that within this base, still several possibilities exist, namely which of the three clutches, C_1 , C_2 or C_3 , is used to lock the internal DoF of the differential. Besides, the NBDM, clutch C_5 could be attached to body 2 or 5, but for this consideration the situation is preferred that the NBDM attaches to body 2, as this also enables the relief of the actuator during sizing, which makes it more resilient to disturbances.

Table 5.9: Number of elements required for each base topology

	C-M-●●	I-M-●●	C-FI-●●	I-FI-●●	C-FC-●●	I-FC-●●
# Clutches	3	4	5 ^a	5 ^a	4 ^a	6 ^a
# Differentials	1	1	1	0	2	1
# Transmissions ^b	0	0	0	1	0	1
# of Elements (Total)	4	5	6	6	6	8

^a One clutch is counted double, because it needs to switch on two accounts.

^b The gearbox which is assumed to be incorporated in the motor is not counted, as it is present in each base topology.

5.4.2 Step 2: Threshold Implementation

The second step in the topology selection is the comparison of the threshold implementation. As described in Section 5.3, four possibilities exist for the threshold implementation. These solutions modify the base. The aim of the current step is to select one of these four possibilities that is the best combination with the base topology C-M-●● from the first selection step.

The selected base topology has still multiple variants for the location of the clutch which locks the internal DoF of the differential. Consequently, some of the four concepts have multiple variants. To account for this, first the best of the four concepts is selected in Section 5.4.2.1, followed by a selection of the variant in Section 5.4.2.2.

5.4.2.1 Step 2A: Concept Selection

The first part of the second selection step consists of a comparison of the four concepts that result from the combination of the four trigger implementations with the selected base topology. Three paragraphs will address subsequently the selection criteria, the descriptions of the concepts and the conducted comparison.

Selection Procedure and Criteria For the comparison of the four concepts, the following criteria are identified:

1. *Simplicity*: As explained in Chapter 1, the introduction, a simple as possible mechanism is desired. The simplicity of the of the various mechanisms are evaluated based on the number of required elements, such as differentials, springs, clutches etc.
2. *Manufacturable*: Also the components itself need to be simple to realize, as complex components are likely harder to miniaturize and therefore larger and heavier.
3. *Compactness*. The size of the mechanism should be small ass possible, because this likely results in a lighter design.

The rating is as follows. A bad score, denoted by $-$, is awarded when the criteria worsens w.r.t. the base. An intermediate score, denoted by a $=$, is awarded when the criteria does not change w.r.t. the base. A good score, denoted by a $+$, is awarded when a criteria is improved w.r.t. the base.

Resulting Topologies The combination of the four concepts for the threshold implementation with the selected base topology results in four concepts. In Table 5.10 these four concepts are listed. This table presents a visualization as well as a description of the concept and an evaluation of its performance. When a concept has multiple variants, this is also indicated in the description.

Table 5.10: Description of Implemented Thresholds

Topology	Visualization	Description
C-M-A-●		<p>In this concept the threshold is implemented using an additional (non-linear) spring. The extension of this spring should not depend on the object size. Therefore, it should not be connected to the ground, but between two of the three in- or outputs (bodies 1,2 and 5) of the differential, hence three possible locations are possible. Combined with the three variants of the clutch locations, this results in 9 permutations, of which one is visualized at the left. This mechanism scores bad on simplicity, as it requires an additional spring compared to the based. Because the spring is a relatively simple component, the manufacturability is not affected.</p>
C-M-R-●		<p>A clutch is able to replace a lock, when this lock has to be engaged when it is subjected to a low load and disengaged when it is subjected to a high load. For the C-M-●-● base, this is the for clutch $C_1 - C_3$. One of these clutches has to constraint the internal DoF of the differential during sizing and allow motion during forcing. Compared to the forcing mode, the differential is subjected to low loads in the sizing mode. Other clutches can not be replaced with a spring. Clutch C_4 is subjected to high loads when it is engaged, because it has to withstand the reaction forces on the position input that occur during forcing. The engagement of clutch C_5 depends on whether the motor is activated. Note that this mechanism has three variants, as it is not yet decided which of the three clutches is used to lock the differential. This mechanism has the same simplicity as the base, as the number of functioning elements does not change. The manufacturability improves, as springs are easier to realize than clutches. Clutches consists of multiple parts which have to alternatively lock or move w.r.t. each other, whereas springs can be as simple as one compliant component.</p>
C-M-I-●		<p>In this concept the non-linear transmission of the SBFA is modified, such that it results in the desired input force characteristic, which functions as threshold. This mechanism has three variants as either C_1, C_2 or C_3 can be employed to lock the internal DoF of the differential. The simplicity is equal to that of the base, because no components are added, removed or replaced. To realize this in a reliable way is challenging, the modification of the transmission is very small, because the potential energy involved with the threshold is small compared to the energy stored in the balancer, this makes the threshold characteristic very sensitive to manufacturing tolerances. In addition finetuning of the mechanism is impeded, as independent finetuning of the balancer and threshold is not possible because they are integrated.</p>
C-M-RI-●		<p>In this concept the clutch C_1 that locks the internal DoF of the differential is replaced with an input force characteristic that is obtained using a modification of the balancer transmission. This modification resembles a spring characteristic between the differential output bodies 1 and 2, and are therefore able to replace clutch C_1. This mechanism improves the simplicity, as it omits the spring or clutch that locks the internal DoF of the differential. Yet, realization of a good input-characteristic is challenging, as the modification is small and finetuning is not possible.</p>

Comparison In this paragraph the four concepts are compared based on the selection criteria. Table 5.11 provides an overview and a brief explanation on the awarded scores of the four concepts on the selection criteria. Although none of the four concepts scores good on all criteria, the concept with the clutch replacement, labeled C-M-R-●, is regarded as the best choice. This is the only concept that improves the manufacturability of the mechanism, as it replaces a clutch with a spring, but does not need

a modification of the balancer transmission.

This concept has three variants, as the location of the locker of the differential outputs is not yet decided, this is next.

Table 5.11: Comparison of concepts for the trigger implementation

Criteria	C-M-A-●	C-M-R-●	C-M-I-●	C-M-RI-●
Simplicity	– Additional spring	= Clutch replaced with spring	= No changes to topology	+ Clutch to lock differential DoF omitted.
Manufacturable	= Additional spring easy to realize	+ Spring easier to realize than clutch	– Sensitive to manufacturing disturbances, no independent finetuning	– Sensitive to manufacturing disturbances, no independent finetuning

5.4.2.2 Step 2B: Variant Selection

As the selected concept, C-M-R-●, has three variants, the second part of this selection step is to select the best one of the three. The following three paragraphs describe respectively the selection criteria, a description of the three variants and a comparison.

Selection Criteria All three variants consists of the same number and type of functioning elements, and also their functionality is equal. This leaves a comparison based on *compactness*. Evaluating this aspect relates also to the speed and mass, as smaller mechanisms have likely less mass and inertia. In this stage of the design it is not possible to quantify the compactness. However, by reasoning about the required stroke, it will be possible to compare concepts relatively to each other.

The comparison of the compactness is conducted based on the required stroke of the springs, expressed as function of the displacement of body 5, the input of the differential. This is done as follows:

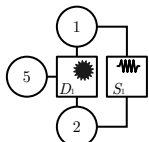
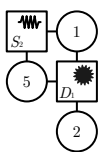
The extension s equals the difference between the displacements of the two differential in- or outputs it is connected to: Δx_1 , Δx_2 or Δx_5 . These displacements are related by the integration of the differential kinematics, see Table 5.1, which resolves to:

$$\Delta x_5 = a_1 \Delta x_1 + a_2 \Delta x_2 \tag{5.1}$$

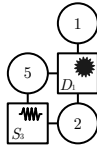
The spring is only extended during forcing, as during sizing the three in- and outputs of the differential need to move with the same speed. During forcing, body 1, needs to be locked, hence $\Delta x_1 = 0$, from which follows: $\Delta x_2 = \Delta x_5 / a_2$. These expressions are used to express the spring extensions of the spring. Recall that the differential ideally realizes a large reduction for the displacement Δx_2 during sizing. This implies that $a_2 \gg 1$.

Description of Variants The tree variants are listed in Table 5.12. In the visualization the three different locations of the spring are depicted. In the description the expressions for the stroke of these springs, as functions of the input displacement Δx_5 are given.

Table 5.12: Description of Concept Variants

Topology	Visualization	Description
Replacement of C_1		For this variant the clutch C_1 is replaced with a spring. The extension of this spring is $s = \Delta x_2 - \Delta x_1$. Application of the differential kinematics yields: $s = \Delta x_5 / a_2$.
Replacement of C_2		The replacement of clutch C_2 results in a spring extension of: $s = \Delta x_5 - \Delta x_1 = \Delta x_5$.

Replacement of
 C_3



For the third variant clutch C_3 is replaced, resulting in a spring extension: $s = \Delta x_5 - \Delta x_2 = \Delta x_5(1 - 1/a_2)$.

Comparison Based on the expressions of Table 5.12 the compactness of the three variants is compared. For the assumed value $a_2 \gg 1$, the replacement of clutch C_2 will always leads to the largest stroke, as this stroke equals Δx_5 . Whether the stroke for the replacement of C_1 or C_2 is the smallest depends on whether a_2 is larger or smaller than 2. Assuming that a_2 is larger than 2, the replacement of clutch C_1 provides the smallest stroke. This is summarized in Table 5.13. Based on this reasoning, the first variant with replacement of C_1 is selected.

Table 5.13: Comparison of the Variants of Clutch Replacement

Criteria	Variant 1: S_1 used	Variant 2: S_2 used	Variant 3: S_3 used
Compactness	+ $s = \Delta x_5/a_2$	- $s = \Delta x_5$	$\pm s = \Delta x_5(1 - \frac{1}{a_2})$

5.4.3 Step 3: Threshold Loading

The third and final step in the topology selection is to compare the three concepts for the threshold loading. First the selection procedure and criteria are explained. Second, the three concepts for the threshold loading are combined with the resulting topology of the previous step, C-M-R- \bullet . Third, the best option is selected.

5.4.3.1 Selection Procedure and Criteria

The three concepts for the trigger loading are combined with the surviving topology from step 2: C-M-R- \bullet . To ease the comparison, an example based on the sliding ladder example is depicted in addition to the rather abstract topologies. The three concepts are compared based on the following three criteria:

1. *Probability of Error* The different types threshold have a different chance on a balancing error. For some concepts it might be guaranteed that the balancing error occurs, whereas for other concepts they might only arise under given conditions. The chance on a balancing imperfection should be as low as possible to realize an energy saving drive
2. *Average Magnitude of Error* Besides the chance of a balancing error, the (average) magnitude of these errors is of importance. This average is ideally small, because the larger the error, the more energy is required to compensate for it.
3. *Simplicity* Avoidance of reduction of the errors might require additional components. This worsens the performance of the mechanism in terms of simplicity.

5.4.3.2 Resulting Topologies

Three methods for the threshold loading are identified, based on whether or not the SBFA output and main spring are bypassed. The first method, C-M-R-TT, has two variants depending on whether anticipation takes place. The four loading methods are explained and visualized in Table 5.14.

Table 5.14: Subtopologies for drive splitter

Type	Representation/Example	Description
C-M-R-TT w/o Anticipation		<p>For this concept the threshold force, originating from contact with the clamp, flows through the SBFA output and through the main spring. The naive solution would be to not anticipate on the threshold force, which flows through the main spring. This causes an extension e of the main spring. Once the threshold force is reached, the position input of the SBFA is locked. As a consequence, the error e is “trapped” in the spring, resulting in a balancing error along the entire stroke of the main spring. In appendix D the mathematics of this concept are presented. For this variant, the balancing error is <i>guaranteed</i> and likely to be <i>considerably large</i>.</p>
C-M-R-TT w/ Anticipation		<p>This concept is almost identical to the previous concept, except for the pretension of the buffer springs that result in an offset equal to e of the main spring. This compensates for the occurring extension e of the main spring once it is loaded with the threshold force. For forces higher than the balancing threshold the mechanism becomes statically balanced. This is proven in appendix D. The balancing imperfection that arises for forces lower than the threshold could be incorporated in the design of the threshold characteristic and do therefore not a problem. However, the position input of the SBFA has to lock exactly when the spring extension equals e, otherwise balancing errors will still arise. As the timing of the locking may for instance vary with the speed of the motion, some stochastic variance is expected, as such it is <i>likely</i> that balancing errors occur, although they are smaller than for without anticipation.</p>
C-M-R-TB		<p>In this concept, the force flows through the SBFA output but bypasses the main spring. To achieve this, a limit-stop is implemented, which prevents the trigger force to elongate the main spring. Instead, it reroutes the force to the position input of the balancer. Due to the unidirectional nature of the endstop, the main spring can still deliver a force to the output during forcing. Strictly speaking, this adds additional components to the topology, and reduces thereby the simplicity of the mechanism. However, in practice this is almost negligible, as a limit-stop is in many cases easily implemented by applying dedicated protrusions and a setscrew. As the locking position is defined by the end-stop, it is expected that the chance of a misalignment is not likely. And if an error would occur, it would be small.</p>
C-M-R-B		<p>For the last concept, the output of the SBFA is bypassed. Contact with the object is transmitted directly to body 1. This concept requires an additional clamp to make contact with the object, this has two major issues: In the first place, ideally the two clamps are collocated, to ensure contact is detected at the exact instance the clamp makes contact. However, in practice the components are not infinitesimal, and therefore this collocation is not possible. As such it is <i>likely</i> that balancing errors arise. This balancing error is likely to be small. In the second place, this concept requires to duplicate the clamp. For a simple clamp this might be easily done, but altering an underactuated robotic gripper with multiple fingers to a variant with twice as much fingers is not easily done.</p>

5.4.3.3 Comparison

Table 5.15 provides an overview on the rating of the concepts. It should be kept in mind that the energetic performance is much more important than the simplicity of the mechanism. The C-M-R-TB scores best on the first two criteria that relates to the energetic performance. Although it is rated intermediate, the realization of an endstop does not require much complicated components. This leads to the conclusion that the topology C-M-R-TB is the best topology.

Table 5.15: Comparison of trigger Loading

Criteria	C-M-RI-TT		C-M-RI-TB	C-M-RI-B
	No Anticipation	Anticipation		
Error Probability	– Guaranteed	± Likely	+ Not likely	± Likely
Error Magnitude	– Large	+ Small	+ Small	+ Small
Simplicity	+ No additional components	+ No additional components	± Additional Limit Stop	– Duplicate fingers/clamps

5.5 Explanation of Selected Topology

The topology selection is a rather abstract procedure. To explain the working principle of the selected one, it will be applied on an example based on a sliding ladder mechanism.

Fig. 5.1a depicts the selected C-M-R-TB topology. It consists of a moving frame driven by a continuous splitter. The threshold replaces a clutch and the threshold force flows through the output but bypasses the main spring via an endstop. The endstop is depicted in grey as in fact are just dedicated geometries of the bodies 1 and 5.

In Fig. 5.1b an example of mechanism with this topology is depicted, based on the sliding ladder mechanism. The differential in this example is a lever. The non-backdrivable mechanism is attached to the same bodies as the motor: The ground and body 5, the input of the differential. The remainder of this section will explain the working principle of this example, according to the three subfunctions of the drive: Sizing, Switching and Forcing.

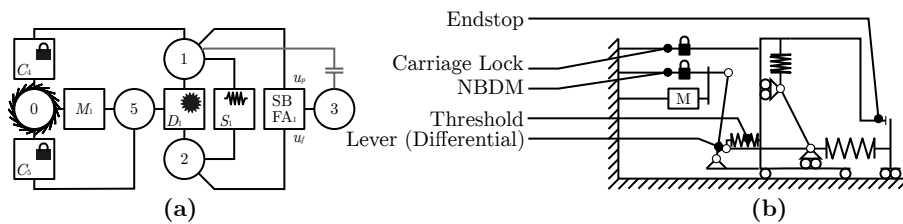


Figure 5.1: Selected concept **a:** Schematic Topology: C-M-R-TB. **b:** Example of a mechanism based on this topology.

5.5.1 Sizing

The first subfunction of the mechanism is sizing. During sizing the carriage lock is disengaged. The threshold spring holds the two outputs of the differential stationary w.r.t. each other. As consequence, a motor displacement will result in a displacement of the SBFA as whole. This is schematically depicted in Fig. 5.2. The clutch on the dashed line indicates the NBDM that is able to relieve the motor.

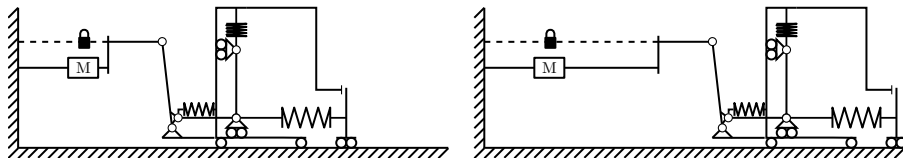


Figure 5.2: Sizing of the example with C-M-R-TB topology. The SBFA moves as whole as the pretension of the threshold springs holds the outputs of the differential together.

5.5.2 Switching

The second subfunction is switching. The mechanism starts with switching once the output encounter an object. The position of the carriage is defined by the endstop. The motor has to overcome the threshold force. During switching the carriage lock mechanism engages. This function is schematically depicted in Fig. 5.3

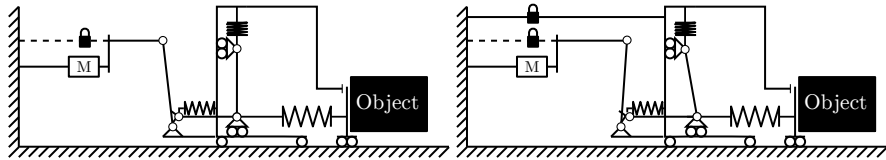


Figure 5.3: Switching of the example with C-M-R-TB topology. The frame of the SBFA is initially hold in place by the end stop. The carriage locker engages during switching.

5.5.3 Forcing

The last subfunction, forcing, is schematically depicted in Fig. 5.4. The carriage lock is engaged and holds the frame of the balancer in place. A limited amount of play might be present in the locking mechanism due to its resolution. As consequence, the carriage might be pushed slightly backwards once the main spring force exceeds the input force. The buffer spring counteracts the main spring, such that the motor is able to adjust the output force almost effortlessly. The non-backdrivable mechanism is able to relieve the motor from continuous static loads.

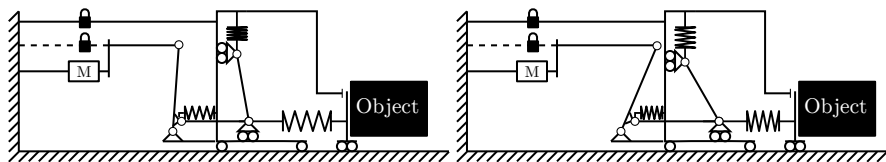


Figure 5.4: Forcing of the example with C-M-R-TB topology. The frame position is locked by the carriage lock. The output force level is effortlessly adapted by the motor.

5.6 Discussion

This chapter aims to find the best topology. In a stepwise selection procedure the C-M-R-TB topology was selected as best one. Before this selection is concluded, its results are subjected to a critical reflection, regarding the completeness of the overview, the used approach and the formulation and evaluation of the selection criteria.

A critical question is whether the described subtopologies span the entire solution space. Unfortunately, it is impossible to be sure of this, because there is no known method which guarantees all possible solutions in the solution space are found. However, as I explored the solution space in a structured way I am convinced at least a large portion of the solution space is explored. The thorough documentation secures the quality and reproducibility of the topology selection.

Another critical question is if whether another approach resulted in a different result. Instead of selecting a base and expanding this base with additional concepts, I could have discussed all 72 permutations and their variants that result from the combination of the four categories of subtopologies. During the design process I took some time to make brief sketches the permutations. From this I learned that the base has a very large influence on the overall lay out. Moreover I learned that the performance effect of differences on the permutations was not always clear. Thoroughly inspecting all permutations would be cumbersome and take much time and pages to explain. Hence I decided for the used stepwise selection approach.

Another critical point are the selection criteria. The results of the selection depend on the formulated criteria and on the rating the of the concepts. I am aware this process is subjected to some subjectivity as as experience and estimations are involved in the formulating and ratings. To be transparent on this, I provided by all criteria formulations and performance ratings a brief explanation.

With the topology selection the second part of this thesis is complete. Up to this part the design was of a drive was conducted from a general perspective. The next two parts will focus on the design and

experimental validation of a drive for an actual gripper. The remaining two chapters will describe a case study: the detailed design and evaluation of an energy saving drive for an existing robot hand.

5.7 Conclusion

This chapter aimed to find the best topology. Using the ACCREx method different subtopologies were found in four categories: The *drive splitter*, the *SBFA mounting*, the *trigger implementation* and the *trigger loading*. In a stepwise selection subtopologies of these four categories are combined.

The first step combined a drive splitter and an SBFA mounting. Based on the simplicity, i.e. the lowest number of components, a continuous splitter with a moving SBFA frame was selected as base. In the second step a threshold implementation was selected that reduces the complexity of the base as it replaces a rather complex clutch with a simpler spring. This spring is mounted between the two outputs of the differential, as this results in the most compact design. In the third step the threshold loading was considered. Ultimately a force path was selected that flows through the SBFA output, but bypasses the main spring by means of an endstop. This reduces both the chance and the magnitude of balancing errors, although it requires a few simple additional parts.

An example of the selected topology is given, based on the sliding ladder balancer.

Part III

Prototype Design

Chapter 6

Design Requirements

6.1 Introduction

The previous chapters discussed the strategy and conceptual design and where from a generic point of view. Now the focus shifts towards the design of an actual prototype. But before start of the design of an actual prototype, its design requirements need to be identified. As such, this chapter is dedicated to the identify those.

Naturally, the drive should not be treated as isolated subsystem. To work properly, it needs to interact with the other components of the hand and robotic system. Therefore this chapter will start with a description of the environment of the gripper in Section 6.2.

When the task and properties of the environment are identified, it is possible to derive the actual design requirements, this will be done in Section 6.3. These design requirements serve as input for the typology selection and the detailed design, which are described in the next two chapters.

The obtained requirements are discussed in Section 6.4 before they are listed as conclusion of this chapter in Section 6.5

6.2 Environment of the Drive

The aim of this chapter is to identify the requirements of the drive, but before this can be done it is important to know what the drive is used for. As such, the environment, i.e. the manipulator and its task and the gripper will be described. These systems are addressed in Section 6.2.1 and Section 6.2.2 respectively.

6.2.1 Manipulator: The Plugless Arm

The robotic drive will be designed for implementation on the *Plugless Arm*. This robotic arm is designed to be extremely energy efficient during pick-and place operations. The arm has 3 DoF, and is able to executes a task in a 2D vertical plane. The high efficiency is realized by energy recuperation using springs. The optimal efficiency is a trade-off between slow movements to reduce the motor torques and a low cycle time to reduce the energetic overhead. The required grasp force is related to the required accelerations for the optimal trajectory of this arm.

In preliminary results¹, a maximum efficiency was found for rather high vertical accelerations a_v , with peaks in the range of $a_v = 35 \text{ m/s}^2$ in both positive and negative direction. Because these results where obtained with a simplified model, the horizontal accelerations are not known. However, for another optimization method [51], the maximum horizontal acceleration a_c was $\sim 40\%$ of the maximum vertical acceleration². As such, the maximum horizontal acceleration is estimated to be $a_c = 14 \text{ m/s}^2$.

The targeted payload is 1 kg. The minimum dislodging force in vertical direction has to be greater than the sum of the static load (gravity) and dynamic load (accelerations), and should therefore be at least 45 N. The minimum dislodging force in horizontal direction should be able to withstand the horizontal accelerations, and should therefore be at least 14 N.

¹Source: E-mail conversation with Linda v.d. Spaa, d.d. 30-01-2017

²These values are not documented in [51], but obtained from an e-mail conversation with Ralph Vosse, d.d. 11-10-2016

6.2.2 Gripper: Delft Hand 3

To accomplish a pick-and-place task, the system needs a gripper to grasp and hold the objects. This thesis focuses on the grippers subsystem with the most influence on the energy consumption: the drive. Therefore an existing gripper was selected of which the drive is replaced. The Delft Hand 3 [17], depicted in Fig. 6.1, is selected to serve as gripper for the following reasons:

1. Due to its clever underactuated mechanical design this gripper is able to grasp a wide variety of objects using just one single actuator.
2. The design is lightweight. The current mass is 330 g, of which 122 g is contributed by the drive, consisting of a geared DC-motor.
3. Its design is well documented in a doctoral thesis, which allows for a good performance prediction.

The Delft Hand 3, depicted in Fig. 6.1a has three fingers, of which one is a thumb, opposing the two other two fingers. Each finger is underactuated, as it has two phalanges, but just one input. The inputs links are driven using a single geared DC motor. The thumb is connected to the stator of the motor and the two opposing fingers are connected via a bevel gear differential and gearbox to the rotor. This is depicted in Fig. 6.1b. The novel drive of this thesis will replace the current drive, a geared DC-motor.

The hand is capable of two grasp types: a *precision grasp*, in which the object is pinched with the fingertips and a *power grasp* in which the object is enveloped by the fingers and the palm. In this thesis only the second grasp is considered as it is more robust.

The next section will quantify the requirements that are related to the use of this hand.

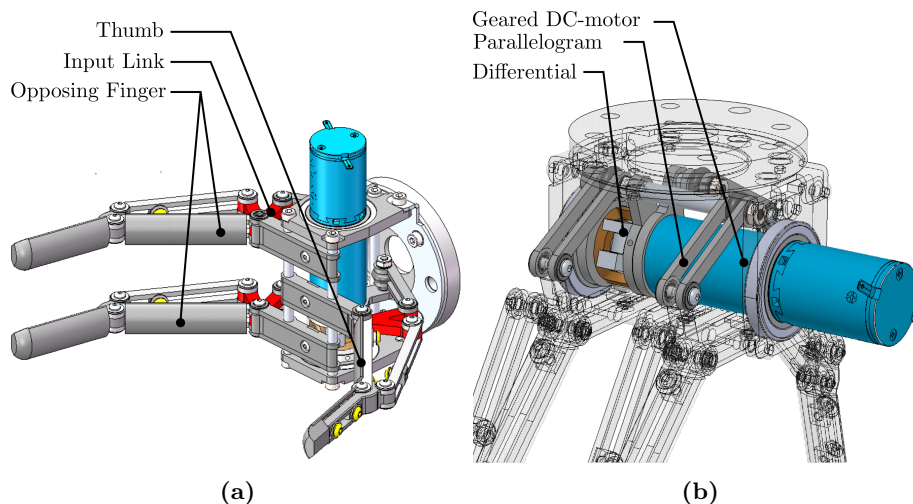


Figure 6.1: CAD-model³ of Delft Hand 3 [17] **a:** The current actuator, a geared DC motor, is highlighted in blue. The input links of the fingers in red. **b:** Close up of existing drive. The actuator is “floating”. The stator is connected to the input of the thumb via a parallelogram. The rotor is connected via a gearbox, differential and parrallograms to the inputs of the two opposing fingers.

6.3 Design Requirements

Now that the environment is described, the design requirements it imposes can be identified. Before the prototype design proceeds, the following questions need to be answered:

- How can the drive be implemented in the hand?
- What is the required drive torque to retain the object?
- Chapter 4 showed that the object stiffness at the balancer output affects the balancing error, so what stiffness appears at the drive output?
- What disturbance forces are to be expected?

The answers to these questions serve as design requirements for the following two chapters.

³CAD-model obtained by e-mail conversation with Cor Meijneke, d.d. 22-12-2016

6.3.1 Implementation

The novel SBFA-based drive has to replace the current drive of the Delft Hand 3. I identified two possibilities to do so. These concepts will be compared and the best one will be selected. The selected implementation will serve as design requirement for the topology, i.e. embodiment, of the various subsystems in the next chapter. This subsection will subsequently address the selection criteria, the descriptions of both possibilities and the comparison.

6.3.1.1 Selection Criteria

It is expected approximately the same performance in terms of energy consumption, speed and mass could be achieved for the two implementation methods. This leaves comparison to depend on practical considerations. The following criteria are taken into account for the comparison of the two implementation concepts:

1. *Manufacturability of the Drive*: The implementation affects the design of the drive itself. One of the critical aspects are the bearings that are required to guide the motion of the different moving components.
2. *Required Adaptations to the Existing Hand*: When the drive changes, also the interface of the hand is likely to change. It is advantageous if these changes are limited to a minimum, as this saves time which can be spend on the focus of this thesis: the drive.

6.3.1.2 Description of Implementation Methods

Now the two implementation methods will be discussed and their advantages and drawbacks are addressed.

Rotational Implementation The first implementation method is to design a rotational device. This device could simply replace the geared motor. It is expected that a rotational mechanism is well manufacturable. A large variety of miniaturized ball bearings is available [52]. These bearings provide relative high load rating in a compact space. For instance the NSK 682 bearing has a static load rating of 50 N with an inner diameter of 2 mm, outer diameter of 5 mm and width of 1.5 mm. The tolerances of the fittings for these bearings are well within the reach of conventional machinery. Regarding the second criteria, this design is advantageous, as it is likely possible to adopt the interface of the current drive in the design.

Translational Implementation The second implementation method is to design a translational device. The existing drive, including the existing differential and parallelogram to the finger inputs is replaced. The inputs of the fingers are driven by a device that converts the translation to a rotation, for instance the input links could be replaced by partial gears, driven by a gear rack.

This method requires linear guides. In general the range of linear guides is smaller and allow for a less compact design [53]. For example, the SKF LBBR 3 linear ball bearing has a static load rating of 44 N, but has an inner diameter of 3 mm, outer diameter of 7 mm and a width of 10 mm, which is much larger than the rotational ball bearing with comparable load rating. Moreover, these guides have to be mounted very precise and bending of these guides should be minimized as much as possible. This impedes manufacturing the drive.

A second drawback is that this method requires much adaptations to the existing hand, as the palm needs to be adopted for a linear input.

6.3.1.3 Comparison

Table 6.1 provides an overview on the comparison of the two implementation methods. A good score (+) or bad score (−) are awarded if the method performs respectively better or worse than its alternative.

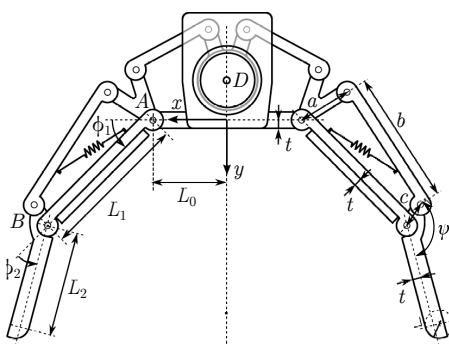
Table 6.1: Comparison of Implementation Methods

Criteria	Rotational	Translational
1 Manufacturability of drive	+ Rotational bearings allow for compact design, are widely available and require moderate tolerances.	– Linear guides are less compact, a smaller range is available and they require stiff design and very precise manufacturing.
2 Changes to hand	+ Existing interface can be (largely) adopted.	– Palm of hand redesigned.

For both the first and second criteria the rotational device outperforms the translational device. The device itself has a better manufacturability and requires less changes to the existing hand. Therefore the rotational method is selected as implementation method.

6.3.2 Grasp Force

An important requirement is the required drive torque to meet the required dislodging force. The dislodging forces depend on the contact forces, which in turn depends on the non-linear transmission ratio. Therefore, the first paragraph is dedicated to the expression of this transmission ratio. The second paragraph describes the dislodging forces in the principal direction and the third paragraph reasons about the minimum required drive torque.

**Figure 6.2****Figure 6.3:** Parameters of Delft Hand 3. Image adapted from [17].

Non-Linear Transmission Ratio This paragraph describes briefly the non-linear transmission ratio of the fingers, based on the parameters of Fig. 6.3. The output torque T_D of the drive and are transmitted via a parallelogram to the input of the fingers. Because of the parallelogram, the torque on the input lever, pivoting around point A equals the drive torque: $T_A = T_D$. The transmission ratios $R_{A,n}$ between the finger input torque T_A and the contact forces F_n depend strongly on the configuration of the hand. In [17] the following expressions are given for the transmissions ratios between the input and the contact force at the proximal and distal phalanx respectively:

$$R_{A,1}(\phi_2) = \frac{F_1}{T_A} = \frac{1}{p_1} \left(1 - R_{A,B} \cdot \frac{p_2 + L_1 \cos \phi_2}{p_2} \right) \quad (6.1)$$

$$R_{A,2}(\phi_2) = \frac{F_2}{T_A} = \frac{R_{A,B}}{p_2} \quad (6.2)$$

Where p_1 and p_2 are the distance between the joints and the contact points of these phalanges and $R_{A,B}$ is the non-linear transmission ratio of the four bar mechanism. The expression for this ratio is reproduced from [48, 17] in appendix E.

Dislodging Forces This paragraph will express the minimum dislodging forces in the three principal directions, followed by a method for a numerical evaluation of these forces.

The minimum dislodging force in y -direction, $F_{y,d\ell min}$, is found by the summation of the y -components of the contact forces:

$$F_{y,d\ell min} = 2(F_1 \cos \phi_1 + F_2 \cos(\phi_1 + \phi_2)) \quad (6.3)$$

When no load is acting on the object, this force equals the contact force with the palm. When the load increases, this contact force decreases. When the load equals $F_{y,d\ell min}$, the contact force with the palm equals zero. Further increase of the load causes the palm to loose contact with the hand.

Two important remarks need to be made on this method. First, it neglects the friction in the contact points. In practice, this friction will counteract the load, and therefore the actual dislodging force is expected to be higher. Second, once contact with the palm is lost, the object is not immediately released. In fact, experiments with a test-bench [17] shows that the actual dislodging force is at its maximum when contact with the palm is lost and the object has displaced a certain amount in y -direction. However, incorporating both effects requires extensive modeling. Because the actual dislodging force is in practice higher, the described procedure can be used to obtain a conservative estimate of the dislodging force. Moreover, this approach ensures the object remains stationary w.r.t. the hand, which allows for accurate positioning.

The dislodging force in z -direction follows from the summation of the forces in the contact points (of all fingers) and multiply it with the friction coefficient μ_f between the finger and the object:

$$F_{z,d\ell min} = \sum F_i \mu_f \quad (6.4)$$

Also the contact force with the palm is incorporated, under the assumption that the load in y direction equals 0.

The dislodging force in x -direction, under the assumption that the load in other directions equals zero, follows from the friction with the palm, as the x -components of the contact forces in the phalanges cancel each other out. Hence,

$$F_{x,d\ell min} = F_{y,d\ell min} \mu_f \quad (6.5)$$

Since typically $\mu_f < 1$, this force is smaller than $F_{y,d\ell min}$.

A numerical evaluation of the forces is not straightforward, as the transmission ratios depend on the configuration of the fingers, which in turn depends on the interaction with the object. The following method [17], based on *loop-vector-closure*, is used for the numerical evaluation: It is convenient to assume a cylindrical object [17], because it is configuration independent along the longitudinal axis, it has a continuous surface and its geometry is described by a single variable: its radius r_o . Moreover, many objects in daily lives approximate a cylindrical shapes, think of many tools, cups, bottles and so on. Solving the *loop closure vector equations* for different object sizes results in the configurations of the hand, which are used in turn to evaluate the transmission ratios. This is described in more detail in appendix E.2.

Based on the results from this procedure, the the contact forces and dislodging forces are evaluated. These forces are plotted as ratio of the drive output torque T_D in Fig. 6.4a.

As follows from this figure, the dislodging force in z -direction is larger than in y -direction. As the loads during movement are the largest in vertical direction, the hand should be orientated such that the z -direction aligned with the vertical. As the hand is stronger in y -direction than in x -direction, the horizontal acceleration should coincide with the y -axis of the hand.

Drive Torque This paragraph reasons about the required drive torque.

The maximum drive output torque for the current design is 1 Nm [17]. As shown in Fig. 6.4a, the the modeled vertical dislodging force $F_{z,d\ell minm} \in [17.2, 43.7]$ N. The discontinuity at $r_o = 47.8$ mm emerges because the proximal phalanx loses contact with the object. Because the force $F_{z,d\ell minm}$ is smaller than the required 45 N, it is desired to increase the drive torque. However, while doing so, the mechanical strength of the fingers should be taken into account. As described in appendix E.4, the practical limit to the output torque is 1.4 Nm, which results in a vertical dislodging force as depicted in Fig. 6.4b. This guarantees that objects with $r_o \in [30, 39.4]$ mm can always be grasped. In practice, upper limit of this range is likely to be larger, as this model assumes a cylinder, which has a constant cross-section. However, for many objects the cross section varies with the height, think of bottles, tools, balls and cups. Because of the underactuated design, the hand is able to adapt to these geometries and enclose the object, resulting in shape grasping in addition to friction grasping, which increases the dislodging force.

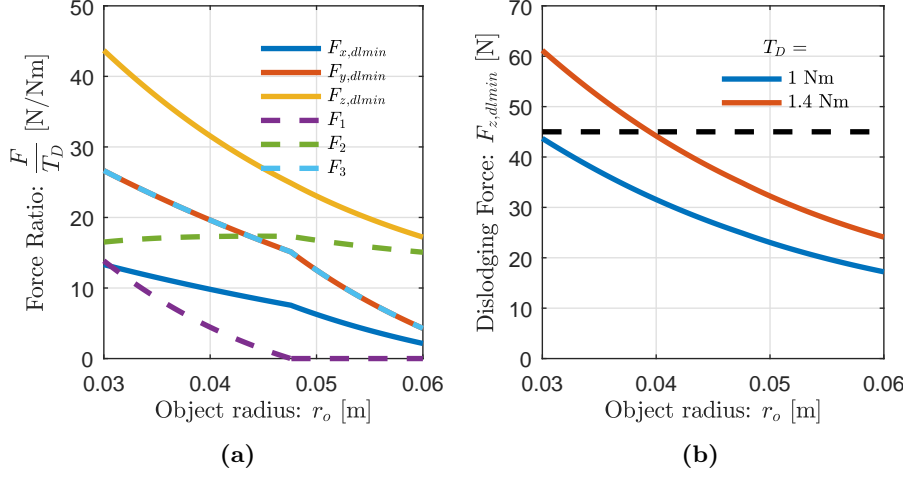


Figure 6.4: **a:** Ratio of forces at finger and torque at finger input. The solid lines indicate the dislodging forces in x -, y - and z -direction, the dashed lines the contact forces at the proximal phalanx (F_1), distal phalanx (F_2) and palm (F_3). **b:** Minimum dislodging forces in z -direction for two different input torques.

6.3.3 Object Stiffness

Due to the transmission, the object stiffness felt at the contact point differs from the stiffness felt at the output of the drive. The stiffness felt at the output of the drive is called the *apparent stiffness*. As shown in chapter 4 the stiffness at the drive output affects the balancing error. The first step to determine this apparent stiffness at the finger input of every contact point. The second step is to express the apparent stiffness at the finger input of multiple contact points. The last step is to determine the apparent stiffness at the drive output for multiple fingers.

Apparent Stiffness at Finger Input of Single Contact Point Using the general expression of the apparent stiffness [20], the apparent stiffness at the finger input at the j^{th} finger as consequence of the stiffness in the i^{th} contact of this finger is expressed:

$$k_{A,i,j} = R_{A,i}^{-2} k_{i,j} \quad (6.6)$$

The derivation of this expression is conducted in more detail in appendix E.

Stiffness at Finger Input of Multiple Contact Points The underactuated fingers are able to distribute the input force over multiple contact forces. In fact, the finger is a (non-linear) differential. This means the contact forces of the various phalanges, and thereby also the effects of the contact stiffness, act in series. An intuitive check for this is by assuming one of the springs has an infinite stiffness. Because of the differential, the other spring could still be tensioned, which means that they are in series. As such, the apparent stiffness at the input of the j^{th} finger follows from:

$$k_{A,j} = \left(\sum_{i=1}^{N_p} (k_{A,i,j})^{-1} \right)^{-1} \quad (6.7)$$

where N_p denotes the number of phalanges. Consequently to the assumed cylindrical object shape, the grasp is always symmetric w.r.t. the y -axis. Therefore, the transmission ratios between the phalanges and finger inputs are the same for every finger, i.e: $R_{A,i,1} = R_{A,i,2} = R_{A,i,3} = R_{A,i}$. Besides, a homogeneous object stiffness k_o is assumed, hence $k_{i,j} = k_o$. As such, Eq. (6.7) resolves to the following expression for the apparent stiffness at the finger input:

$$k_{A,j} = \frac{k_o}{R_{A,1}^2 + R_{A,2}^2} \quad (6.8)$$

Apparent Stiffness at Drive Output The apparent stiffness at the actuator output follows from combining the apparent stiffness at the different finger inputs. While doing this, it should be taken into

account that these fingers are also connected in series. As such, the apparent stiffness k_D at the drive input follows from:

$$k_D = \left(\sum_{j=1}^{N_f} \left(R_{D,j}^{-2} k_{A,j} \right)^{-1} \right)^{-1} \quad (6.9)$$

where N_f is the number of fingers, $R_{D,j}$ is the transmission ratio between the drive and input of j^{th} finger. The thumb is connected to the housing of the gearbox via a parallelogram. As such the transmission ratio for this finger equals $R_{D,1} = 1$. The two opposing fingers are connected via a parallelogram to the outputs of a bevel gear differential. This differential is driven by the output shaft of the actuator, and distribute the shaft torque equally over the finger inputs. As such, $R_{D,2} = R_{D,3} = \frac{1}{2}$. Substituting these values in Eq. (6.9) results in the following expression for the total apparent stiffness at the actuator output:

$$k_D = \frac{2}{3} \frac{k_o}{(R_{A,1}^2 + R_{A,2}^2)} \quad (6.10)$$

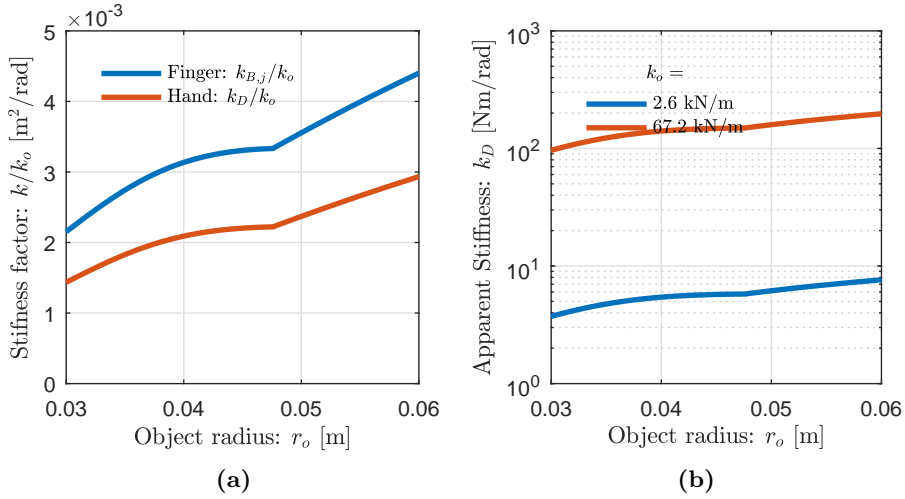


Figure 6.5: Apparent Stiffness. **a:** Apparent stiffness divided by the object stiffness at input of single finger and output of the drive. **b:** Apparent stiffness at drive output for two different values of the object stiffness k_o .

In figure Fig. 6.5a the stiffness factor, i.e. the ratio of the apparent stiffness to the object stiffness is plotted for both the the finger input and the drive output. This factor has as unit meter squared per radians (m^2/rad) because of the conversion from translational to rotational stiffness. Due to the serial connection the apparent stiffness at the drive output is lower than than the apparent stiffness at the finger input. The non-smoothness at $r_o = 47.8$ mm arises as the proximal phalanx does not make contact for objects with a radius exceeding this value.

As follows from Fig. 6.5a: $k_D/k_o \in [1.43 \cdot 10^{-3}, 2.93 \cdot 10^{-3}]$ m²/rad. To compute the apparent stiffness itself the object stiffness needs to be known. In [47] the stiffness of a standardized set of everyday life objects is measured. These values are in a range from $2.6 \cdot 10^3$ N/m for a cracker box to $67.2 \cdot 10^3$ N/m for a coffee can. The apparent stiffness for these objects is plotted in Fig. 6.5b and lies in the following range: $k_D \in [3.73, 197.1]$.

6.3.4 Disturbance Force

Due to the inertia of the components, a disturbance force will appear at the fingers as soon as the gripper accelerates and decelerates. This subsections aims to quantify the required threshold force to prevent unwanted motions.

Recall that the hand is positioned with the z -axis in vertical direction and the y -plane in line with the the horizontal movement of the gripper. As the fingers can only move in the $x - y$ plane, the vertical accelerations in the z -direction do not cause unwanted movements. The effect of the accelerations in the horizontal y -direction are are estimated based on a simplified model, in which the fingers are modeled as

rigid links.

The equilibrium condition of the fingers will be derived while the differential is incorporated. Then the effect of positive and negative disturbances are described. Ultimately the threshold is numerically evaluated.

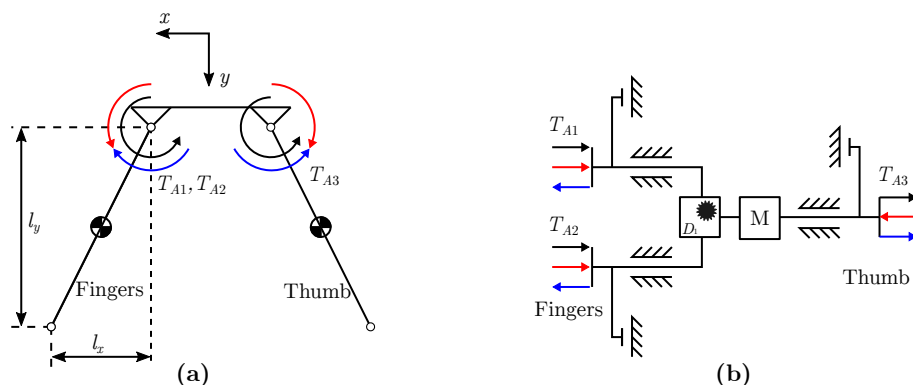


Figure 6.6: Simplified model of finger to quantify effects of disturbance. Black arrow: Defined positive direction of torques. Red: Torques when $\ddot{y} \geq 0$. Blue: Torques when $\ddot{y} < 0$.

Equilibrium Conditions The first step to find the required threshold force is to consider the equilibrium conditions of the fingers.

A differential is placed between the thumb and two finger, this is schematically depicted in Fig. 6.6. The counterclockwise torques on the fingers are represented as positive forces in Fig. 6.6b.

The differential is in moment equilibrium when the sum of the torques on the finger inputs equals zero: $T_{A,1} + T_{A,2} + T_{A,3} = 0$. The drive is placed between the thumb and the differential and a the direction of its output torque is defined positive when it counteracts the thumb: $T_D = -T_{A,3}$. As the differential is a “standard differential”, $T_{A,1} = T_{A,2}$. This results in the following equilibrium condition:

$$T_D = -T_{A,3} = 2T_{A,1} = 2T_{A,2} \quad (6.11)$$

Effect of Horizontal Accelerations This paragraph describes the effect of horizontal accelerations on the equilibrium condition of the hand. This will be done for positive and negative accelerations subsequently, while the hand is in a fully opened configuration.

When the hand accelerates with $\ddot{y} > 0$, the thumb tends to rotate counterclockwise (CCW) and the two opposing fingers tend to rotate clockwise (CW). To oppose these motions, a torque $T_{A,1} = T_{A,2} = \frac{l_x}{2} M_f |\ddot{y}|$ need to act on the two opposing fingers and a torque $T_{A,3} = -\frac{l_y}{2} M_f |\ddot{y}|$, as is indicated in red in Fig. 6.6. These torques can only be delivered by the endstops, as the equilibrium condition for the differential, $T_{A,1} + T_{A,2} + T_{A,3} = 0$, can never be satisfied.

When the hand accelerates with $\ddot{y} < 0$ in negative direction, the endstops itself can not oppose the unwanted motion. On the fingers an input torque $T_{A,1} = T_{A,2} = -\frac{l_x}{2} M_f |\ddot{y}|$ is required and on the thumb an input torque of $T_{A,3} = \frac{l_y}{2} M_f |\ddot{y}|$. This is indicated in blue in Fig. 6.6. When the drive would exert a torque with the value $-T_D = l_x M_f |\ddot{y}|$ no movements occur. The two opposing fingers are in force equilibrium, and the thumb is pushed unto its endstop. So to prevent the motion a threshold torque at the output of the should satisfy the following condition: $-T_{D,t} \leq l_x M_f \ddot{y}$. To make the mechanism more versatile the constraint is applied in a both positive and negative direction, which results in:

$$|T_{D,t}| \geq |l_x M_f \ddot{y}| \quad (6.12)$$

Numerical Evaluation The found criteria for the threshold is numerically evaluated, using estimated parameters based on the CAD-model.

Based on the CAD-model, the estimated mass of the finger is $M_f = 25$ g, and the estimated lengths are $l_x = 78$ mm and $l_y = 80$ mm. With an acceleration of $\ddot{y} = a_h = 14$ m/s², this evaluates to $|T_{D,t}| \geq 0.027$. This seems a reasonable value, as it is $\sim 2\%$ of $T_{D,max}$. The design of this threshold will be discussed later.

6.4 Discussion

The aim of this chapter was to derive the design requirements for the design of a prototype drive for an existing hand. But before these requirements are summarized in the conclusion, they are subjected to a critical reflection.

Regarding the grasp force one might object that the selection Delft Hand 3 might seem not a very good choice for this task, as the range of the object is reduced. Indeed, for the theoretical model, assuming a cylindrical object this is indeed true. Yet in practice, many objects are not cylindrical, but have a varying cross section, think of bottles, balls and screw drivers. The underactuated design of the hand enables it to constrain the object also by the shape rather than only the forces. For these objects the grasp force will be higher than the modeled force. As such, the gripper is likely to retain a larger range of object sizes than modeled. As already mentioned, the selection of a well documented existing hand enabled me to focus on the drive. Moreover, this hand was readily available at the laboratory, which saved even more time and efforts.

The apparent stiffness at the output drive is evaluated based on a rather broad range of values for the object stiffness. This is done because the aim of the hand is to be versatile and suitable for many different objects. For applications in industry the gripper may handle its whole lifetime the same product. For these applications it is advisable to make an estimate of the object stiffness and anticipate in the design of the buffer spring on this stiffness, as this likely saves energy.

The disturbance force is based on a simplified model of rigid link. This estimation is regarded as conservative, as the finger has a kind of tapered shape. This means that the CoM lies closer to the joint than modeled. The threshold prevents motion the finger joint does not rotate. In the finger a weak spring is integrated to keep the finger stretched and temporarily fixate the joint between the proximal and distal phalanx. In the evaluation of the grasp force this spring is neglected, as this spring force is small compared to the actuation force or torque.

6.5 Conclusion

This chapter aimed to identify the design requirements for a prototype drive which will be implemented in the Delft Hand 3. This hand will be mounted on the Plugless Arm, an extremely energy efficient pick-and-place robot arm. The resulting requirements to ensure this manipulator and hand are able fulfill their task are:

- The drive is a rotational device
- The maximum output torque of the drive is 1.4 Nm.
- The drive should be able to withstand a disturbance torque of 0.027 Nm.
- The drive should be able to cope with an object stiffness ranging from 3.73 Nm/rad to 197.1 Nm/rad.

Chapter 7

Typology Selection

7.1 Introduction

In the Chapter 5 a topology was defined, which describes how the different components of the drive should be connected. Nonetheless, the *typology* of the components is not yet decided. For instance, the SBFA could be implemented as a lever mechanism or a cam mechanism. This section will select the embodiments for the subsystems of the drive, such that they result in a compact rotational device, as is specified by the design requirements of Chapter 6. The typology of the SBFA, carriage locker, non-backdrivable mechanism and the differential will be discussed subsequently in sections Sections 7.2 to 7.5. The results will be discussed in Section 7.6. The chapter is concluded in Section 7.7.

7.2 SBFA

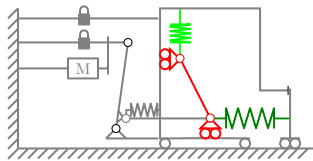


Figure 7.1: Balancer Subsystem.

One of the “core-components” of the drive is the Statically Balanced Force Amplifier. This subsystem is highlighted in color in Fig. 7.1. This section will briefly describe the topology selection of the SBFA.

This selection based on an outdated design insight. Initially, one of the criteria related to the maximization of the stroke, as this reduced the *relative* amount of work. Ultimately this was falsified as the *absolute* amount of work determines the energetic performance. Because this was discovered relatively late in the design process, the typology of the SBFA was not re-evaluated. Appendix F.1 elaborates on the typology selection and the changing design insight. The consequences are discussed in the discussion, Section 7.6.

As described in Hoeven’s master thesis [45], a statically balanced mechanism could be obtained as a compliant or rigid-body mechanism. The advantage of a compliant mechanism is that the friction between various components is eliminated. Drawbacks are that these mechanisms still dissipate energy due to hysteresis and it *approximates* the balanced condition. In rigid body mechanisms, friction might occur, but the balancing condition can be derived in an analytic way. He concluded that a rigid-body mechanism resulted in a more compact balancer with a better force reduction. Based on this results, a rigid-body SBFA is selected.

Hoeven divided the balancers in two categories: *cam-based* a *linkage-based*. For linkage-based balancers he showed that only the one with two orthogonal translating springs is a viable solution, under a given set of assumptions that ensures a simple and compact design. In chapter 6 was decided that the mechanism should be a rotational device. This leaves the cam-based mechanisms.

The selected embodiment is a rotational cam connected to the main spring. Upon this cam engages a rotational follower.

7.3 Carriage Locking Mechanism

This locking mechanism, highlighted in Fig. 7.2, has to lock the relative motion between the carriage and the ground once the drive enters the forcing mode.

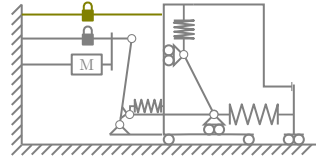


Figure 7.2: Carriage Lock subsystem

7.3.1 Selection Criteria

For the design of the locking mechanism, the following criteria are compiled:

1. *Many locking positions*: The required locking position of the carriage is dependent on the size of the object. As shown in chapter 4, a position error with respect to this required position results in a balancing imperfection. Therefore the carriage should be locked as close as possible to the required position. Hence, the locking mechanism should have a fine resolution, i.e. many locking positions.
2. *Low energy consumption*: Ideally, the locking mechanism should not consume much energy, because the goal of this thesis is to develop an energy-saving drive.
3. *Compact*: Ideally the locking mechanism is compact. This ensures the locking mechanism can be easily integrated in the drive and is probably lightweight, which is beneficial for the performance of the drive in terms of speed and mass.

7.3.2 Locking Mechanisms

Plooij et al. [27] provide an extensive overview on locking mechanisms. They use two different categorizations to classify the locking mechanism.

The first categorization is already discussed in Chapter 4, it distinguishes *active* and *passive* mechanisms. The second categorization distinguished locking mechanisms based on three working principles, which are explained subsequently.

7.3.2.1 Mechanical Locking Mechanisms

These mechanisms rely on the position of a mechanical component that determines whether the locking is (dis)engaged, for instance a ratchet wheel with a pawl. Most mechanisms have just a few locking positions, except for ratchets and hydraulic locks. Because they are relatively simple to realize, they are typically compact, small and lightweight. They have typically a low energy consumption, because for even the active variants, the only thing the actuator has to do is to momentarily change the position of the blocking component.

7.3.2.2 Friction Locking Mechanisms

These mechanisms rely on friction to lock the relative motion. Friction locks have typically an infinite number of locking positions, as the friction pad can engage anywhere in the motion range. The locking force/torque is limited by the delivered normal force, which requires large internal forces in the mechanism. Hence, these mechanisms are relatively large and heavy. For state of the art mechanisms, such as the brake that employs a SBFA [24], the energy consumption is low, although this is a fairly complex mechanism.

7.3.2.3 Singular Locking Mechanism

These mechanisms exploits the singular position of a mechanism to lock the relative motion. As the singularity typically arises in just one configuration, the number of locking positions is just one. They are also relatively simple to realize, but are typically larger than mechanical locking mechanisms. They also have a low energy consumption.

7.3.3 Comparison

Table 7.1 summarizes the performance of the three working principles of locking mechanisms.

Table 7.1: Comparison of Locking Mechanisms for Carriage Lock

Criteria	Mechanical	Friction	Singular
1 Many locking Positions	± Most mechanisms have a few locking positions, except for ratchets and hydraulic locks	+ Infinite number of locking positions as friction pad can engage anywhere.	- Singularity typically arises just at 1 or 2 configurations
2 Low Energy Consumption	+ Even for active mechanism almost no energy consumption is required	+ For state of the art mechanisms the energy consumption is low.	+ Low
3 Compact	+ Typically small	- Typically large and heavy, as a large normal force is required	± Typically larger than mechanical lockers

Based on Table 7.1 the mechanical locker is selected as locking mechanism, as it has with two good scores and one average score, the best overall score. According to [27] there are two types of mechanical lockers with more than a few locking positions: Hydraulic lockers and ratchets.

Although hydraulic lockers have an infinite number of locking positions, their implementation might be challenging, as for instance proper sealing is required. Ratchets are much simpler to realize and still allow for a large number of locking positions. Therefore a ratchet is selected as locking mechanism for the position of the carriage.

7.4 Non-Backdrivable Mechanism

The second locking mechanism is a NBDM that relieves the motor from the static load, which might for instance arise due to balancing imperfections. This mechanism is highlighted in Fig. 7.3. Similar to the carriage locking mechanism, the three working principles identified by [27] are compared to find the viable working principle. To do so, the selection criteria are formulated. Then the NBDMs of the three categories are described, followed by a selection of a viable one.

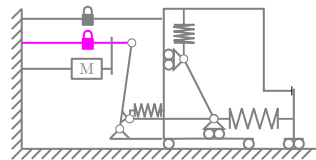


Figure 7.3: Non-Backdrivable Mechanism subsystem

7.4.1 Selection Criteria

The following selection criteria are formulated for the selection of a typology of locking mechanism for the NBDM:

1. *Many Locking Positions* The resolution of the NBDM determines the resolution of the output force, because the NBDM locks the extension of the spring once the motor is deactivated. A large number of locking positions enables a fine resolution in the output force, which improves the mechanism's ability to deliver any desired output force.

2. *Bidirectional* Beforehand it is not known in which direction the forces arising from the balancing imperfections act, hence the mechanism should be able to block the motion in both directions.
3. *Low Energy Consumption* Because the goal of this thesis is an energy saving drive, the locking mechanism should not consume much energy.
4. *Compact* A compact locking mechanisms is likely to reduce the mass and inertia of the drive, which is beneficial for the performance of the drive in terms of speed and mass.

7.4.2 Possible Locking Mechanisms

The three working principles for locking mechanisms are now assessed.

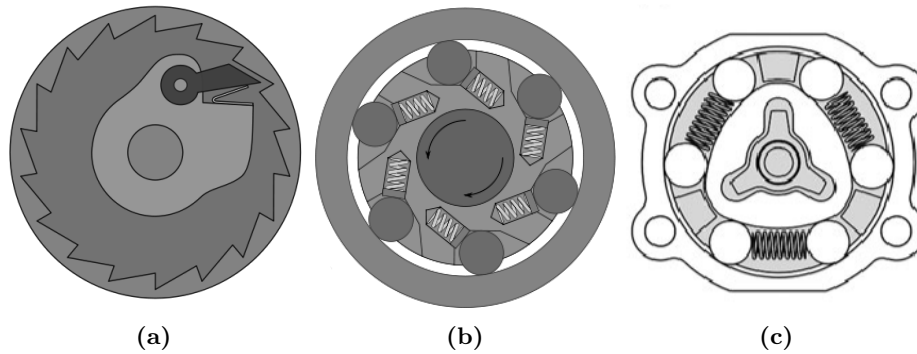


Figure 7.4: Nonbackdrivable mechanisms. **a:** Ratchet freewheel. Image adapted from [54]. **b:** Friction freewheel. Image adapted from [54]. **c:** Advanced friction freewheel, for bidirectional use. Image taken from [22]

7.4.2.1 Mechanical Locking Mechanisms

In [27] one mechanical locking mechanism is reported that can act as NBDM: a passive ratchet, also known as freewheel. See Fig. 7.4a. The pawl is loaded by gravity or a spring and permits the ratchet to move in just one direction. As soon as the motion direction changes the pawl blocks the motion. Ratchets can be employed as compact mechanisms [27], and as it is passive it has a low energy consumption.

7.4.2.2 Friction Locking Mechanisms

A first way to obtain a non-backdrivable mechanism based on friction is a non-backdrivable gearing, such as a wormwheel or lead-screw. These mechanisms have an infinite number of locking positions, are bidirectional and are typically very compact. A drawback is that these mechanisms have a relative poor efficiency when they are disengaged.

Another type of nonbackdrivable mechanisms is an overrunning clutch, which works basically the same as the ratchet described in the previous paragraph, except that the friction is employed to block the motion. An example is depicted in Fig. 7.4b. This mechanism relies on cylindrical rollers between a wedged innerring and a smooth outer ring. These rollers jam when the mechanism moves in a certain direction. An advanced form of these overrunning clutches is reported by e.g. [21, 22] and depicted in Fig. 7.4c. The advantage of these mechanisms is that they are bidirectional, contrary to the conventional overrunning clutches. The designs of [21, 22] are relatively compact, but still slightly larger than the ratchet [27]. The energy consumption is low, as efficiencies are reported of 95% [21]. These mechanisms have an infinite number of locking positions.

7.4.2.3 Singular Locking Mechanisms

When a singular locking mechanism is in its singular configuration, the transmission ratio between the input force and the blocked force is infinite. Hence, theoretically an infinite small input force is able to block an infinite large force on the output. These mechanism are bidirectional and require a low energy consumption. An important drawback is that these mechanisms have typically just 1 or 2 locking positions, which makes it unsuitable as non-backdrivable mechanism.

7.4.3 Comparison

Table 7.2 provides an overview on the performance of the various working principles.

Table 7.2: Comparison of NBDMs for Cancellation of Motor Static Load

Criteria	Mechanical			Friction		Singular		
	Ratchet			NB Gearing	Overrunning Clutch			
1 Many locking Positions	±	Finite number	+	Infinite number	+	Infinite number	–	1 or 2
2 Bidirectional	–	Monodirectional due to tooth geometry	+	Always bidirectional	+	Bidirectional for advanced models	+	Bidirectional
3 Low Energy Consumption	+	Low energy consumption due to passive design	–	Poor efficiency for unlocked mechanism	+	High efficiencies (~ 95%) reported for unloked mechanism in [21])	+	High efficiency
4 Compact	+	Very compact according to [27]	+	Very compact according to [27]	±	Medium compact according to [27]	±	Medium compact according to [27]

The singular and mechanical based locking mechanism are not feasible as they have respectively just a few locking positions or are not bidirectional. This leaves the friction based lockers, of which the advanced overrunning clutch scores better than the non-backdrivable gearing, since it has a better efficiency. Therefore, an overrunning clutch is selected as NBDM to relieve the motor from the static load.

7.5 Differential

The differential resolves the motor input in two outputs for sizing and forcing respectively. In this subsection the selection of a suitable differential is covered.

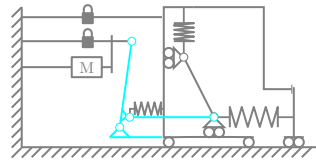


Figure 7.5: Differential subsystem.

7.5.1 Selection criteria

The following selection criteria are applicable for the selection of a suitable differential.

- *Efficient* To comply with the main goal of this thesis, the reduction of the energy consumption of the gripper drive, the transmission should have a large efficiency.
- *Manufacturable* The differential should be easily realized, hence purchasing a stock component is preferred over a custom manufactured one.

7.5.2 Description of Differentials

In [38] an overview is given on differentials commonly used in robotic hands, but there are much more possibilities than they report. In fact, a differential is a generalized form of a transmission [28]. This implies that any transmission can be used as differential by replacing its connection to the ground with a moving output. To reduce the number of possibilities to evaluate, only differentials with coaxial rotational in- and outputs are considered, as this complies with the rotational build form. Planetary gears, cycloid drives and harmonic drives are where found in this category.

7.5.2.1 Planetary Gear

Planetary gears are commonly applied in robotics. They are widely available as stock components. An efficiency of ~ 90% per stage is typical [55] for the size of gears applied in robotics, although higher

efficiencies, in the range of $\sim 97\%$ are also claimed [56]. For a reduction ratio of $i = 100$ typically three stages are required [55], this complies with the reported values for a single stage in the range of $i = 3$ to $i = 7$ [56], which results in an overall maximum gear efficiency of 92% [56].

7.5.2.2 Cycloid Drive

An example of a cycloid drive, depicted in Fig. 7.6, relies on a cam mounted on an excenter. The lobes of the cam rolls along a set of rollers, which results in a reduced rotational speed of the cam. This rotation is transmitted by a set of pins and holes to an output shaft.

Although Cycloid Drives are available as stock components, they are typical used for industrial applications with a nominal torque ration of $> 10 \text{ Nm}$ [57, 58]. I could not find miniaturized versions. In [59] an efficiency of 71% is measured for custom cycloid drives with ratios of $i = 100$. In the commercial available versions efficiencies of $70 - 92\%$ are reported [57, 58]. Interestingly this efficiency is the smallest for the smallest transmissions, which suggests that miniaturization is indeed difficult.

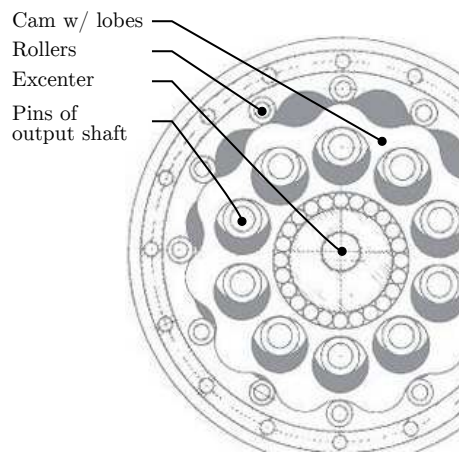


Figure 7.6: Cycloid drive. The cam with lobes is driven by an eccentric input shaft. This results in a reduced rotation of the cam, which is transmitted to an output shaft by means of pins that go trough the holes in the cam.

7.5.2.3 Harmonic Drive

Miniaturized versions of harmonic drives are commercially available [60] and employed in robotics, for instance in [36]. [59] reports efficiencies in the range of $67 - 79\%$ for harmonic drives with a ratio of $i = 100$.

7.5.3 Comparison

An overview of the performance of the three differentials is given in Table 7.3. From this table it follows that a planetary gear is preferred, as it has the highest efficiency and miniaturized versions are commercially available.

Table 7.3: Comparison of Differentials

Criteria	Planetary Gear	Cycloid Drive	Harmonic Drive
Efficient	+ 92% for a ratio of $i = 100$. [56]	- 71% for a ratio of $i = 100$. [59]	\pm 67 - 79% for $i = 100$ [59].
Manufacturable	+ Stock parts commercially available	- No miniaturized commercially available	+ Stock parts commercially available

7.6 Discussion

The typology selection is based on selection criteria. As already mentioned, the formulation and evaluation of these criteria is subjected to some subjectivity. Again, I explained all criteria and ratings, in order to make the process transparent.

A greater issue is the selection of the SBFA embodiment based on an outdated design insight. As this outdated design criteria was only relevant for one of the two selection criteria, the other one is still valid. When the options are compared only on this second criteria, just two possibilities are left, both consisting of a rotational cam and follower, but only with the swapped connections to the springs. This implies that indeed rotational cams and follower should be used, although the best location is not yet known. Based on this reasoning I think the impact of this advancing insight is not very serious, as it does not imply a completely different embodiment.

7.7 Conclusion

For the various components of which the mechanism exists an embodiment was selected. For the SBFA this was a rotational cam with rotational follower. For the carriage locking mechanism this is a ratchet, as it has many locking positions, has a low energy consumption and is compact. For the non-backdrivable mechanism this a friction overrunning clutch is selected, as it scores well on the same three criteria as well as it is suitable for bidirectional use. A planetary gear is selected as differential, as they are widely available and have a high efficiency.

Chapter 8

Detailed Design

8.1 Introduction

Now that the typology and topology selected are completed, one design step remains: the detailed design, in which the dimensions of the components are determined. The focus of this chapter is to explain the basics of the functionality and the important principles. More details are incorporated in appendix G.

Before the design of all subsystems can be explained, it need to be explained how these subsystems cohere in the design of the drive. This overall working principle is addressed in Section 8.2.

The sections Sections 8.3.1 to 8.3.6 are each dedicated to one of the subsystems. In Section 8.3.1 the design of the carriage lock will be discussed as it is largely dependent on practical considerations and its resolution determines the positional error. With the knowledge of this error the spring stiffness of the balancer can be determined. This is addressed in Section 8.3.2. Then the design of the third subsystem, the differential, is discussed in Section 8.3.3 as it determines the diameter of the mechanism together with the first two subsystems. Section 8.3.4 discusses the threshold mechanism. The design of the NBDM is discussed in Section 8.3.5, followed by a description of the feedback of the mechanisms in Section 8.3.6. Although in the subsystems are discusses subsequently, in the design process they are designed more or less simultaneously, as all subsystems have a large influence on each other.

The realized prototype is presented in

The design is discussed in Section 8.5. A conclusion follows in Section 8.6.

The primary aspect of this thesis, the ability to save energy, is also the leading aspect in the detailed design of the prototype. The secondary aspect in the design is the manufacturability, to ensure a *working* proof of principle is obtained. This also includes the limitation to use stock components and materials (Al 7075 and RVS 304) as much as possible. The ternary aspects are the mass and compactness.

8.2 Global Description

Before the detailed design of the various subcomponents is discussed, it is important to understand how these components cohere in the overall design. As such, this section is dedicated to a global description of the prototype. This falls apart in two parts. First the overall working principle will be explained, followed by a summary of some specifications.

8.2.1 Working Principle

The prototype functions the same as the example explained in Section 5.5, except the motions are rotational instead of translational. For simplicity the schematics of this translational example and a cross-sectional view of CAD model of the rotational prototype are depicted side by side in Fig. 8.1. The different components are color-labeled in both images. For instance, the buffer springs are in both figures light green and the non-linear transmission red.

The mechanism consists of a housing, depicted in grey, in which the blue carriage and orange output shaft are suspended with ball bearings. In the center of this blue carriage the red cam shaft is mounted with ball bearings. A balancing cam and threshold cam is mounted on this shaft. At the end of this shaft the main spring is mounted. Around this central shaft multiple shafts are suspended in the carriage, which

are equipped with spring loaded followers of the cams. Three paragraphs will explain how the prototype achieves its three subfunctions: sizing, switching and forcing.

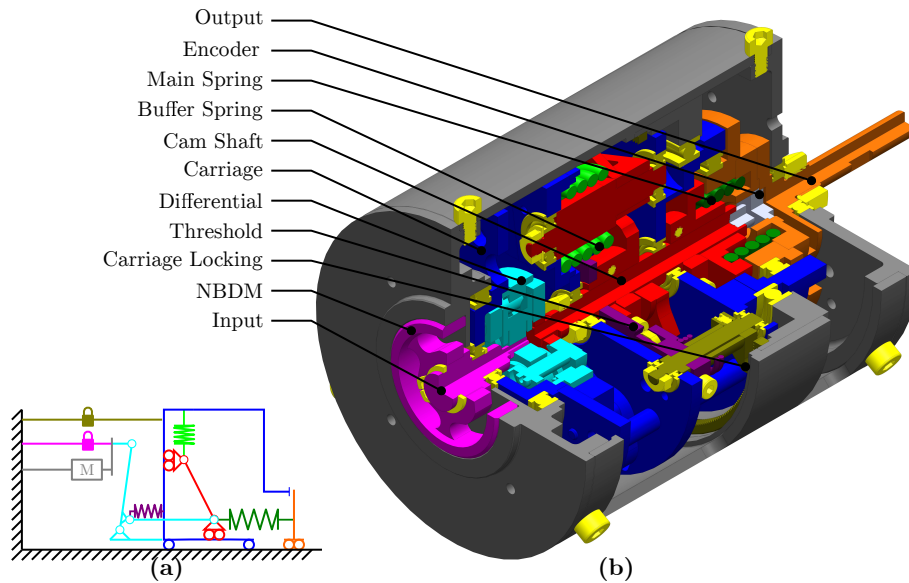


Figure 8.1: Working principle of prototype. The components of both subfigures are labeled with the same colors. **a:** Schematic example of a translational mechanism. **b:** Cross-sectional view of CAD-model of prototype. The yellow parts in this subfigures are fasteners and bearings. Note that the motor is not depicted.

8.2.1.1 Sizing

During sizing the input and output move synchronously. The pretension of the non-linear spring characteristic of the threshold is realized by the purple spring loaded cam mechanism and constraints a relative movement between the blue carriage and red cam shaft. As consequence, the blue carriage and red cam shaft rotate with the same speed. An endstop transmits this motion from the blue carriage to the orange output shaft.

8.2.1.2 Switching

Once the hand encounters the object, the motion of the orange output shaft is blocked. The endstop prevents also rotation of the blue carriage. Once the motor has overcome the pretension of the purple threshold mechanism, the red cam shaft starts to rotate with respect to the blue carriage. A reduced speed of this shaft is realized using the lightblue differential. Consequently to this motion, the green main spring starts to exert a torque on the output. Besides, the motion of the threshold cam follower causes the engagement of the olive-green carriage locking mechanism.

8.2.1.3 Forcing

Once the position of the blue carriage is locked, the mechanism is in the forcing mode. The lightblue differential reduces the input motion, resulting in a rotation of the red cam shaft. The rotation of this shaft tensions the dark-green main spring. Theoretically no force is required to do so, as the lightgreen buffer springs counteract the main spring torque. The NBDM enables the mechanism to maintain the torque level once the motor is deactivated, as it prevents balancing imperfections to cause rotations.

8.2.2 Specifications

To gain insight in the size and weight of this mechanism, the basic dimensions and properties are listed in this subsection.

- Outer Diameter Housing: 64 mm
- Length Housing: 75.5 mm
- Estimated weight in CAD-model: 460 g

8.3 Design of Subsystems

8.3.1 Carriage Locking Mechanism

The carriage locking mechanism, depicted in Fig. 8.2, has to lock the blue carriage with respect to the grey housing. This locker consists of a ratchet and two pawls. The ratchet is glued to the housing. The two pawls are mounted on two different shafts, which are supported by the carriage frame. The pawls are (dis)engaged by a rotation of the shaft, which is caused by the threshold mechanism. This section will describe briefly the detailed design of this locker. More details are incorporated in appendix G.

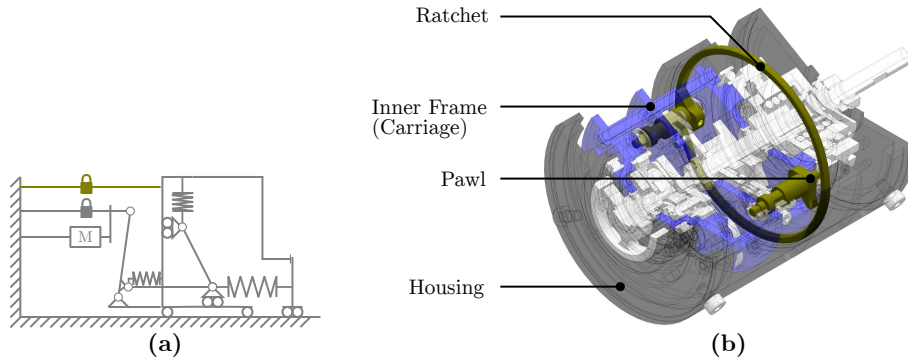


Figure 8.2: Carriage locking subsystem. **a:** Schematic. **b:** Cross-sectional view of CAD-model. The olive green ratchet locks the motion between the blue transparent inner frame and the dark grey housing.

The ratchet and pawls are made of 301 stainless steel, by means of respectively wire-EDM and water-cutting.

The resolution of the ratchet determines the position error and should therefore be as fine as possible. This resolution is dependent on the inner ratchet diameter and the tooth size. The inner diameter of 54 mm is determined simultaneously with the design of the balancer and gearbox to obtain a compact design. The pitch, i.e. the distance between the teeth, is determined based on practical considerations. This resulted in a teeth number $Z = 300$ and thereby a resolution of 1.2° . The teeth width of 2 mm and the teeth-geometry is in accordance with the guidelines of [61]. The mechanical strength is validated using a Finite Element Analysis (FEA).

The stroke to engage the ratchet is 6° . The first 1.5° overcomes a safety margin between the pawl and teeth. The subsequent 4.5° is required to move the pawl from the position where it just touches the tooth to where it fully engages. The latter portion of the motion is self-engaging, which means that the mechanical design ensures that once the ratchet and tooth make contact, the pawl will move automatically to the engaged position.

8.3.2 SBFA

The balancer is depicted Fig. 8.9. The balancer enables effortless tensioning of the main spring. It consists of a cam with two followers, with ball bearing as rollers. The followers are position axisymmetric, such that they cancel out the reaction forces on the shaft. The cams and followers are mounted on dedicated shafts, which are all connected to the carriage with ball bearings. A helical torsion spring is placed coaxial with these shafts and exert torques between the followers and carriage. This section will describe the selection of the springs and the realization of the non-linear transmission using a cam.

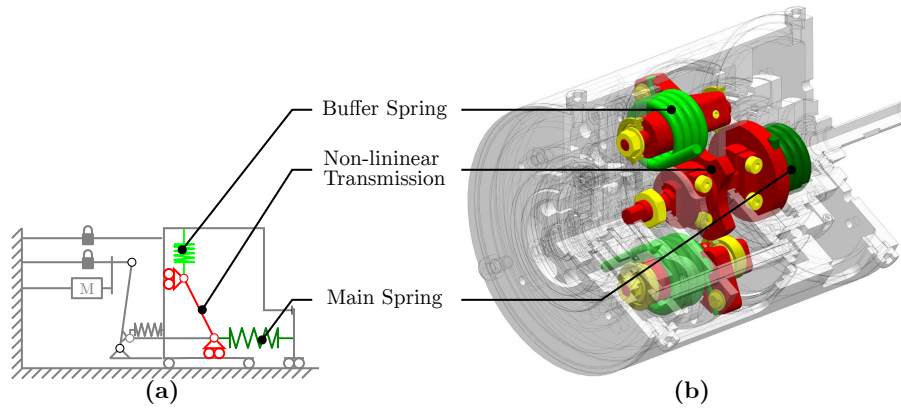


Figure 8.3: SBFA subsystem. **a**: Schematic **b**: Cross-sectional view of CAD model.

8.3.2.1 Spring Selection

The spring selection consists of three steps. The first step is to find the desired spring stiffness based on the design metrics of Chapter 4. The second and third step are to select suitable springs from a catalog as main spring and buffer spring.

Desired Stiffness In Chapter 4 two design metrics were provided which describes the required work and force reduction for a stiffness range, force range and error range. These metrics will be applied to find the desired stiffness of the main spring.

For the numerical evaluation of the design metrics, the following parameters are used: As summarized in Section 6.5 the maximum output torque equals $T_{M,max} = T_{D,max} = 1.4$ Nm and the stiffness range equals $k_O \in [3.73, 197.1]$ Nm/rad. The maximum error equals the resolution, which is 1.2° as described in the previous subsection.

In Fig. 8.4 the two design metrics are plotted versus the maximum stroke of the mechanism. This means that the average balancing error is at most 5 % of the output torque. This result in a stroke $s_{M,max} \geq 35^\circ$ and a stiffness of $k_M \leq 0.04$ Nm/ $^\circ$. The stroke should be not much larger than this, as this will increase the required work. This bounds will be used in the next step to select the main spring.

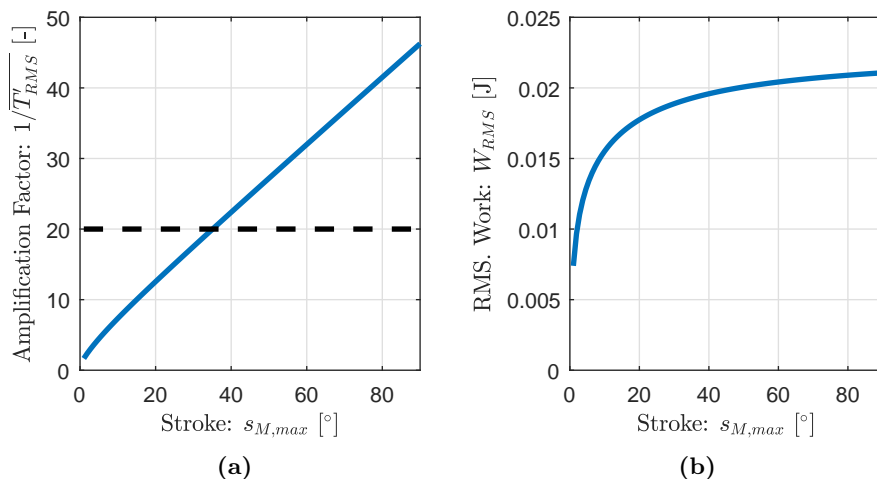


Figure 8.4: Design Metrics **a**: Amplification Factor. The lower limit of 20 is indicated by the dashed line. **b**: RMS Work

Main Spring Selection The design of the springs was limited to off-the shelf components to ensure fast realization of a prototype. The spring selection is done as follows: A database of springs was created. Based on several selection criteria the feasible springs were selected and their external dimensions are

visualized in graphs. Based on these graphs the springs that resulted in the most compact design where selected.

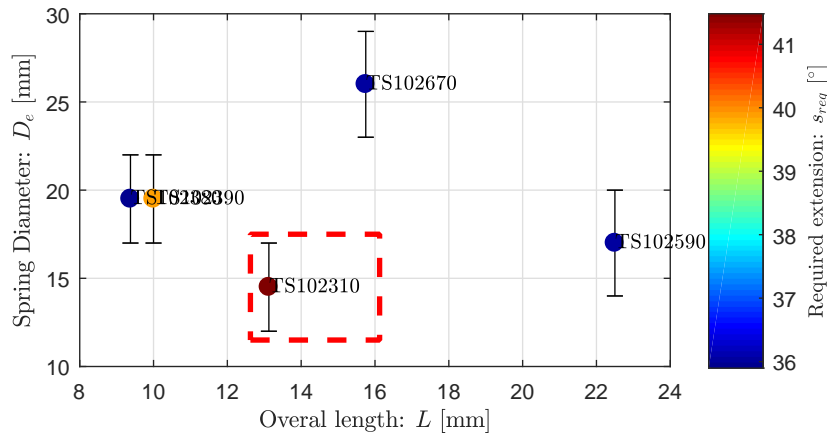


Figure 8.5: Main Spring Selection. The red dashed box indicates the selected spring.

It was assumed that a single catalog per spring type would provide enough options for the design. For the helical springs, the catalog of Tevama [62] was loaded in the database. For the spiral springs, the catalog of Lesjofors [63] was loaded.

The main spring has to produce a torque of $T_{M,max} = 1.4$ Nm with a stroke of at least 35 degrees, but ideally not much larger. For each spring of the database the required extension s_{req} is evaluated to achieve the desired torque, using:

$$s_{req} = T_{M,max}/k_s \quad (8.1)$$

Where k_s is the stiffness of the inspected spring. The required extension should satisfy the following two constraints:

$$35^\circ \leq s_{req} \leq 1.25 \cdot 35^\circ \quad (8.2)$$

$$s_{req} \leq s_{s,max} \quad (8.3)$$

Where $s_{s,max}$ is the rated maximum stroke for a lifetime of 10,000 cycles. Fig. 8.5 provides an overview of the smallest springs from the database that satisfy these conditions. The mean diameter and length is depicted by a scatter plot. The color indicates the required extension s_{req} . The error bars indicate the inner and outer diameter of the required space to mount the springs.

Ultimately the following spring was selected: TEVEMA TS102310 as it has the smallest external diameter. The spring is used for a stroke $s_{M,max} = 41.5^\circ$ to obtain a torque $T_{M,max} = 1.4$ Nm.

Balancing Spring Selection The buffer springs have to balance the main spring. This paragraph describes the selection of this balancer springs. Similar to the main spring, the balancer springs are selected to satisfy certain constraints.

Two balancing springs are preferred over one, as this enables a axisimetrical embodiment in which the reaction forces on the main shaft are canceled out. This results in smaller bearings and less friction in these bearings. The balancing springs must be able to store together at least the same amount of potential energy as the balancing spring, as static balancing implies a 100% energy exchange between the buffer and main springs [23]. Moreover, the required extension to store this energy should less than 90° to ensure the follower works in only one quadrant which is required for a good cam design. This results in the following two criteria:

$$s_{reg} \leq s_{max} \quad (8.4)$$

$$s_{reg} < 90^\circ \quad (8.5)$$

Where s_{max} is the maximum extension specified by the manufacturer for a lifetime of at least 10.000 cycles. s_{req} is the required extension to store enough energy, expressed by:

$$s_{req} = \sqrt{\frac{T_{M,max}(s_{M,max} + s_{M,safety})}{N_s k_s}} \quad (8.6)$$

Where $T_{M,max}$ and $s_{M,max}$ are properties of the selected mains spring, $N_s = 2$ the number of buffer springs and k_s the spring stiffness of the investigated spring. To incorporate a safety margin of $s_{M,safety} = 3^\circ$ to avoid the singular positions, this margin is added to the maximum extension of the main spring.

The smallest springs that satisfy these conditions are plotted in Fig. 8.6. The TEVEMA TS102310 is also selected as buffer spring. The use of two identical springs reduce the change of balancing imperfections due to variations in the spring stiffness. When the actual stiffness varies from the specified value, this will likely occur for both spring. Consequently, the effect is canceled, as Eq. (4.3) shows that the transmission depends on the ratio of the spring stiffness and buffer spring stiffness k_M/k_B . This advantage outweighs the fact that although the spring is relatively small compared to many of its competitors, it is not the smallest spring possible.

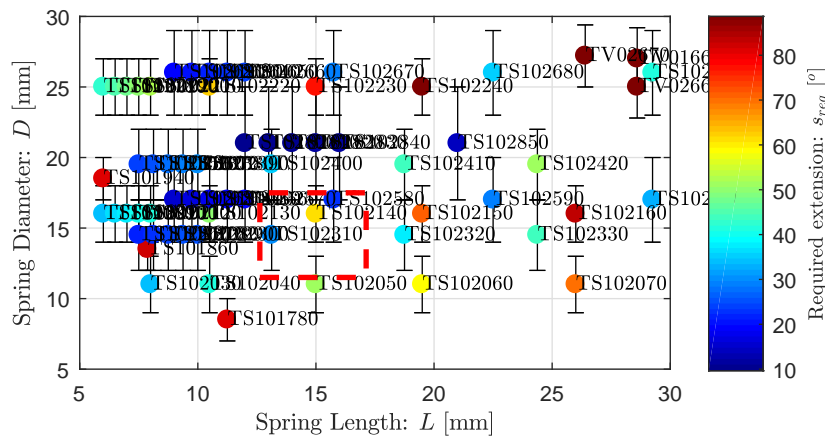


Figure 8.6: Buffer Spring Selection. The red dashed box indicates the selected spring.

8.3.2.2 Cam Geometry

The non-linear transmission ratio between the main and buffer springs is realized with a cam mechanism. First the desired trajectory for the rotation of the cam follower is derived. This trajectory is then used to generate a cam geometry, using a procedure similar to [64]. During this process it should be taken into account that the contact force between the cam and follower should not exceed the static load rating of the bearing, which is verified using a static analysis.

Follower Trajectory In Chapter 4 the extension of the balancing was expressed as function of the extension of the main spring. This relation is used to express the desired trajectory of the follower. The angle ψ_M describes the cam rotation. Because one end of the main spring is attached to the cam, the main spring extension equals ideally the cam rotation: $s_M = \psi_M$.

The angle of the follower is denoted by $\psi_B = s_B + \psi_{B,0}$, where $\psi_{B,0}$ is the angular position for which the balancing spring is at rest and s_B the extension of the buffer springs, which follows from Eq. (4.3). This is indicated in Fig. 8.7. Note that the balancing spring stiffness k_B in this equation needs to be multiplied with the number of balancing springs N_s , because the buffer springs act parallel. To avoid the singular configuration, the buffer spring is designed for a main spring with a stroke that is $s_{M,safety}$ larger than required for the output for the output of 1.4 Nm. Hence the singularity condition would occur for a main spring extension of $s_{M,max} + s_{M,safety}$, which is beyond the motion range of the mechanism. As such, this singularity is prevented. To ensure the mechanism is still balanced, $s_{M,max}$ is replaced with

$s_{M,max} + s_{M,safety}$ in equation Eq. (4.3). This results in:

$$\psi_B(\psi_M) = \sqrt{\frac{k_M \left((s_{M,max} + s_{M,safety})^2 - \psi_M^2 \right)}{N_s k_B}} + \psi_{B,0} \quad (8.7)$$

The cam geometry has to achieve this trajectory.

Cam Geometry The procedure to convert the desired trajectory in a cam geometry is inspired by Tsay and Lin [64]. The basic idea is that the angle trajectory of the follower can be converted in a path of the center of the roller of the follower. The cam geometry follows from a coordinate transformation of this path to a *rotating* local coordinate frame. This results in the following expression for the cam geometry in the local coordinate frame, spanned by the \hat{x} and \hat{y} axes:

$$\hat{\mathbf{S}} = \begin{bmatrix} S_{\hat{x}} \\ S_{\hat{y}} \end{bmatrix} = \begin{bmatrix} a \cos \psi_M - \cos(\psi_B(\psi_M) + \psi_M) \\ -a \sin \psi_M - b \sin(\psi_B(\psi_M) + \psi_M) \end{bmatrix} - \hat{\mathbf{n}} r_b \quad (8.8)$$

Where a and b are properties of the cam as depicted in Fig. 8.8a; r_b is the radius of the roller and $\hat{\mathbf{n}}$ the normal vector of the cam surface, as expressed in appendix G.

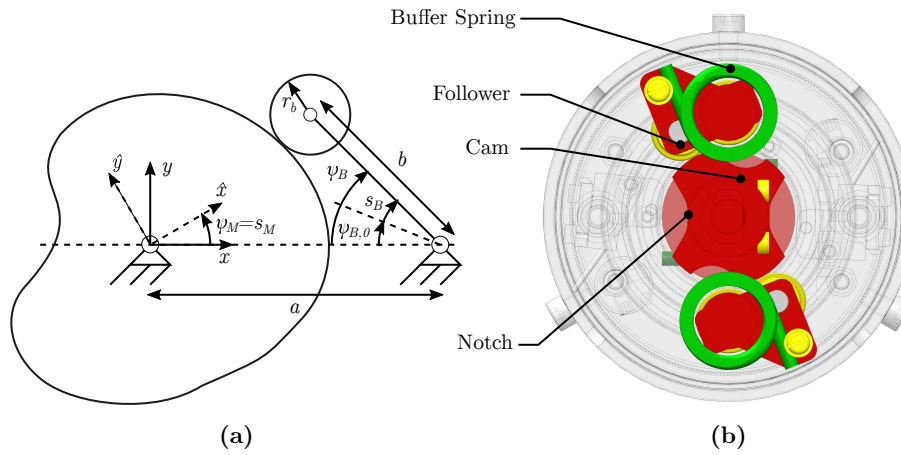


Figure 8.7: Cam Geometry. **a:** Design variables for cam. **b:** Realized cam in CAD model.

Static Analysis A static analysis is conducted to verify the contact force, as this load should be positive and not exceed the rated bearing load.

As the follower is a roller bearing, the friction is negligible. As such, the contact force is equal to the normal force. A static analysis, described in detail in appendix G results in the following expression for this normal force:

$$F_N = \frac{T_B}{(n_y b \cos \psi_B + n_x b \sin \psi_B)} \quad (8.9)$$

Where n_x and n_y are the components of surface normal vector at the contact point, defined in the global frame. This normal force should be positive but not exceed the static load rating of the bearing that functions as follower roller.

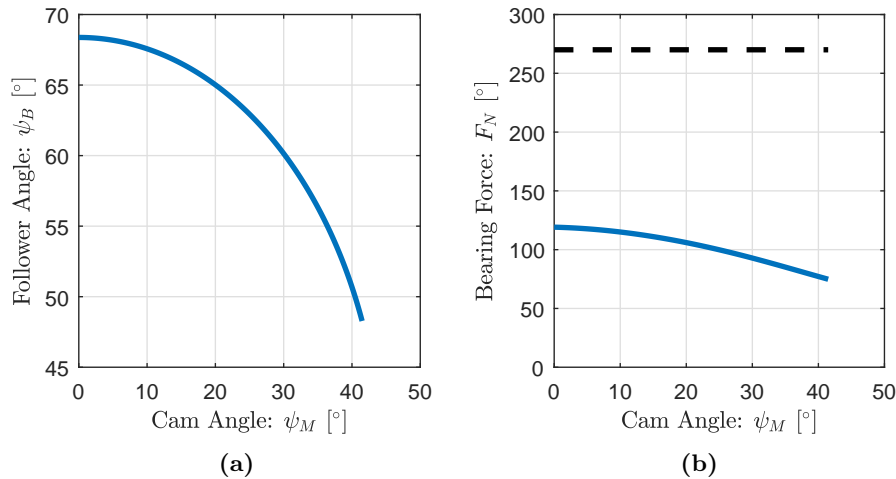


Figure 8.8: Properties of the follower. **a:** Follower trajectory **b:** Normal fore between the cam and bearing. This force should not exceed the static load rating of the bearing, indicated by the dashed line.

Resulting Cam The above equations are used in several design iterations. The resulting design is shown in Fig. 8.8. $a = 18$ mm to provide enough space for the planetary gear. With the help of numerical optimization it was found that a value of $b = 9$ mm and $\phi_{B,min} = 36.9^\circ$ in combination with a NSK MR104 bearing as follower ensures the the normal force is positive and does not exceed the static load rating of the bearing. The resulting trajectory is plotted in Fig. 8.8a and the bearing force is plotted in Fig. 8.8b.

The springs need to be at rest for a follower angle $\psi_B = \psi_{B,0}$. A notch that corresponds to this follower angle is incorporated in the cam geometry. This notch is used to define the rest position of the buffer springs while they are mounted.

8.3.3 Differential

The differential, realized with a planetary gear, distributes the single motor input over two inputs. The aim of this subsection falls apart in two goals: First, a selection is conducted of one of the six possible permutations of how the tree in- and outputs are connected to its surrounding components. Second, the selection of a suitable planetary gear. In addition, the general equilibrium condition of the differential is discussed, as this is relevant for the design of the threshold.

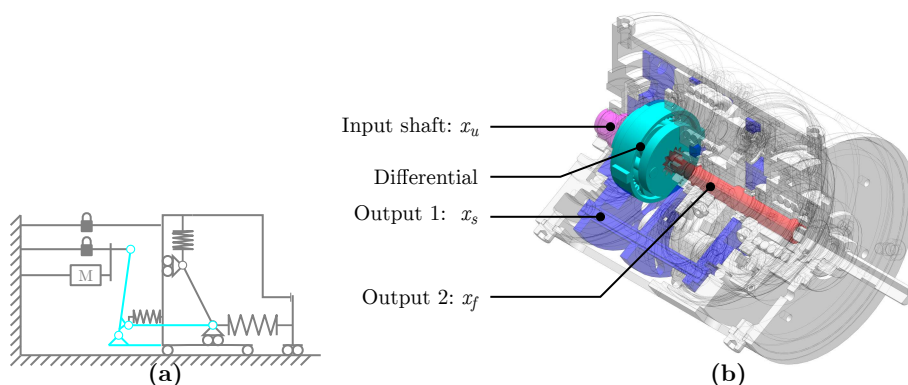


Figure 8.9: Differential subsystem. **a:** Schematic **b:** Cross-sectional view of CAD model. The lightblue planetary gear acts as differential and resolves the motion of the pink transparent input shaft in a motion of the blue inner frame and the red cam shaft.

8.3.3.1 Planetary Gear as Differential

In the typology selection a planetary gear was selected as differential. Because the differential has three in- and outputs, there are six different permutations possible for the connections to the environment, resulting in different transmission ratios. Although in appendix G an elaborate analysis is conducted to select the best one, this can also be explained in an intuitive way.

Typically miniature planetary gear stages are employed with the outer ring fixed and the sun as inputs. The reduction ratio i_{Diff} of the gear is specified for this condition. Arguably, they are optimized to obtain the highest ratio in the smallest volume. This implies that the most compact way to realize a reduction during forcing i_2 is to use the sun gear as input and keep the ring gear fixed. This can be achieved by mounting this outer ring to the carriage, as the carriage is fixed during forcing. The output is connected to the cam shaft. This reduction ratio equals then the gear ratio: $i_2 = i_{Diff}$. During sizing the carriage and cam shaft move simultaneously, which means that the internal parts of the gear does not rotate and the transmission ratio $i_1 = 1$. Consequently, the normalized ratio equals $\iota = i_2/i_1 = i_{Diff}$. An elaborate analysis of the kinematics in appendix G confirms indeed that this is indeed the best permutation. From this analysis also follow that the coefficients $a_1 = 1 - i_{Diff}$ and $a_2 = i_{Diff}$.

8.3.3.2 Selection of Differential

The second step regarding the detailed design of the differential is to select a suitable gear from a catalog. To do so the loads are estimated, resulting in a desired normalized ratio. This normalized ratio is converted to a transmission ratio corresponding to the ratios mentioned in catalogs. Based on this information, a gearbox is selected.

Loads The gearbox ratio depends on the loads that occur during sizing and forcing. Unfortunately these forces are not deterministic, as they depends on practical deficiencies and friction, which also is accompanied with a lot of variation. Yet, a rough estimate is made of these friction forces.

For forcing the friction is estimated based on the friction torque of the bearings of the mechanism, based on a simple model provided by SKF. This model provides the following expression for the friction torque of a bearing

$$T_w = 0.5\mu F_{eq}d \quad (8.10)$$

where μ is the friction coefficient, F_{eq} the equivalent bearing load and d the bore diameter of the bearing. For deep groove ball bearings, $\mu = 0.0015$. The model is valid for $F_{eq} \sim 10\%$ of the dynamic load rating. Only the bearings that support the carriage and output w.r.t. frame rotate. The specifications and resulting friction torques of these bearings are listed in Table 8.1. These friction torques add up to a friction torque of $T_{w,sizing} = 11.27 \cdot 10^{-3}$ Nm.

The torques during forcing is estimated using an average balancing imperfection of 5% of the maximum output torque, resulting in a torque of $T_{w,forcing} = 0.07$ Nm.

From an energetic perspective it is desired that the work points i.e. motor torque and speed, for both modes are approximately equal, because this way the motor and gearbox can be optimized for this work point. The geared motor torques are respectively $T_{Mot,sizing} = T_{w,sizing}/i_1$ and $T_{Mot,forcing} = T_{w,forcing}/i_2$. The motor torques are equal if:

$$\frac{T_{w,forcing}}{T_{w,sizing}} = \frac{i_2}{i_1} = \iota \quad (8.11)$$

Evaluation of this expression using the estimated friction torques results in a ratio $\iota = 6.2$.

Gearbox Selection Based on the above reasoning the targeted gearbox ratio is $i_{Diff} = 6.2$. Under normal operation, as described above, the gear be rated for at least 0.07 Nm. Yet, for a first prototype this nominal load rating is increased to at least 1.4 Nm, the maximum torque of the springs. This allows the mechanism to operate without either the buffer springs or main springs removed, which is usefull if the separate characteristics of the springs need to be measured. The MATEX 26-5SAI4 [56] is ultimately selected for its excellent efficiency of $\approx 98\%$. Its gear ratio of 4.5 is close to the targeted ratio and its rated torque of 1.96 Nm allows for evaluation of the unbalanced spring characteristics.

Table 8.1: Friction torque in bearings during sizing

Bearing Type	Dynamic Load Rating C [N]	Inner diameter d [mm]	Friction Torque T_w [Nm]
NSK NB705	1930	25	$3.62 \cdot 10^{-3}$
NSK NB707	2810	35	$7.38 \cdot 10^{-3}$
NSK MF137	540	7	$0.28 \cdot 10^{-3}$
Total			$11.27 \cdot 10^{-3}$

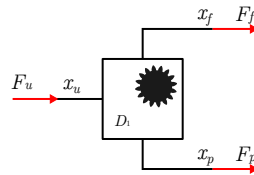
8.3.3.3 Equilibrium Condition

For the design of the threshold mechanism, which is addressed in the next section, the equilibrium condition of the differential needs to be known, because of the large interplay between the differential and threshold.

Fig. 8.10 depicts schematically a differential with its three in- and outputs, x_u , x_f and x_p , and the associated forces. The equilibrium condition can be easily derived from the differential kinematics using the principle of virtual work, as is done in appendix G. This results in the following equilibrium condition:

$$F_u = \frac{-F_p}{a_1} = \frac{-F_f}{a_2} \quad (8.12)$$

The very same relation is valid for moment equilibrium in case of a rotational differential.

**Figure 8.10:** Static Equilibrium of differential.

8.3.4 Threshold Mechanism

To prevent the mechanism from accidentally shifting between the modes, a threshold mechanism is incorporated in the design. In Chapter 4 a conservative force was selected as threshold and in Chapter 5 it was determined it should be realized by a non-linear spring placed between the outputs of the differential. The threshold is highlighted in Fig. 8.11. It consists of the purple cam mounted on the red cam shaft, on which two axisymmetric purple followers engage. A helical torsion springs exerts a torque between the blue carriage and purple followers. The followers are mounted to which also the pawls of the ratchet locking mechanism are mounted. A rotation of the followers results in the (dis)engagement of this pawl. The exerted threshold force is a function of the two outputs of the differential, i.e.: $F_T(u_f - u_p)$. This torque-characteristic has to satisfy a set of criteria that ensure proper functioning.

The characteristic manifests itself in two situations: During switching between the modes and when unwanted disturbances arise. The resulting requirements of these two situations are derived in Sections 8.3.4.1 and 8.3.4.2 respectively. The realization of the cam mechanism is addressed in Section 8.3.4.3.

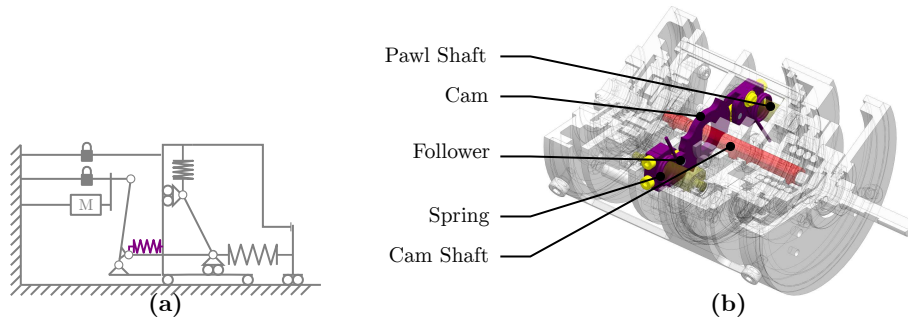


Figure 8.11: Threshold Subsystem. **a:** Schematic. **b:** Cross-sectional view of CAD-model. The threshold consists of a cam on the cam shaft, on which two spring-loaded followers engage.

8.3.4.1 Equilibrium While Switching

The first inspected situation is switching. First the switch from sizing to forcing will be discussed. Then will be explained what happens when the mechanism switches back to sizing.

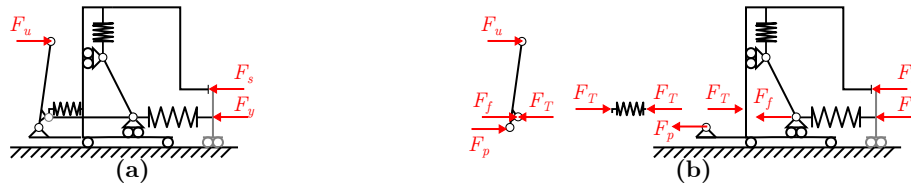


Figure 8.12: Force/Torque Equilibrium during Switching

Switch from Forcing to Sizing As soon as the output hits the object, the mechanism starts to switch its mode from sizing to forcing. The tricky part is that the lock does not engage instantaneously, as a small pawl displacement required to engage the pawl. During this “engagement displacement”, static equilibrium of the carriage needs to be ensured. A static analysis is conducted for the linear variant, schematically depicted in Fig. 8.12. This analysis is also valid for the rotational prototype.

This analysis goes as follows, first the equilibrium condition of the whole mechanism is considered. Then the components of this expression are related to the threshold. Substituting these back in the equilibrium condition results in a requirement for the characteristic.

The force equilibrium follows from Fig. 8.12a, and states: $F_u - F_s - F_y = 0$. Where F_u is the input force, F_y the main spring force acting on the output and $F_s \geq 0$ the excessive force that flows through the endstop. The carriage does not move as long as it is pressed against the object, which is the case when:

$$F_u \geq F_y \quad (8.13)$$

The input force F_u is related to the threshold characteristic by means of the equilibrium condition for the differential, Eq. (8.12), which results in: $F_u = -(F_f - F_T)/a_2$. F_f denotes the force on the input u_f of the SBFA. In Chapter 4 was shown that this force equals zero when no balancing imperfections occur. Hence, $F_u = F_T(x_f - x_p)/a_2$.

The output force F_y equals to the force in the main spring: $F_y = k_M(x_f - x_p)$. Hence Eq. (8.13) resolves to:

$$F_T(\Delta x_f) \geq k_M \Delta x_f a_2 \quad (8.14)$$

Where $\Delta x_f = x_f - x_p$ denotes the extension of both the non-linear threshold spring and the main spring. This criteria needs to be satisfied as long as the pawl is not in the self engaging region. The corresponding cam rotation required to engage the the carriage is denoted as $\Delta x_f \in [0, \Delta x_{f,t}]$, where $\Delta x_{f,t}$ denotes the displacement of the forcing input of the differential for which the carriage lock becomes fully engaged. From an energetic perspective, the required cam stroke to engage the lock should be as small as possible, as the threshold mechanism is not work-neutral during switching. A value of $\Delta x_{f,t} = 3^\circ$ was deemed as smallest value that resulted in a manufacturable cam design.

Forcing to Sizing From forcing to sizing the exact same conditions apply for static equilibrium, with the only difference that the motion of the input is in opposite, i.e. negative direction. This has as consequence that negative work is done, since the static equilibrium still requires F_u to be positive.

8.3.4.2 Equilibrium during Disturbance

The second situation that needs to be analyzed is when disturbances on the output arise. As the balancing spring generates a negative stiffness to compensate the positive stiffness of the main spring, the mechanism might become unstable in the sizing mode, resulting in an unwanted relaxation of the buffer spring. Again it is the aim to express the threshold that prevents this unwanted behavior. A positive disturbance has a different effect than a negative disturbance, as they flow differently through the mechanism. Therefore they will be discussed separately.

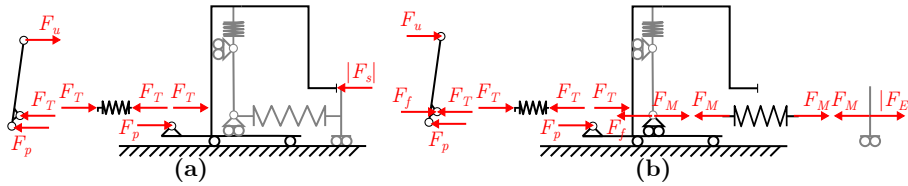


Figure 8.13: Free body diagram of mechanism during disturbances. **a:** Negative disturbance. **b:** Positive disturbance

Negative Disturbance Force This paragraph aims to express the required threshold force to prevent unwanted motions due to a negative disturbance force.

For this static analysis it is assumed the mechanism is in the sizing mode. The free body diagram of the carriage, threshold mechanism and differential are depicted in in Fig. 8.13a. The carriage is in equilibrium when:

$$F_T + F_p - |F_E| = 0 \quad (8.15)$$

Where $|F_E|$ is the magnitude of the disturbance of the negative disturbance, i.e. $F_E \leq 0$ N. On the position output of the differential acts the frame reaction force F_p and on the forcing input the threshold force F_T . No other forces act on this input, as the mechanism is still in sizing mode. The equilibrium condition, Eq. (8.12), resolves to:

$$\frac{-(-F_p)}{a_1} = \frac{-(-F_T)}{a_2} \quad (8.16)$$

Substituting this condition in Eq. (8.15) and rearranging yields:

$$F_T = \frac{|F_E|}{1 + \frac{a_1}{a_2}} \quad (8.17)$$

This condition should be satisfied for $\Delta x_f = 0$, such that unwanted motions are completely prevented.

Positive Disturbance Force This paragraphs derives the required threshold for a positive disturbance force.

When a positive force acts on the output, it can not be counteracted by the endstop. Hence it flows through the spring to the forcing output of the differential. The free-body-diagram in Fig. 8.13b is used to analyze equilibrium. The carriage is in equilibrium when:

$$F_T + F_p = 0 \quad (8.18)$$

Furthermore, $F_f = |F_E|$, to ensure an internal equilibrium in the balancer. As this force and the threshold force act both on the forcing output of the differential, but in opposite condition, the equilibrium condition for the differential is:

$$\frac{-(-F_p)}{a_1} = \frac{-(-F_T + F_f)}{a_2} \quad (8.19)$$

The substitution of Eq. (8.18) in Eq. (8.19) results in:

$$F_T = \frac{|F_E|}{1 + \frac{a_2}{a_1}} \quad (8.20)$$

Again, this condition should be satisfied for $\Delta x_f = 0$, such that unwanted motions are completely prevented. Note the subtle but important difference in the denominator between Eq. (8.17) and Eq. (8.20).

8.3.4.3 Cam Design

The design of the threshold cam mechanism consists of three steps. First a required characteristic is proposed that satisfies the identified constraints to prevent unwanted motion. Second, a suitable spring is selected. Third, the cam geometry is generated.

Required Characteristic The threshold characteristic should satisfy the three constrains, to prevent unwanted motion during switching and negative or positive disturbances, described by respectively Eqs. (8.14), (8.17) and (8.20).

The expected disturbances are set to $|T_E| = 0.03Nm$, based on the the third design requirement of Chapter 6. The cam is mounted on the cam shaft, as such Δx_f can be replaced with the rotation of the cam ψ_m . The required rotation to achieve switching is set to $\psi_{M,t} = 3^\circ$. In the previous subsection the parameters $a_1 = -3.5$ and $a_2 = 4.5$ are obtained. The resulting constraints are depicted in Fig. 8.14a. From this figure follows that to be resilient to disturbances, the threshold mechanism needs to be pre-tensioned. In the range of $\psi_M \in [0, \psi_{M,t}]$ the targeted characteristic is set to a constant force of $T_T = 0.135$ Nm. This avoids on the hand a negative stiffness and at the other hand minimizes the accumulation of potential energy. Once the mechanism is in the forcing mode, the threshold should not impede the SBFA. Therefore the threshold force is set to zero during for $\psi_M > \psi_{M,t}$. The characteristic is expressed with the following expression:

$$T_M = \begin{cases} T_T & \text{for } \psi_M \leq \psi_{M,t} \\ 0 & \text{for } \psi_M > \psi_{M,t} \end{cases} \quad (8.21)$$

Now that this characteristic is proposed, a suitable spring can be selected and a cam geometry can be defined.

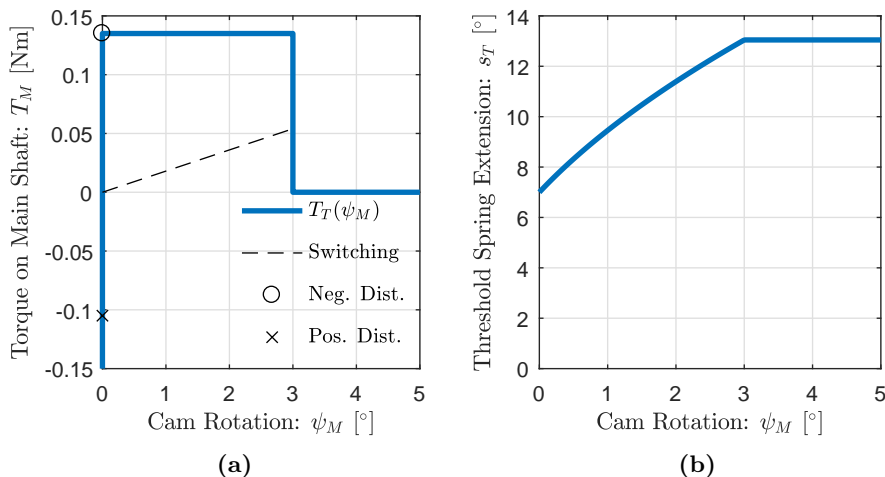


Figure 8.14: Threshold Mechanism. **a:** Proposed characteristic that satisfies the constraints for switching and negative disturbances, expressed by respectively Eqs. (8.14), (8.17) and (8.20). **b:** Extension of threshold spring for desired characteristic.

Spring Selection The spring selection of the threshold mechanism is very similar to the selection of the main and buffer springs. A database with springs is evaluated to find compact springs that satisfy

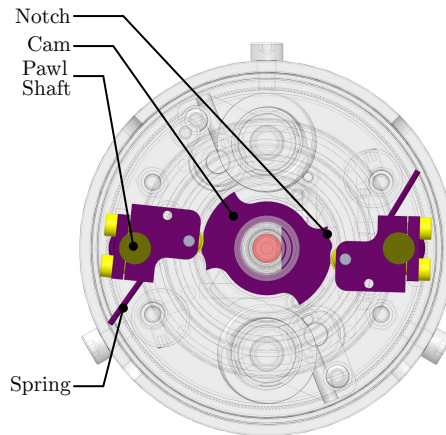


Figure 8.15: Threshold cam in cross-sectional view of CAD-model.

certain design criteria. Because the threshold spring is small compared to the other springs, its selection is not very important as it has no large impact on the design. As such, the threshold spring selection is described in detail in appendix G.

Ultimately TEVEMA TS101720 is selected with an outer diameter of 10 mm and a length of 4.5 mm.

Cam Geometry The procedure to obtain the cam geometry of the threshold cam is as follows: First the potential energy of the characteristic is expressed. Then this characteristic is converted into a desired trajectory for a follower. This trajectory is converted to a cam geometry using the same procedure as for the balancing cam.

To define the trajectory of the threshold follower, the potential energy of the characteristic needs to be expressed. This follows from integration of Eq. (8.21). To ensure the follower bearing is always pressed on the cam, the threshold spring will be pretensioned with an extension $s_{T,0}$, as such the potential energy of the characteristic equals:

$$V_T = \begin{cases} \psi_M T_T + \frac{1}{2} k_T s_{T,0}^2 & \text{if } \psi_M \leq \psi_{M,t} \\ \psi_{M,t} T_T + \frac{1}{2} k_T s_{T,0}^2 & \text{if } \psi_M > \psi_{M,t} \end{cases} \quad (8.22)$$

Where k_T is the stiffness of the threshold spring.

The linear balancing springs have to store this energy. As this spring is tensioned by the follower, the follower trajectory follows from rewriting the expression that describes the energy stored in the threshold spring: $V_T = 1/2 k_T s_T^2$. This results in the following expression for the follower trajectory:

$$\psi_T = \sqrt{\frac{2V_T}{N_s k_T}} + \psi_{T,0} \quad (8.23)$$

Where $\psi_{T,0}$ denotes the rest position of the spring.

Using the same procedure as the balancing cam, the specified trajectory can be converted in a cam geometry. The resulting cam geometry is depicted in Fig. 8.15. Also in this cam a notch is incorporated to tune the rest position of the springs during mounting.

8.3.5 Nonbackdrivable Mechanism

The incorporation of the NBDM enables the deactivation of the motor while the mechanism is still resilient to balancing imperfections or disturbances. As mentioned before, in the prototype as much as possible off-the-shelf components are used. In line with this paradigm an existing NBDM is used, namely one that was incorporated in a gearbox of a BOSCH EASYDRILL 12 cordless drill driver¹

¹Many thanks to Glenn Matthijsen from the VUB for pointing out that high-end accudrills incorporate these bidirectional overrunning clutches.

8.3.6 Feedback

The designed energy saving drive is able to vary the magnitude of the output torque. To provide feedback on its magnitude a small non-contact rotational encoder is incorporated, which measures the extension of the main spring. The 12 bit RLS RM08 incremental encoder was selected for this purpose because of its very small size and its resolution of 4096 counts per revolution, which results in a torque resolution of 3 mNm.

8.4 Realization of Prototype

This section shows the realized prototype and describes the deficiencies and how they are soled.

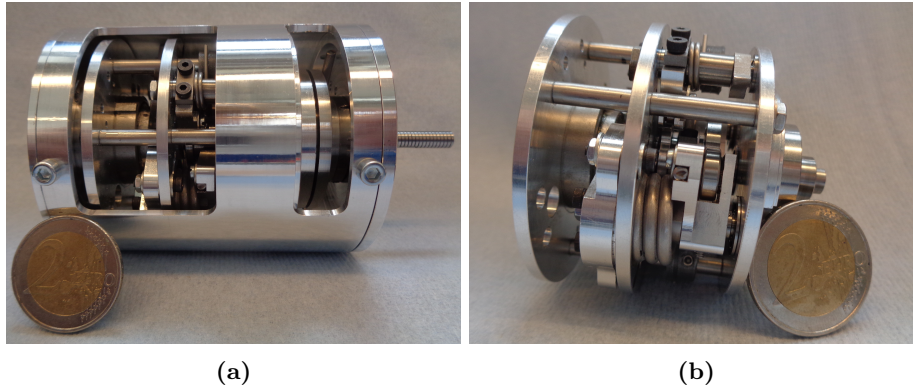


Figure 8.16: Realized Prototype with coin for scale. **a:** Picture of assembled drive.
b: Picture of carriage

Fig. 8.16 shows a picture of the assembled drive and the carriage. The mechanism is machined from aluminum, except for the stock components, ratchet, cams and shafts. The shafts are made of Stainless Steel 304.

During the build process some deficiencies in the design were discovered. The major ones are listed together with their solution:

- Initially the threshold mechanism did not work. A rotation of the main shaft caused the threshold follower to rotate in the wrong direction and snap through its singular point. There were two reasons for this. In the first place the cam was made using water-cutting, which resulted in a slightly rough surface. This roughness caused deviations in the direction of the contact force. The second reason is that the follower is at its initial cam rotation is 6 degrees, which is close to the singular position, this means it is rather sensitive to manufacturing tolerances in the cam shaft geometry or location of the pawl shaft suspension. The hypothesized solution, a slightly larger and smoother cam, was verified by a simple test in which a smooth piece of duct tape with a thickness approximately 0.2mm was applied on the cam surface. After this successful test a new threshold cam was produced using CNC milling, of which the outer surfaces have an offset of 0.2mm with respect to the earlier design. A drawback of this solution is that the modification of the cam geometry will cause a deviation from the designed threshold characteristic. It is expected that finetuning the pretension of the threshold spring might partially compensate for this.
- The balancer follower could not reach the notch in threshold, which was incorporated to tune the rest position of the spring, because the rotation of the main shaft is obstructed by a collision between the threshold cam and buffer springs. To solve this, a custom tension tool was made, which could be used in combination with a vernier protractor, i.e. an accurate angle meter, to set the pretension. This tension tool is described in appendix G.5.

8.5 Discussion

Regarding the detailed design of the components, the obtained design is, compared to the current drive of the Delft Hand 3 rather large and heavy. Yet, it should be kept in mind that it is not a fair comparison,

as the designed mechanism is a first prototype with this working principle, whereas the geared DC motor is a fully optimized drive, based on a long-known principle.

As this mechanism is a first prototype, the manufacturability and reliability was highly valued. This is manifested in among others the following aspects:

- To ease trouble shooting and adaptations, the prototype is designed to be demountable. As such, many components are connected using detachable connections, for instance bolts and nuts. These connections require typically more space than for example an adhesive bond.
- As this mechanism is a one-off prototype, stock-components are used as much as possible, which is likely to result in overdimensioned designs, because the specifications does not exactly match the requirements. A good example is the main spring. It is rated for an extension of 52° , but is employed with a maximum extension of 41.5° . The use of custom-components instead, might enable further reduction of the size and weight.
- The use of high-strength steels might further reduce the size of various components. Also additional effort can be put in the optimization of the strength and stiffness of the parts with respect to the weight.
- The design is based on some practical estimates, such as the minimum possible size of the teeth. More design iterations and trail-and-error could be undertaken in future work to reach the edge of what's possible.

Improving these aspects is possible but also time consuming and costly. These expenses are only justified when the principle shows potential, which in turn justifies a first proof of principle in which these aspects are not yet optimal.

In addition it should be noted that some properties of the mechanism are also dependent on practical deficiencies, such as manufacturing tolerances and friction, which are hard to model accurately and often have a stochastic nature. For now they are estimated using in a conservative way, to ensure the mechanism is likely to work. Conducting experiments with the obtained design will increase insight in these parameters and enable further optimization of the design.

Naturally, for a follow-up version of a prototype, the discovered deficiencies listed in Section 8.4 should be solved. Moreover, I think the design of the ratchet could also be improved, as it is overconstrained in the current mechanism: Theoretically the pawls engage simultaneously, but this is in practice not necessarily the case, due to practical deficiencies, such as a deficiency in the cam symmetry of the threshold cam or the concentricity of the carriage, ratchet ring and housing. This might cause internal stresses and forces, which ultimately might result in more friction. A possible solution is to add some compliance between the threshold follower and the pawl. It would be interesting to investigate whether it is possible to integrate this compliance in the pawl itself, or example by executing it as a cantilever beam.

Adding this compliance also would enable to mount multiple pawls on the same shaft, which engage on different dephased ratchet rings. This would improve the accuracy with a factor that is equal to the number of installed rings. This will reduce the balancing error.

8.6 Conclusion

This chapter described the design of the prototype and its subcomponents in detail according to the design requirements of chapter 6. The overall design results in a mechanism with an outer diameter of 64 mm, a length of 78.5 mm and a weight of 460 gram. An actual prototype is realized.

Part IV

Experimental Validation

Chapter 9

Experimental Validation of Working Principle

9.1 Introduction

To validate the working principle of the prototype, two experiments are conducted. The first experiment will measure the main spring characteristic. This provides important information about the maximum output torque of the mechanism. A linear model will be fitted on the data, which can be used later on to estimate the delivered output torque.

The second experiment will measure the input characteristic of the mechanism. Based on this results the working principle of the threshold and balancer are evaluated. The two experiments are addressed in Sections 9.2 and 9.3. Both sections are structured in three subsections addressing respectively the methods, results and a discussion.

This chapter ends with a discussion regarding the working principle in Section 9.5 and a conclusion in Section 9.4.

9.2 Main Spring Characteristic

In the first experiment the main spring characteristic is measured. This is important, as it provides information about the following two aspects:

- *The Maximum Output Torque* The drive is designed for a maximum output torque of 1.4 Nm. By evaluating the maximum torque of the output it is validated whether this target is realized.
- *Calibration of Torque Estimation with Encoder* The magnetic encoder is used to measure the deflection of the main spring. To be able to predict the output torque with the measured encoder output, a linear model is fitted on the measured output torque.

This section will address respectively the methods, the results and a discussion respectively.

9.2.1 Methods

This subsection describes the methods of the first experiment. First the experimental setup itself is described. Second, the conducted experiment is described. Finally the model will be introduced which will be used to estimate the output torque based on the encoder output.

The setup depicted in Fig. 9.1 is used to measure the torque and angular displacement. This setup is a modification of a setup by Michiel Plooij. It consists of two loadcells connected by a lever, of which the center is mounted to the output shaft of the designed drive, such that the output torque is measured. The data of the loadcells is acquired using a BECKHOFF EHERCAT module. The loadcells are calibrated using multiple weights. The torque $T_{measured}$ is computed using the following relation:

$$T_{measured}(t) = (F_{LoadCell1}(t) - F_{LoadCell2}(t)) \cdot r \quad (9.1)$$

Where $F_{LoadCell1}$ and $F_{LoadCell2}$ are the forces measured with the loadcells and $r = 150$ mm the moment arm, i.e. half the lever length.

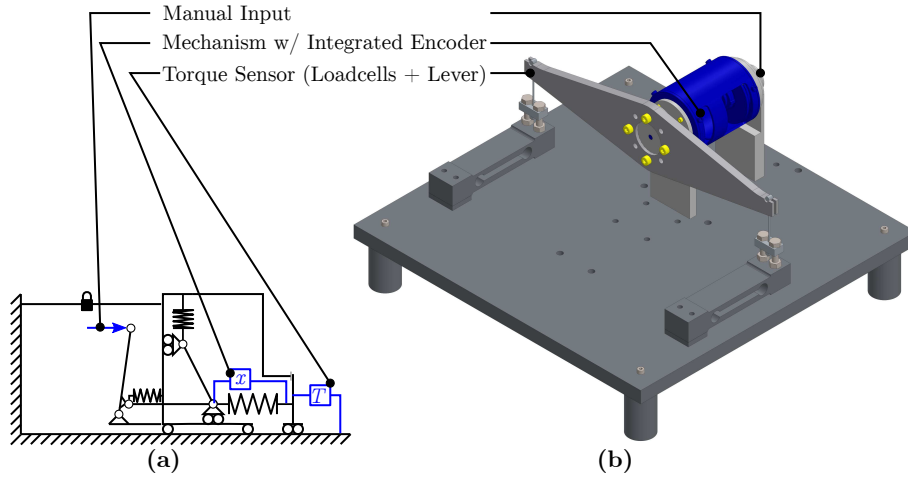


Figure 9.1: Experimental setup for first experiment. The torque at the drive output is measured with the loadcells via the lever. The spring deflection is measured by an integrated miniature encoder. **a:** Schematic. The manual input, torque sensor and integrated encoder are depicted in blue. **b:** CAD-model of setup.

The integrated miniature magnetic encoder was used to measure the deflection of the main spring. A COPELY ACCELNET AEM motor controller is connected to the ETHERCAT network to read out this encoder. The locations of this encoder and the “torque sensor”, i.e. the loadcells with lever, are indicated in Fig. 9.1a. Fig. 9.1b depicts a CAD model of this setup.

The data was acquired using Simulink xPC running at 1 kHz at a target PC, which was also connected to the ETHERCAT network. For this experiment the input of the mechanism is actuated manually.

The conducted experiment consists of two stages, namely an idle time for calibration of the torque signal and the actual experiment.

Although the loadcells are calibrated individually, an offset might arise due to pretension in the connection to the lever. To account for this, the first 5 seconds of the experiment the mechanism is left at rest. The average torque measured during this rest is subtracted from the measured torque signal.

The actual experiment consists of 5 repetitions in which the input shaft of the mechanism was rotated manually forwards and backwards in a slow and smooth way. The obtained torque and position signal is filtered with a 5th order Butterworth filter with a cutoff frequency of 5 Hz. This filter is applied in both forward and reverse time direction with the MATLAB command `filtfilt`. For each repetition the data is truncated to the positive torque, as a negative torque belongs to the situation where the shaft is turned too far backwards and therefore tensions the spring in negative direction.

The following linear spring model will be fitted on the data of each repetition using a least-squares fitting algorithm:

$$T_{est}(s_M) = k \cdot s_M + T_0 \quad (9.2)$$

Where k is the spring stiffness, s_M the deflection measured with the magnetic encoder and T_0 an offset.

9.2.2 Results

In Fig. 9.2 the measured output torque is plotted versus the measured deflection of the spring for the 5 repetitions.

The first goal of the experiment is to determine the maximum output torque. The average maximum measured torque for the five repetitions is 1.073 ± 0.002 Nm. The second goal of the experiment was to fit a linear curve on the data in order to estimate the output torque. Averaging the estimated parameters fitted for the five repetitions leads to a stiffness $k = 26.3 \pm 0.3$ mNm/° and an offset of $T_0 = -0.059 \pm 0.009$ Nm. The root-mean-square-error (RMSE) of the fitted model and the measured data of all 5 repetitions is 0.0557 Nm.

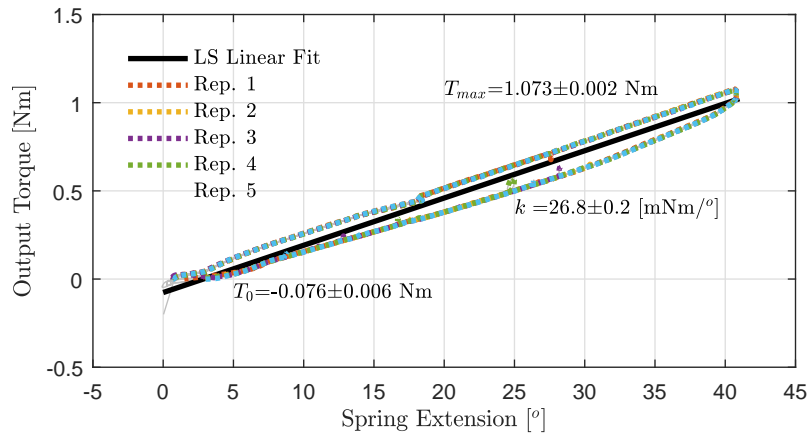


Figure 9.2: Main spring characteristic. The gray lines depict all filtered data. The colored lines belong to the 5 repetitions which are isolated from this data. The black line shows the fitted linear function.

9.2.3 Discussion

In this section the results of the first experiments are discussed. First the results for the two goals are addressed, followed by additional observations.

The maximum measured torque of 1.073 Nm is smaller than the targeted 1.4 Nm. The reason for this difference is that the actual spring stiffness of 26.8 mNm/° is 20.6% smaller than the catalog value [62] of 33.75 mNm/°.

The RMSE indicates that the fitted model is able to predict the actual output torque with an average error of 0.0557 Nm, which is 5.19 % of the maximum output torque. A more accurate prediction could be obtained by extending the model. This is beyond the scope of this experiment, as the obtained model allows for an evaluation of the working principle. For a spring deflection close to zero the model predicts the torque more negative than measured. This might be explained by play, which will be addressed in more detail later on in this discussion.

The negative offset can be explained by the fact that the encoder is incremental, which means that the zero position is initialized when the COPELY motor controller is turned on. As such, this zero position does not necessarily correspond to exactly zero torque. Also the play at the beginning of the spring extension contributes to this offset.

The measured data in Fig. 9.2 reveal a hysteresis loop. This hysteresis reveals play and friction. By means of numerical integration the work per cycle is computed to be $0.0806 \pm 0.007 \text{ J}$. The friction torque of this hysteresis has multiple potential origins:

- As shown in Fig. 9.3a the spring is wound such that the windings touch each other. When the spring is deflected, the windings will slide alongside each other. [49] indeed indicate this as a potential source of a friction..
- Internal hysteresis.
- The output shaft is suspended in two ball bearings, which are likely to have friction. Yet, this is no full explanation as it would result in approximately 0.014 J work for a friction torque in the same order of magnitude as the estimated friction torque in the ball bearings during sizing. In Chapter 8 this friction torque was estimated as 11 mNm. The main spring is suspended in less and smaller ball bearings, hence its friction torque is likely smaller.
- The main spring is positioned in a spring housing, as depicted in Fig. 9.3b. The windings or poke of the main spring might touch this housing during the deflection, also causing friction.

For future work the cause of this hysteresis should be investigated in more detail, as this hysteresis should be minimized. The first three points could be investigated by testing the springs and/or bearings while unassembled. The possible interference between the spring and its housing or surrounding could be investigated by covering the spring with pigments and inspect the surrounding elements after the completion of a few cycles.

The play is observed for the torques close to zero. This play likely occurs at the mountings of the pokes of the main spring. In the adjacent components channels are machined in which the pokes of the main spring fits. For assembly purposes this is a loose fit. If the direction of the spring torque changes, the pokes will resetttle in this channel, which is observed as play. In the experiment the torque direction changes when the spring is turned too far backwards.

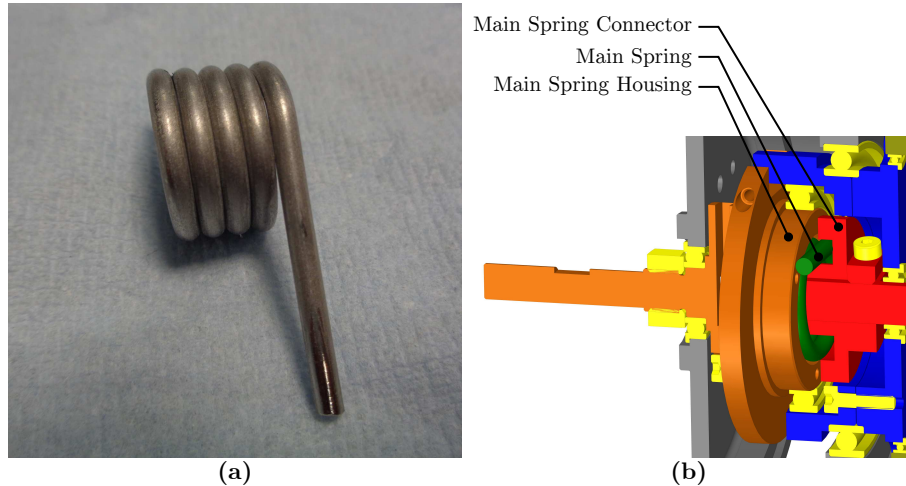


Figure 9.3: Possible causes of hysteresis in main spring characteristic. **a:** The windings of the main spring are touching each other. **b:** Inteferece might occur between the main spring and its housing.

9.3 Input Characteristic

The second experiment aims to measure the input characteristic. This input characteristic reveals the following properties of the mechanism:

- *Torque Reduction:* The realized torque reduction of the drive follows from comparing the in- and output torque.
- *Required Input Work:* The mechanism is designed to obtain a high output torque at a low energetic cost. Hence, the required input work at the input of the mechanism is of importance.

The input characteristic depends on the object size, as this determines when the mechanism switches. Five different object sizes will be emulated by limiting the output motion to five different ranges.

9.3.1 Methods

This subsection describes respectively the experimental setup, the conducted experiment and the expression for the torque reduction.

The setup from the first experiment is largely reused in this experiment except for a few modifications. The geared DC-motor is supported by two rotational ball bearings and attached to the two load cells with the lever. As such, the loadcells are now measuring the torque exerted torque by the geared motor. The geared DC motor is connected with a dedicated shaft to the input the differential instead of via the NBDM. A disk with threaded holes is mounted at the output. By inserting bolts in these holes the motion range of the output is limited to a value in the following set: $\{35.04, 71.28107.52143.76180.00\}^\circ$. The increment of 36.24° is deliberately chosen, as this corresponds to a step of 30.2 times the locker resolution of 1.2° . As the locker only locks for an integer value of this resolution, the position errors increases each time with $0.2 \cdot 1.2^\circ = 0.24^\circ$. Consequently, the expected balancing error is equally spaced within the range $e \in [0, 1.2]^\circ$. Note that the exact error is not known, as the ratchet is mounted without aligning its angular orientation.

The setup is schematically depicted in Fig. 9.4a and a CAD-model is shown in Fig. 9.4b. The geared DC motor is controlled with a second COPELY ACCELNET AEM motor controller.

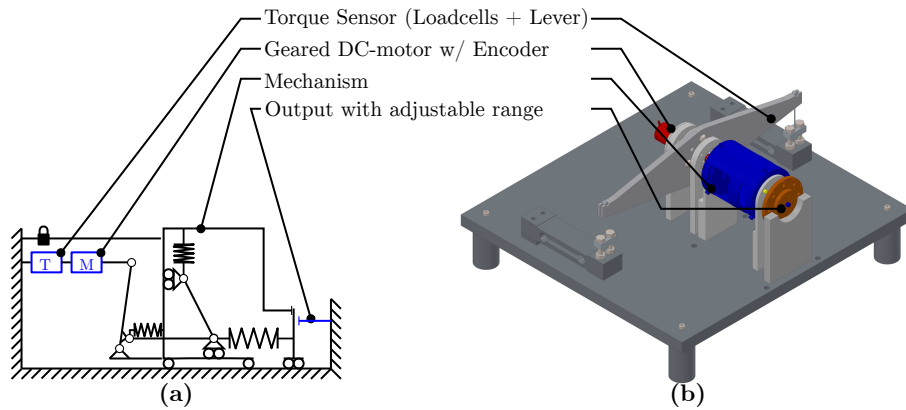


Figure 9.4: Experimental setup for second experiment. The output of the mechanism is connected to a disk of which the motion range can be adjusted by inserting bolts in the threaded holes. The input torque delivered by the geared DC motor is measured by the two loadcells that are connected via the lever to the housing of this motor. **a:** Schematic. The torque sensor, adjustable output and geared DC-motor are depicted in blue. **b:** CAD-model.

The experiment is conducted for five conditions of the motion range. Each condition consists of five repetitions. For every repetition the following three stages are repeated:

1. The input shaft is moved manually to determine the motion range. This motion range is used to determine a trajectory for the motor.
2. The setup is idle for 5 s. During this 5 s the offset of the torque signal is determined, to account for the connection of the loadcells to the lever.
3. The motor moves 5 times forward and backwards within the motion range with a gearbox shaft velocity of 5 RPM.

The measured torque signal is corrected for the offset that arises from the connection to the lever, by averaging the torque signals measured during the idle-time before each condition. One signal was removed, as its average idle torque was an outlier with a magnitude twice as big as the other four idle times. The data is filtered in forward and backwards direction with a 5th order Butterworth filter with a cutoff frequency of 5 Hz.

The torque reduction is evaluated using the following equation:

$$TR = \left(1 - \frac{\max(|T_{in}|)}{\max(|T_{est}|)} \right) \cdot 100\% \quad (9.3)$$

Where T_{in} is the measured input torque and T_{est} is the estimated output based on the measured spring deflection during forcing. The max operator returns the maximum value of the signal. Note that the input torque during forcing and sizing will be excluded, by only evaluating the data that is larger than $T_{est} > T_{est,T}$, where $T_{est,T}$ is the estimated output torque for which relates to the end of the threshold peak. This value will be determined based on the results.

The work of the mechanism is evaluated by numerical integration of the measured input torque over the input angle.

9.3.2 Results

The measured input torque and estimated output torque are plotted Fig. 9.5. A correction was applied for the high peaks in the input torque at the end of the stroke. The uncorrected data is plotted in light grey. The peaks in this data appear, because the deflection range of the spring is limited by the cam design. When the motion range of the motor is set beyond the deflection range of the spring, the spring is not able to deflect further and the output torque stalls. Due to the finite stiffness of the mechanisms parts, the motor is able to rotate further, but this requires high input torques. To exclude this effect for each repetition only the data is taken into account that corresponds to an estimated output torque

that is at most 99 % of the maximum estimated output torque of that repetition. The corrected data is depicted in Fig. 9.5 colored curves.

In this data the switching occurs when the main springs starts to deflect and deliver and output torque, and the input torque shows a peak. Before switching the mechanism is in the sizing mode. The peak threshold peak diminishes for a spring deflection which corresponds to an output torque of approximately 0.1 Nm, as such $T_{est,T}$ is set to this value.

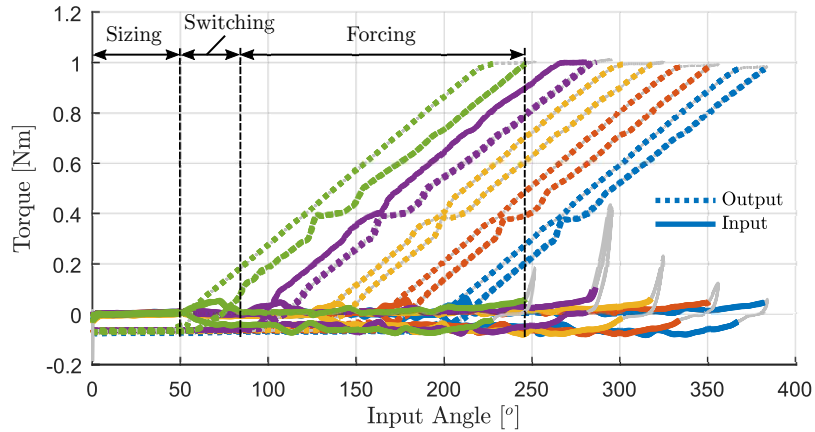


Figure 9.5: Measured input torque and estimated output torque. Each color belongs to one of the five conditions. For the condition in green the three subfunctions, i.e. sizing, forcing and switching, are indicated.

In Fig. 9.6 the measured input torque is plotted. The uncorrected data is also plotted in grey. The resulting torque reductions for each repetition are listed in Table 9.1. In this table also the mean and standard deviation (SD) are listed for the different conditions and the complete dataset. The dataset used to evaluate the torque reduction, which only contains the data corresponding to forcing is, is visualized in appendix H.1.

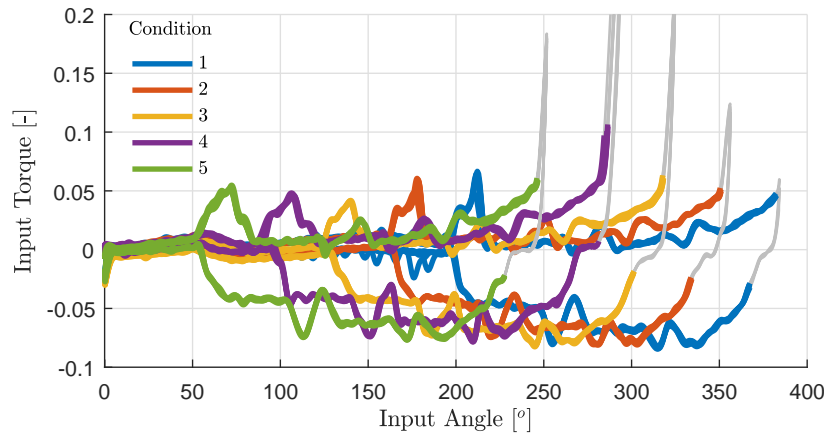


Figure 9.6: Input torque for the five different conditions.

Table 9.1: Torque Reduction

Condition	Repetition					Mean	SD
	1	2	3	4	5		
1	91.4%	91.6%	91.6%	91.6%	91.4%	91.5%	0.10%
2	91.8%	91.9%	91.8%	91.9%	91.9%	91.9%	0.04%
3	91.8%	91.9%	92.0%	91.9%	91.8%	91.9%	0.08%
4	90.4%	90.0%	90.0%	89.6%	89.5%	89.9%	0.36%
5	92.4%	92.4%	92.4%	92.5%	92.4%	92.4%	0.06%
Average						91.5%	0.88%

Table 9.2: Input Work

Condition	Repetition					Mean	SD
	1	2	3	4	5		
1	0.252 J	0.248 J	0.244 J	0.250 J	0.255 J	0.250 J	0.0042 J
2	0.246 J	0.242 J	0.243 J	0.242 J	0.243 J	0.243 J	0.0015 J
3	0.233 J	0.231 J	0.230 J	0.232 J	0.232 J	0.232 J	0.0012 J
4	0.228 J	0.229 J	0.230 J	0.229 J	0.232 J	0.230 J	0.0013 J
5	0.231 J	0.222 J	0.220 J	0.220 J	0.222 J	0.223 J	0.0047 J

9.3.3 Discussion

This section discuss the second experiment. It will first address the two goals of this experiment, followed by some additional observations are discussed.

Regarding the first goal, the evaluation of the torque reduction it should be taken into account that the output torque is an estimated value, rather than a simultaneously measured value. In the first experiment the was estimated to be 5.19% of the maximum measured output torque. This uncertainty propagates to the evaluation of the torque reduction. For the case that the actual output torque is indeed 5.19 % lower for every measurement would the average torque reduction becomes 91.1%, which still close to the estimated average.

The torque reduction might seem sensitive to the definition of the edges of the corrected dataset. This is only the case when the extreme value indeed occurs at the edge of the dataset, which might be the case for the forward motion. A closer look to the results showed that this is the case for just one condition. For all other conditions the maximum value occurs during the backwards motion, for which the extreme values are not at the edge of the data set.

Based on literature [25, 24] the expected force/torque reduction of the isolated balancer is approximately 95%, which corresponds to a normalized input torque of $\max(|T_{in}|) / \max(|T_{est}|) = 1 - 0.95 = 0.05$. In the designed a differential with a transmission ratio of 4.5 is incorporated, what would result in a normalized input torque of $0.05 \cdot 4.5 = 11 \cdot 10^{-3}$ or an overall torque reduction of 98.9%. This suggest the drive is not yet as good as it can be.

Indeed Fig. 9.6 reveals a large hysteresis loop suggests a potential balancing imperfection. The hysteresis loop will be discussed later on. Especially during the backwards motion a high friction torque seems to occur. An explanation for this is that the main springs and buffer springs might not be perfectly balanced. This results in a resultant torque that opposes the friction torque during the forward motion and sums up to the friction during the backwards motion. The balancing imperfection is not necessarily constant along the stroke, this might explain the peak at the end of the stroke. It is expected that by additional finetuning the extreme values of the input torque might be brought closes to zero. This will improve the torque reduction.

Table 9.1 shows that the the minimum torque reduction for a single repetition is 89.5%. When the buffer springs would not compensate the main spring, the torque reduction would be at most 77.8 %, as the maximum input torque would be at most a factor 4.5 lower than the maximum output torque due to the differential. This shows that the balancer works in combination with the differential for every repetition of every condition.

The results for the second goal, the measurement of the input work, shows that it equals approximately 0.24 J for each condition. The average input work is just 0.03 J more for the first condition than for the last condition, even though its displacement during sizing is 4 times larger. This suggests sizing costs almost no energy, but all energy is spent during forcing. Fig. 9.6 shows indeed a large hysteresis loop. The potential causes of this hysteresis will be discussed:

First of all, play was observed between the gearbox output and cam-shaft. This play appears in the results of Fig. 9.6, as the ripples in the torque signal occur at a different location for the forward motion than for the backward motion, and the loop in the output torque signal.

The cause of this play is that plastic deformation has occurred in the gearbox adapter, as shown in Fig. 9.7a. Therefore the shaft is no longer fully constrained. The reason that the adapter is so weak is that the the gearbox output in the supplier's CAD-model does not correspond to the reality, as such the actual adapter had to be smaller and thinner than the designed one. The difference between the actual adapter and the incorrect model is shown in Fig. 9.7b. An additional effect of this play is that it troubles the transparency between the torques acting on the cam shaft and the measured torque, as this play might result in a sudden snap-through when the direction of the torque on the cam-shaft changes. This might for instance explain the bump in the (forward) output torque between 0.3 and 0.4 Nm, as the actual output torque is temporarily ahead with respect to the expected value based on linear interpolation of the remainder of the signal. Besides, it is likely that this weak adapter also has a very limited stiffness, which causes even more deficiencies between the motor angle and cam-shaft rotation.

Second of all, the friction torque might be explained by the touching windings of the springs. Recall that identical springs are used as main and buffer springs, for which a hysteresis of 0.08 J was measured in the first experiment. Because the buffer springs have to store each half of the maximum main spring energy and the quadratic scaling of the energy, their maximum extension is $1/\sqrt{2}$ times the maximum extension of the main spring. Assuming the hysteresis scales linearly with their extension and the the hysteresis of 0.08 J fully originates from these touching windings, the total hysteresis would equal $(1+2/\sqrt{2})\cdot 0.08 = 0.19$ J. This suggest that the touching windings might almost fully explain the observed hysteresis loop. To validate this either the properties of the an unassembled spring could be measured or alternative springs could be mounted in the mechanism. Both will require some effort, as either the test setup or mechanism needs to modified in order to mount the springs.

The discussion ends with some additional observations:

- The removed outlier in the calibration procedure belonged to the condition that was first tested. A reason for this outlier might be that the just before this experiment the setup was assembled. Some settling might have taken place, which affected the offset.
- Although according Fig. 9.5 the estimated torque is negative, the actual torque might be equal or larger than zero. Recall that this output torque is simplified and estimated based on the first experiment. In the results of this experiment the fitted torque curve is for a small spring extension lower than the measured data.
- Fig. 9.6 shows ripples in the input torque. As these ripples occur fairly consistent for the different repetitions of the same condition, they are not of stochastic nature. During forcing, they might be caused by deficiencies in the cam-surfaces, which are likely to arise due to the tolerances of the CNC-milling machine and numerical errors in the CAD-model or CNC-programming. During sizing this might be caused by imbalance of the carriage. An imbalance of 4 grams at 28 mm out of the center, which corresponds to the rim of the carriage, would result in a torque deviation of approximately 1 mNm. Also the stiffness of the sensor cable, which has to displace during sizing might contribute to the deviation.
- For each condition the threshold is clearly visible, once the output torque starts to build up a peak is visible in the torque signal. The peak of this spike is at approximately 0.05 Nm, which is larger than designed 0.03 Nm. This might have several reasons. First of all, the threshold was realized with a small offset, to solve the issue of the follower snapping trough. Second, the spring stiffness might differ from the catalog value, as this is also the case for the main spring. Third, the pretension might differ from the targeted value. Fourth, due to the limited stiffness of in other components in the drive line, such as the adapter, even a perfect block-impulse characteristic might have slopes at the sides.

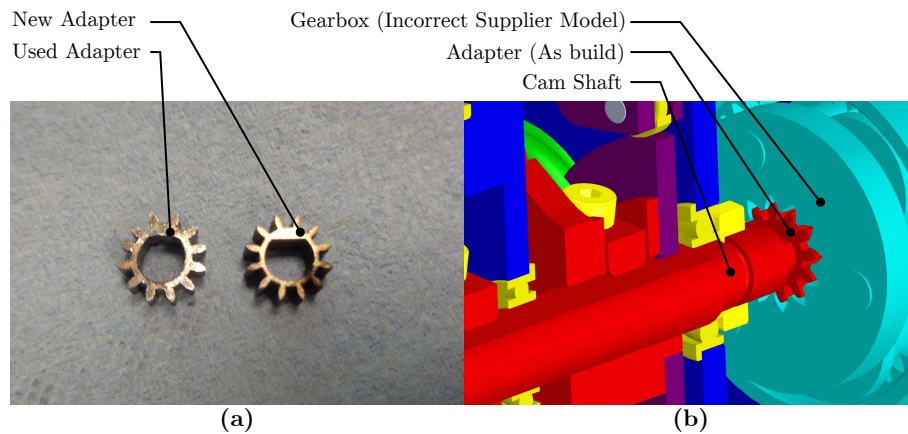


Figure 9.7: Issue with gearbox adapter. **a:** A used gearbox adapter shows plastic deformation with respect to an unused gearbox adapter. This allows play between the cam shaft and gearbox output. **b:** The actual adapter that fits in the actual gearbox is smaller and has a much thinner wall than the first one that was designed based on the incorrect CAD-model of the gearbox supplier.

9.4 Discussion

Based on the conducted experiments the functionality of the working mechanism is discussed. Fig. 9.5 shows the mechanism's ability to perform:

- *Sizing:* The mechanism is able to adjust to an emulated object size and start with the force build up at different locations.
- *Forcing:* The mechanism is able to generate an output torque using the implemented balancer.
- *Switching:* The mechanism is able to switch automatically between sizing and forcing.

This shows that the working principle of the drive works. Moreover, it proves the feasibility to combine an SBFA with a differential to obtain two different drive branches with different transmission ratio actually works. During the experiments the NBDM was not implemented. In preliminary tests the NBDM was compared with the plain drive shaft for a situation where the pretension setting of the buffer springs resulted in a large balancing imperfection, causing a spring-like behavior on the mechanisms input. When the plain drive shaft was rotated manually, it returned back to its initial position once released. The NBDM on the other hand, was observed to maintain its position. In future work the NBDM should be implemented on the mechanism to fully test its functionality and evaluate its impact on the performance, for instance due to additional friction.

Future work should focus on the improvement of the reliability and the performance. The current design suffered from play due to play in the gearbox adapter. It turns out that a 12-teeth metric gear with module 0.5 fits exactly in the gearbox output, so it could be investigated if a commercially available gear, for instance [65] could be used. Also the current threshold cam resulted in unreliable behavior. Unlike the intended design, the threshold cam can be turned to far backwards, as the cavity in which the follower initially rests is not deep enough. This causes the mechanism to lock at unwanted moments, which sometimes causes a complete jam of the mechanism. Adjusting one side of the cavity will likely solve this problem.

To increase the performance additional finetuning of the spring pretensions should take place. Also the hysteresis in the input torque should be subjected to a closer look. A good starting point might be to verify whether the touching windings of the springs are the origin.

9.5 Conclusion

In the experimental validation the working principle of the mechanism is proven, as the data shows that the mechanism is able to perform sizing, forcing and switching. An average torque reduction of 91.5% is measured for five different emulated object sizes.

Chapter 10

Discussion

The aim of this thesis is to develop and evaluate an energy saving drive. The core of this thesis consists of four parts, describing respectively the strategy selection, concept selection, prototype design and experimental evaluation. This chapter will discuss the relevance and implications of the developed drive.

During the concept selection the SBFA was selected based on a newly proposed performance metric, as this mechanism showed the potential to reduce the energy based on three aspects:

1. A transmission ratio change, which allows for a *high-speed* and a *high-force* branch.
2. Static load cancellation using a non-backdrivable mechanism (NBDM), which requires only activation of the motor during the prehension or release phase. Because of this intermittent activation, the nominal torque can be temporarily exceeded.
3. Torque reduction using the SBFA, which decreases the required actuation torque without to produce an adjustable output torque.

The main novelty is the integration of an SBFA in the drive, as no reported implementation of an SBFA in grippers was found in literature. It was combined with the other two current state-of-the-art aspects in a design of a gripper drive. The combination of the first and third aspect was experimentally validated using a realized prototype. The NBDM was tested manually in preliminary tests.

As the proposed mechanism consists of springs and clutches and aims to control the energy flow, it belongs to the category of *Clutched Elastic Actuators* [28]. Like in statically balanced brakes [45, 24], the level of the output force becomes a position-related task rather than a force-related one, because of the force reduction of the SBFA. The novelty of the newly proposed drive is that it is able to produce this output force at an initially unknown distance.

Although this new type of CEA is intended for the implementation in fixturing grippers and related devices, such as robotic grippers, prosthetic hands and all kind of clamps, it might also be applied in other machinery, such as stamping-machines. The mechanism might be especially useful in situations where the available input force is limited, such as manually operated devices.

In future work, these drives could be modeled in detail using the proposed method of Plooij et al. [28] with the addition of the SBFA component, which is proposed in Chapter 4. As mentioned, the developed drive is able to produce a adjustable output torque at an initially unknown distance. From this perspective, an interesting topic for future research is to investigate the possibilities to balance an initially unknown spring, i.e. an initially unknown stiffness at an initially unknown distance. As such, it would be possible to counteract the object stiffness of various objects.

Future research and finetuning of the drive is required to improve the current torque reduction of 91.5% and to analyze the energy consumption of the mechanism. There is an interesting possibility to improve the performance of the drive, at the cost of adding an extra differential, placed *after* the balancer, see Fig. 10.1. This reduces a paradoxical effect that is observed for the current design, in which the differential is placed *before* the balancer: Although the differential is required to increase the input Torque, it also reduces the motion required to build up the SBFA output Torque. The larger the differential's ratio, the longer it takes to obtain the desired output level. In the evaluation of the performance metric the time for the force build up was neglected. When the differential is placed *after* the balancer, it transmits no displacement but still enlarges the SBFA output torque. This will enable a faster force build up and

complies better with the performance metric. The additional differential is also expected to affect the balancing error and apparent stiffness. Analyzing these effects is subject of future research.

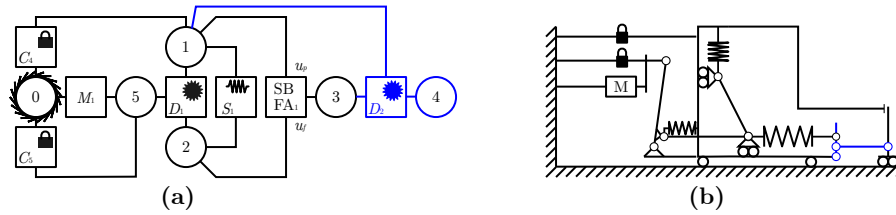


Figure 10.1: Concept with additional differential *after* the balancer. This transmission increases the output force but does not transfer motion. It requires one additional transmission, depicted in blue, in addition to the current concept. **a:**Topology. **b:** Example.

Another natural question is whether this prototype could be actual applied in for instance an industrial environment. Aside from finetuning the functionality and performance, there is one other key factor that should be improved: Its bulk. The current version, with its housing of $\varnothing 64 \times 78.5$ mm and mass of approximately 460 g is too large and heavy to use within a gripper for other purposes than research. As discussed in Section 8.5, there is potential to reduce the mass and size of the mechanism by using permanent connections, rather than detachable ones and by using custom designed components.

This might also reduce the number of required components, which is advantageous as the current mechanism is fairly complex, although I do not think the complexity will be an actual problem. Current state-of-the-art drives, such as the *Automatic Clutch* [35], are also mentioned to be complex [37]. Also [28] observes an increasing complexity in CEAs over time.

Chapter 11

Conclusion

The goal of this thesis was to develop and evaluate an gripper drive that reduces the energy consumption.

As drive strategy an actuator in combination with an internal torque mechanism was selected, because this allows for autonomous grasping and passive retention in any orientation. Based on a newly proposed performance metric, which relates to 1) the minimum dislodging torque in any direction, 2) the average closing speed and 3) the nominal power rating, the *Statically Balanced Amplifier* (SBFA) was selected as internal force mechanism. The performance increase of an SBFA with respect to a geared DC-motor falls apart in three factors:

1. A transmission ratio change, which allows for a *high-speed* and *high-force* branch.
2. Static load cancellation using a non-backdrivable mechanism (NBDM), which requires only activation of the motor during the prehension or release phase. Because of this intermittent activation, the nominal torque can be temporarily exceeded.
3. Force reduction using the SBFA, which decreases the required actuation torque.

A concept of a drive was developed which included the above three aspects. An actual prototype for the implementation in the existing Delft Hand 3 which performs a pick-and-place task was designed and realized.

Experiments where conducted with the prototype without NBDM. The results confirms the feasibility of the working principle, as the mechanism is able to perform 1) *sizing*, 2) *forcing* and 3) *switching between sizing and forcing*. The force build up starts automatically once mechanism has adjusted to the emulated object size. The mechanism is capable to produce a maximum output torque of 1.073 Nm. For 5 different object sizes an average torque reduction of 91.5% was measured. The NBDM was observed to engage in a manual test. This shows the feasibility of combining a Statically Balanced Force Amplifier with a NBDM and transmission ratio change.

Epilogue

Finally, after almost a year's work this master project has come to an end. Although I have the feeling that this project is still unfinished, I have to end it to make room for the next adventure, which was put in motion a while ago: a year working abroad.

At the time I requested "green-light" I already was aware that a functional prototype would be ambitious. Yet, I did not foresee the delay of almost a month in the manufacturing of the components, for which I was dependent on craftsmen. The breakdown of the encoder magnet during assembly caused some additional delay. This resulted in a lack of time to solve the "childhood-diseases" in the prototype and to finetune the mechanism and test setup for a proper evaluation of the performance. Ultimately a few days instead of a few weeks were left for testing. I am pleased that I at least was able to validate the working principle, although I aspired to do more.

I could not have come this far on my own. So many people supported me in this work, for which I am very grateful.

First of all I would like to thank my daily supervisor, Wouter. Thank you for your guidance, valuable feedback and I appreciate that you were always available to assist with questions. Second, I would like to thank Jan. Thank you for your engagement and valuable advice in the design of the prototype. Third I would like to thank the craftsmen from the workshop, Reinier, Mario and Wim. Thank you for your help with the realization of the prototype. I admire your skills and finesse with the workshop machinery. Fourth, I would like to thank Ralph and Linda. I enjoyed working with you on the Plugless Arm. Fifth, I would like to thank Just Herder, Martijn Wisse, Michiel Plooij, Gerwin Smit, Cor Meijneke and Dick Plettenburg. Thank you for the time you took to advise me in one or more of the various stages of this project.

Sixth I would thank my valuable friends for their support during the last year. Especially Ewout and Arnoud, thanks for your advice. Finally I would like to thank my lovely wife, Eline. Thanks for your patience, encouragement, cheerfulness and love.

Appendix A

Additions to Chapter 2

A.1 W.E.N-Principle

The current section explains the W.E.N.-principle, which is applied in the *WILMER* prosthetic hand. Unfortunately the design of this hand is not very well documented¹ and only the general working principle is described in [26]. As such, some details on the implementation of the hand are not known.

The hand is schematically depicted in Fig. A.1. The key of this hand is that the grasp force in the finger tips is changed by moving the spring, without affecting its elongation: The grasping force of this hand is controlled by moving one of the ends (point P) of the spring in a curved slot, as is indicated in Fig. A.1b and Fig. A.1c. As such, the moment the spring around the hinge A changes, and thereby the contact force in the finger tip. If the curved slot is made such that it forms a radius around point B , the spring is moved without length change and no work is done.

In the original subcaption it is claimed the sizing, as depicted in Fig. A.1a, occurs effortlessly. However, as the groove is fixed this is not possible, because the attachment of the spring does not coincide with the joint of the hinge, and therefore the length of the spring will change during sizing. According to Plettenburg¹ the groove could move together with the finger during sizing, and is locked in place during sizing.

The actuation of this prosthesis hand is not described, as such it is not known whether this hand was powered manually or by an actuator. It is also not known if the control requires 1 or 2 inputs.

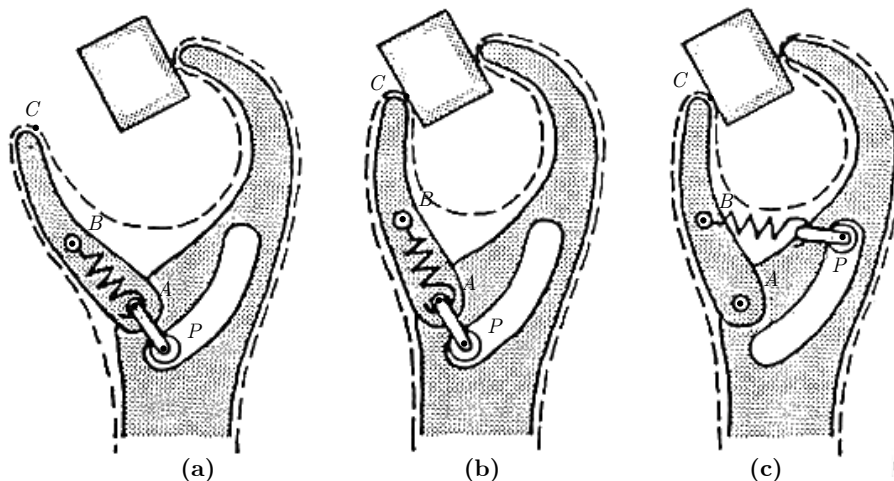


Figure A.1: *WILMER* hand with *W.E.N.-Principle*. **a:** Sizing mode, the thumb is able to adjust to the object size. **b:** Contact is made between the object and thumb. The mechanism transfers to the forcing mode. **c:** Forcing mode, the force in the fingertip can be adjusted effortlessly, because the spring changes its direction without changing its elongation. Image taken from [26].

¹ Personal communication with Dr.Ir. Plettenburg d.d. October 13th, 2016.

When this principle is generalized, it is a (lockable) spring connected to a CVT. The key concept for this strategy to operate is that the spring is kept at a constant length (and constant force). As such no work is done. Using the variable transmission ratio of the CVT, the force at the output is varied. The spring needs to be lockable, to ensure the length does not change during sizing (when the clamp is not in contact with the object). In Fig. A.1b, the spring is indeed in a singular position. As described by Plooij et al [27] this is one of the three principles on which locking mechanisms operate.

Yet another way to look at these mechanism is as a Variable Stiffness Actuator (VSA) because the effective stiffness in the contact point changes. When the groove and finger move together, (Fig. A.1a) no stiffness is “felt” at point C . When point P is moved (Fig. A.1b and Fig. A.1c), the stiffness felt in point C changes.

Appendix B

Additions to Chapter 3

B.1 Alternative Performance Metric Visualization

This section presents an alternative visualization of the performance metric. The performance is plotted in Fig. B.1 as function of ι for two different tasks.

The first task is a pick-and-place task, where prehension and release takes both 0.5s and the forward and backward movement both 2s. Only during the forward motion an object is retained. This results in $D_{PR} = \frac{1}{5}$ and $D_{PRR} = \frac{3}{5}$, or $D_{PRR}/D_{PR} = 3$. The second task is an assisted living robot that picks up objects in the kitchen and brings them to the living room. The retention and release take again 0.5s, but the movement from the kitchen and living room take 30s. This results in $D_{PR} = \frac{1}{61}$ and $D_{PRR} = \frac{31}{61}$, or $D_{PRR}/D_{PR} = 31$.

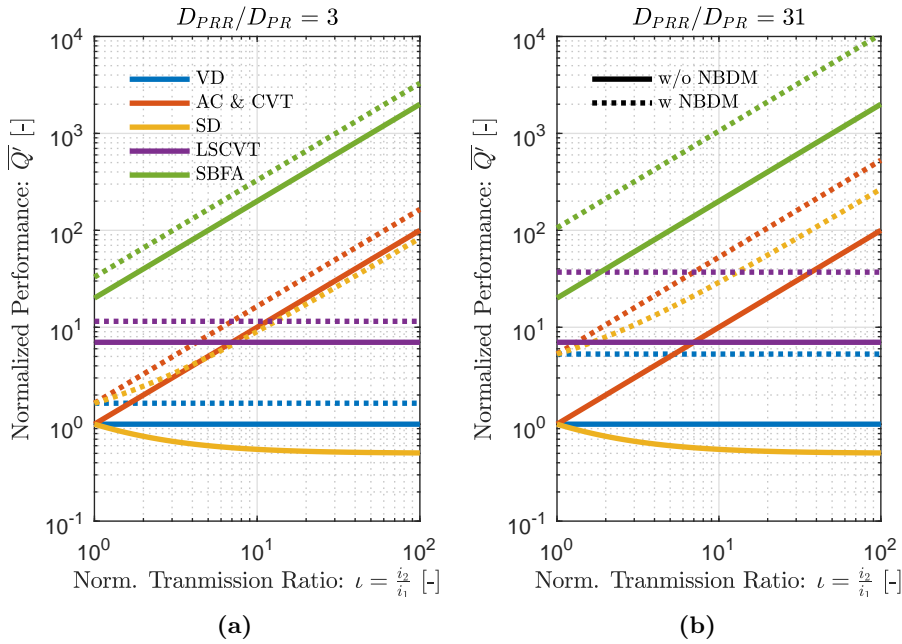


Figure B.1: Normalized performance of the different strategies. The line color represent the strategy. The linestyle, solid or dotted, represent without NBDM or with NBDM respectively. For the LSCVT is assumed: $\alpha = 7$. For the SBFA is assumed: $\zeta = 0.95$. **a:** Typical pick and place task. **b:** Typical assisted living task.

Appendix C

Additions to Chapter 4

C.1 Concept with Intermittent Transmission

The mechanism depicted in Fig. C.1b is a modified version of a statically balanced mechanism described by [23]. It works as follows: During sizing, lock C_1 is disengaged and C_2 engaged. The mechanism is statically balanced and can perform sizing. Once the sizing is completed, C_1 engages locked and C_2 is disengaged, the tension in the buffer sprign S_B is maintained and the main spring is causes a contact force.

The grasping force for this mechanism can not be controlled, as the output force is a constant. The reason for this is that hen one of the springs is ommitted in the system depicted in Fig. C.1a, this would result in a mechanism delivering a constant force in the horizontal direction [23], hence the output force is always equal to this constant. This violates the second subfunction, as the contact force can not be controlled.

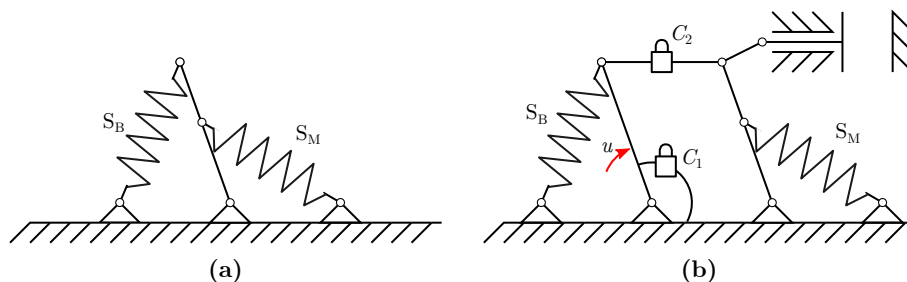


Figure C.1: Intermittent SBFA. **a:** A possible emobidiement of a statically balanced mechanism as described by Herder [23] **b:** Intermittent SBFA. Using input u the mechanism adapts to the object size effortlessly, because S_1 and S_2 are statically balanced. Once adjusted properly, the position of S_B is locked using C_1 . The locker C_2 is unlocked simultaneously. As such the transmission is intermittent and the object is clamped by spring S_M . As such, no force adaptations can take place.

Appendix D

Additions to Chapter 5

D.1 Derivation of SBFA forces

The forces of the SBFA can be derived by the partial derivatives of the potential energy. To do so, the expression $s_M = u_f - u_p$ and $s'_M = u_f - y$ are substituted in Eq. (4.9). As for this analysis only the SBFA itself is regarded, the object stiffness is not taken into account, $k'_M = k_M$. If it is desired to take the object stiffness into account in the topology analysis, it can be introduced as additional spring connected to the output. The resulting expression for the potential energy is:

$$V' = \frac{1}{2} (k_M(u_f - y)^2 +) \quad (\text{D.1})$$

Taking the partial derivatives results in the forces on the in- and outputs:

$$F_f = \frac{-\partial V'}{\partial u_f} = k_M(y - u_p) \quad (\text{D.2})$$

$$F_p = \frac{-\partial V'}{\partial u_p} = k_M(u_p - u_f) \quad (\text{D.3})$$

$$F_y = \frac{-\partial V'}{\partial y} = k_M(u_f - y) \quad (\text{D.4})$$

These equations are used to describe the SBFA block.

D.2 Topology Generation using Graph Theory

The first method for the generation of topologies is based on graph theory. Graph theory is widely used in engineering, for both the synthesis [66, 67] and analysis of mechanisms [68], whether or not evaluated using dedicated algorithms. Likewise, CEAs might be represented by graphs, which would allow for a computer aided concept generation.

This section is structured as follows. First the conventional way of mechanism representation is discussed, and it will be argued this conventional representation is not sufficient. Therefore a novel representation, based on *bipartite graphs* will be proposed. Then this representation will be used to explore the solution space and estimate the number of possible topologies.

D.2.1 Conventional Mechanism Representation using Graphs

Typically, when graphs represent the kinematic structure of a mechanism, the *vertices* (points) of the graph represents the bodies and the *edges* (lines connecting the points) represent the connections between the bodies, i.e. revolute joints, prismatic joints, springs, gear meshes etc. [66, 67]. Although this represents the mechanism in a very detailed way, this has two difficulties. First, it is too detailed. The aim is to describe the topology rather than the typology, and therefore the structure on part level is not of interest yet. As is shown by [67], each added body causes an immense increase in possibilities. A representation involving less vertices implies a significant reduction in the number of possible graphs. The difference in the complexity of the representation is also shown in Fig. D.1, where several graph representations describe the same differential mechanism.

Second, when kinematic structures are evaluated on part level, as in [66, 67], they use *simple* graphs, i.e. graphs without *loops* and *multiple edges*. Loops are edges of which the ends connects to the same vertex. Multiple edges means multiple edges connect the same two vertices. As such, parallel connections, e.g. a clutch in parallel with a spring between two bodies, could not be represented by graphs. (Unless special measures are taken, e.g. define the mechanism by multiple graphs simultaneously [67].)

Therefore I propose in the next subsection a more compact form, in which a differential might be represented by a single vertex (Fig. D.1c). Also the relation will be shown with *hypergraphs* where a differential might be represented as single *hyperedge* (Fig. D.1d).

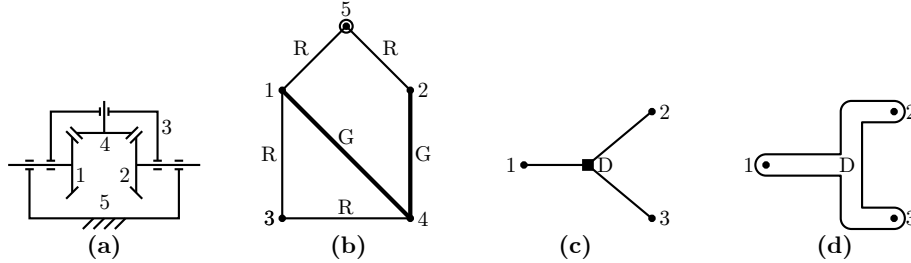


Figure D.1: Different representations of differentials. **a:** Schematic representation of bevel gear differential. **b:** Graph representation of kinematic structure. Vertices 1, 2 and 4 represent the bevel gears. Vertex 3 represents the rotating carrier and the encircled vertex 5 represents the ground. Edges with a label “G” represent a gear mesh connection between two bodies, edges with a label “R” represent a revolute joint between two bodies. **c:** Bipartite Graph representation. The vertices 1-3 represent the bodies, the vertex “D” represents the differential connecting the three bodies. **d:** Hypergraph representation of differential. The hyperedge “D” represents the differential, connected to three bodies, represented by vertices 1-3.

D.2.2 Representation of CEAs using Bipartite Graphs

This section describes a novel way to represent the topologies of CEAs by graphs. This method is based on *bipartite* graphs. Also the relation to *hypergraphs* will be shown.

A bipartite graph $\mathcal{G}(U_{\mathcal{G}}, V_{\mathcal{G}}, E_{\mathcal{G}})$ consists of an edgeset $E_{\mathcal{G}}$ and two sets of vertices $U_{\mathcal{G}}$ and $V_{\mathcal{G}}$, such that these two vertices are disjoint: $U_{\mathcal{G}} \sqcup V_{\mathcal{G}}$. This means that two adjacent (i.e. connected by an edge) vertices are always part of different sets. In other words, the vertices u_i and v_j can only be adjacent if $v_i \in V_{\mathcal{G}}$ and $u_i \in U_{\mathcal{G}}$. Two vertices in the same subset can never be adjacent.

These properties of bipartite graphs matches perfectly with the topology representation as described in Section 5.2. The bodies and functioning elements (e.g. springs, clutches, differentials) are each represented by a different subset of vertices. The properties of a bipartite graph implies that two rigid bodies can never be connected directly, because two vertices in the same subset can never be adjacent. This is logic, if two bodies are rigidly connected to each other, they ought to be represented as a single body. The same holds for the functioning elements, they can never be connected directly, but always require an intermitten body. This is in line with the representation described in Section 5.2

In Fig. D.1 a differential is represented as bipartite graph. The circular vertices represent the rigid bodies. The square vertex represents the functioning element, in this case a differential. Note that the edges represent nothing else then connection between a functioning element and a body.

Further support of this representation is the notion that a differential might also be represented as a hypergraph [68]. Unlike graphs, the hypergraphs consist of hyperedges which are allowed to connect to more than two vertices [69]. In this representation the vertices represent the bodies and the hyperedges represent the functioning elements connecting those bodies. A differential is shown as example in in Fig. D.1d¹.

As is described in [70] a hypergraph can be represented as a bipartite graph by its incidence graph. The hypergraph is denoted as $\mathcal{H}(V_{\mathcal{H}}; E_{\mathcal{H}})$, where $V_{\mathcal{H}}$ is a set of vertices where $E_{\mathcal{H}}$ is a set of hyperedges. The two vertex-subsets of the bipartite graph are equal the vertexset and edgeset of the hypergraph

¹The representation of Fig. D.1d does not correspond to the representation in [68], where the differential is represented by three vertices and three edges, although it is clearly stated that it is a hypergraph

respectively, i.e. $V_G = V_{\mathcal{H}}$ and $U_G = E_{\mathcal{H}}$. Two vertices $e_i \in U_G$ and $v_j \in V_G$ are only adjacent if and only if, $v_j \in e_i$ in the hypergraph \mathcal{H} . When this procedure is followed, this results in a bipartite graph, with a vertex-subset representing the bodies and a vertex-subset representing the functioning elements.

Although the hypergraph representation and bipartitegraph representation are both valid, the latter is more useful, because bipartite graphs are a special form of graphs, whereas hypergraphs are a generalization of graphs. As such, software available for the analysis of graphs deal easily with bipartite graphs, but requires more effort to handle hypergraphs.

D.2.3 Analysis of Possibilities

Based on the gained knowledge on bipartite graphs, it is possible to estimate the number generated topologies.

A first way to do this would be by simply evaluating the number of existing connected bipartite graphs with for N vertices. This sequence is documented by [71] and listed in Table D.1. (Connected means that all vertices of the graph are directly or indirectly connected to each other. The graph does not contain “Islands”. This ensures the graph represents a single mechanism.)

However there are two difficulties with this approach. The first difficulty is that on beforehand it is not known which vertex-set represents the rigid bodies. This has to be determined when the bipartite graphs is generated. When one of the vertex-sets contain an one degree vertex (i.e. a vertex connected to one edge) this vertex-set represents automatically the rigid bodies, because functioning elements should at least be connected to two bodies. For some graphs both vertex-sets could represent the rigid bodies. These graphs have a “double interpretation”, this increases the number of topologies. A second difficulty is that not all bipartite-graphs result in feasible topologies. For instance, when both vertex-sets contain a one degree vertex, none of the vertex-sets could represent the functioning elements. This reduces the number of topologies.

The number of possible graphs for each number of vertices is evaluated as follows. Using the build-in library of WOLFRAM MATHEMATICA 11.0, *all* unlabeled simple graphs with N vertices are loaded. Unlabeled means that no identifier (number/name) is appointed to the vertices of the graph. When this would not be the case, this introduces more permutations. For example, the graph depicted in Fig. D.2a could have 3 permutations, because the isolated vertex could be labeled 1, 2, or 3. For each individual graph is determined whether it satisfies the eight constraints listed below. The first two constraints ensure the graph is connected and bipartite. The other constraints checks whether the graphs represent a feasible topology. For each given number of vertices (N), the number of graphs that satisfy all constraints are stored in the array $a[N]$.

Furthermore the graphs are counted that have a second interpretation, i.e. the graphs for which both vertex-subsets could represent the bodies. This is the case when the graph does not contain any vertices with a degree of one or larger than four. Otherwise, the vertex-set containing this vertex would automatically appointed as the set representing the bodies, because all functioning elements are either connected to two or three bodies. The number of graphs for that have a double interpretation are stored in the array $b[N]$.

What follows is a list of constraints. These constraints are visualized in Fig. D.2. The first constraint corresponds to Fig. D.2a, the second to Fig. D.2b and so on.

1. The graph should be connected. The graph should not contain isolated vertices, because this would result in loose bodies or elements.
2. The graph should be bipartite. The vertex-set of the graph should consist of two disjoint subsets, vertices within the same subset should not be adjacent. As such, the graph represents elements and bodies.
3. The graph should contain at least one vertex with a degree of two. Every solution should incorporate an actuator, which is represented by a vertex with two degrees.
4. All vertices with a degree of one should be in same vertex-subset. As explained, only the clamp and ground may have a single connection. Both the clamp and ground are rigid bodies and not functioning elements, and should be therefore in the same vertex-subset.
5. If one of the subsets contains a one degree vertex, the other subset should contain a two degree vertex. The vertex with degree appoints its vertex-subset to represent the bodies. As consequence,

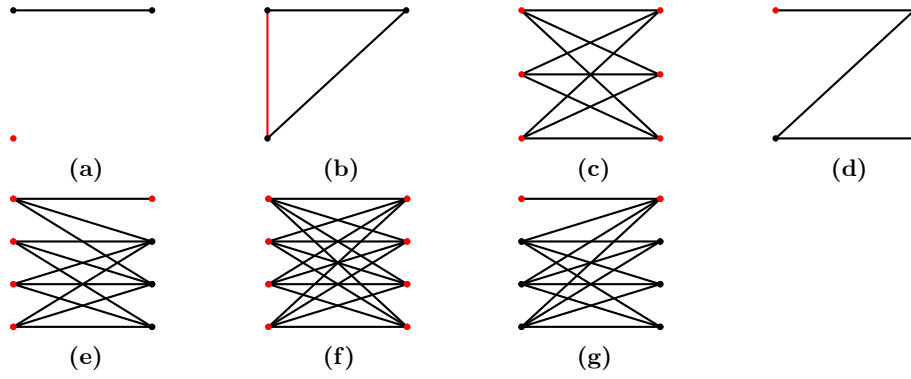


Figure D.2: Visualization of the constraints. The subfigures **a-f** correspond to constraints 1-7 respectively. The vertices or edges that violate the constraints are colored red for clarifications. Note that for each subfigure only 1 constraint is taken into account.

the other subset contains the functioning elements. This subset should contain at least a motor, represented by a vertex with a degree of two.

6. All vertices of one of the vertex-subsets should have a degree lower than four. No functioning-elements are defined with more than four connections. As such, at least one of the two subsets should consist of vertices of which their degree is lower than four.
7. All vertices should have a degree lower than four in one vertex-subset, if the other vertex-subset contains a vertex with a degree of one. Because a vertex of one degrees represents a body, its vertex-subset is the vertex-subset containing the bodies. As such, the other vertex-subset are the functions. All functions have a maximum of three connections.

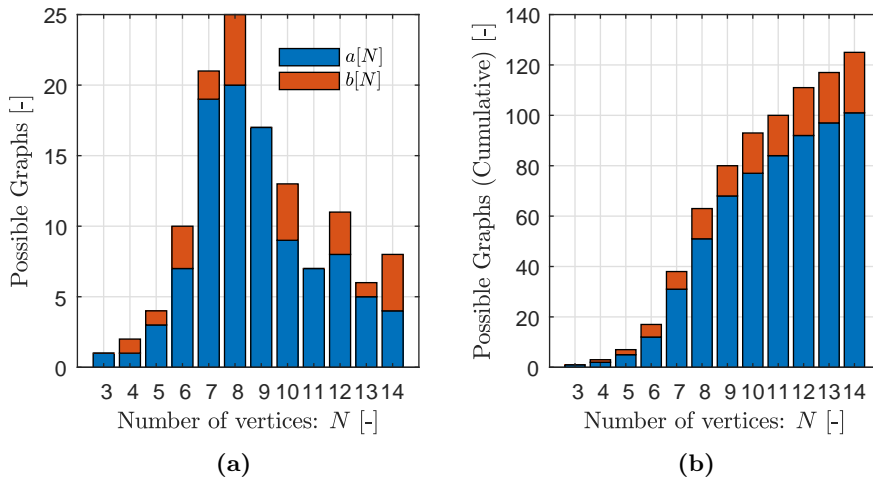


Figure D.3: Number of graphs that satisfy the seven constraints ($a[N]$) and number of graphs that both satisfy the seven constraint have a double interpretation ($b[N]$). **a:** Per number of vertices. **b:** Cumulative

Table D.1: Number of Possible (Unlabeled) Graphs

Vertices	Connected Bipartite Graphs [71]	Graphs satisfying constraints	Graphs satisfying constraints with double interpretation
N		$a[N]$	$b[N]$
3	1	1	0
4	3	1	1
5	5	3	1
6	17	7	3
7	44	19	2
8	182	20	5
9	730	17	0
10	4,032	9	4
11	25,598	7	0
12	212,780	8	3

D.2.4 Discussion

It is likely that using this method all possible topologies (up to a certain number of vertices) can be generated. However, it should be mentioned that this method is sensitive to the constraints for filtering the feasible concepts. Because these constraints are rather abstract, the risk exists of posing these constraints to tight or to loose, i.e. the risk of respectively excluding feasible topologies or including infeasible solutions.

As is shown in Table D.1 a huge reduction of possible graphs is achieved when the constraints 1-8 are satisfied, compared to the default sequence of connected bipartite graphs. Because of the constraints on the maximum and minimum degree of vertices, even the monotonically increasing behavior of the number of the graphs is lost.

Yet, for up to 10 vertices (which equals the complexity of the mechanism in ??) the cumulative number of graphs is ~ 80 , see Fig. D.3. Furthermore, when the graphs are labeled, i.e. a functions are appointed to the functioning elements, this might result in several permutations for each graph. Therefore, manual evaluation of all generated topologies is cumbersome.

This approach could be fruitful for the conception of topologies for less complex clutched elastic actuators, or when it is implemented in an optimization procedure, for example an evolutionary algorithm as in [67]. However, this is beyond the scope of this thesis.

D.3 Mathematical Description Threshold Loading

This section expresses the balancing error for the two variants of the C-M-R-TT topology.

D.3.1 Without Anticipation

The error e is “trapped” in the spring. Assuming that the object is infinite stiff, the balancing error follows from $\lim_{k_O \rightarrow \infty} V'$ where V' is expressed according to Eq. (4.9). This results in:

$$V' = \frac{k_n}{2} (e - s_M)^2 + s_{M,max}^2 - (s_M)^2 \quad (\text{D.5})$$

When $e \neq 0$, V' is no longer a constant. The magnitude on the deviation is non-linear and depends on e and s_M .

D.3.2 With Anticipation

This section proves that an offset compensates for the balancing imperfection. The spring extension e resulting from the load of the threshold is known beforehand and can therefore be incorporated in the Eq. (4.3), the expression for the:

$$s_B = \sqrt{\frac{2C - k_M(e - s_M)^2}{k_B}} \quad (\text{D.6})$$

This results in the following expression for the actual potential energy:

$$V' = \frac{1}{2} (k_M s_M^2 + k_B s_B^2) = \frac{k_M}{2} ((e - s_M)^2 + s_{M,max}^2 - (e - s_M)^2) = C \quad (\text{D.7})$$

This equation results in a constant and is therefore statically balanced.

Appendix E

Additions to Chapter 6

E.1 Non-Linear Transmission in Fingers

The expressions for the non-linear transmission ratio is described in both [17, 48]. Using the parameters depicted in Fig. E.1 the transmission ratio of the differential equals

$$R_{A,B} = \frac{h}{h + L_1} \quad (\text{E.1})$$

Where:

$$h = c(\cos(\phi_2 - \psi) - \sin(\phi_2 - \psi) \cot \beta) \quad (\text{E.2})$$

With:

$$\cot \beta = \frac{c \sin(\phi_2 - \psi) \sqrt{4a^2b^2 - N^2} + M(L_1 + c \cos(\phi_2 - \psi))}{-(L_1 + c \cos(\phi_2 - \psi)) \sqrt{4a^2b^2 - N^2} + Mc \sin(\phi_2 - \psi)} \quad (\text{E.3})$$

$$M = -L_1(L_1 + 2c \cos(\phi_2 - \psi)) + a^2 - b^2 - c^2 \quad (\text{E.4})$$

$$N = L_1(L_1 + 2c \cos(\phi_2 - \psi)) - a^2 - b^2 + c^2 \quad (\text{E.5})$$

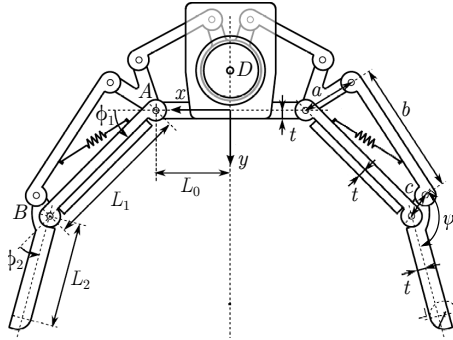


Figure E.1: Parameters of Delft Hand 3. Image adapted from [17].

E.2 Hand configurations

This section describes the procedure to compute the hand configuration for a given object size.

This procedure, reproduced from [17, Ch. 6] uses *loop closure vector equations*. The parameters for this analysis are depicted in Fig. E.1. Under the assumption that the object is a cylindrical object, positioned with its centerpoint at the y -axis of the gripper, the configuration is determined for a given object radius r_o by solving the following set of equations:

$$\begin{bmatrix} L_0 + p_1 \cos \phi_1 \\ p_1 \sin \phi_1 \end{bmatrix} = \begin{bmatrix} (r_o + t) \sin \phi_1 \\ y_o - (r_o + t) \cos(\phi_1) \end{bmatrix} \quad (\text{E.6})$$

$$\begin{bmatrix} L_0 + L_1 \cos \phi_1 + p_2 \cos(\phi_1 + \phi_2) \\ L_1 \sin(\phi_1) + p_2 \sin(\phi_1 + \phi_2) \end{bmatrix} = \begin{bmatrix} (r_o + t) \sin(\phi_1 + \phi_2) \\ y_o - (r_o + t) \cos(\phi_1 + \phi_2) \end{bmatrix} \quad (\text{E.7})$$

These equations are solved using the MATLAB command `fsolve` for $r_o \in [28, 60]$ mm. This results in the configuration depicted in Fig. E.2

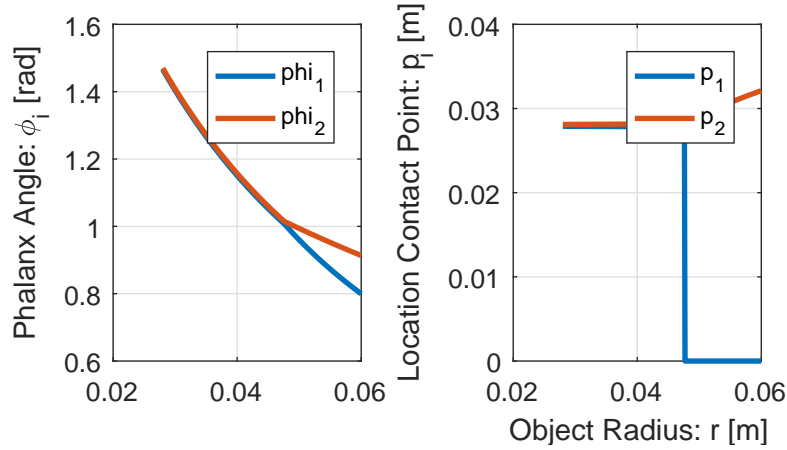


Figure E.2: Hand configuration for a cylindrical object

E.3 Apparent Stiffness of Finger

This section elaborates on the derivation of Eq. (6.6). Application of the general equation for the apparent stiffness [20] results in:

$$k_{A,i,j} = \left(\frac{\partial q_{i,j}}{\partial \phi_A} \right)^2 k_{i,j} \quad (\text{E.8})$$

where $k_{i,j}$ the stiffness at this contact point and $\frac{\partial q_{i,j}}{\partial \phi_A}$ is the (non-linear) transmission from the finger input to contact point. To relate this transmission to the transmission ratios $R_{A,1}(\phi_2)$ and $R_{A,2}(\phi_2)$, the principle of virtual work is applied:

$$T_A \delta \phi_A = F_{i,j} \delta q_{i,j} = F_{i,j} \frac{\partial q_{i,j}}{\partial \phi_B} \delta \phi_B \quad (\text{E.9})$$

When this expression is rearranged and combined with Eqs. (6.1) and (6.2), this results in:

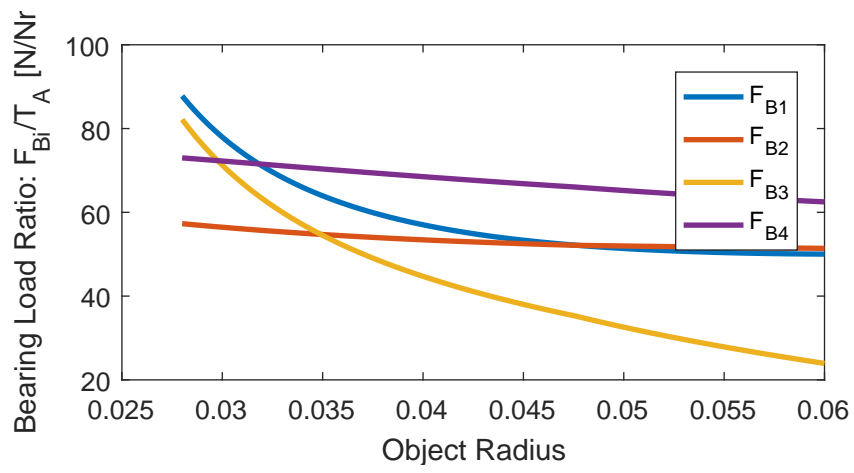
$$\frac{\partial \phi_A}{\partial q_{i,j}} = \frac{F_{i,j}}{T_A} = R_{A,i,j} \quad (\text{E.10})$$

Substituting Eq. (E.10) in Eq. (E.8) results indeed in Eq. (6.6):

$$k_{A,i,j} = R_{A,i}^{-2} k_{i,j} \quad (\text{E.11})$$

E.4 Mechanical Strength of Hand

A brief inspection of the mechanical strength of the existing hand revealed that the bearings are weakest components and therefore pose a limit to the drive torque. An analytic expression for the bearing loads was derived and evaluated for the configurations obtained in appendix E.2. The results of this expression are verified with a graphic method. The bearing loads are plotted as ratio of the drive torque in Fig. E.3. This ratio has a maximum value of 87.8 N/Nm. The bearings, of type NSK MF63 and NSK MR63, have a static load rating of 74 N. Each joint is equipped with two bearings. Hence, an upper limit to the drive torque is 1.69 Nm. To include a safety margin of 20 % the maximum drive torque is set to 1.4 Nm.

**Figure E.3:** Bearing loads

Appendix F

Additions to Chapter 7

F.1 Outdated Typology Selection of the SBFA

This section describes the typology selection of the SBFA based on an outdated design principle. First this outdated design principle and its implications will be explained, then the original typology selection is conducted. Because the design principle was falsified relatively late in the design process, the typology selection of the SBFA is not completely re-evaluated.

F.1.1 Outdated Design Principle

Initially the energetic performance of the SBFA was evaluated on the relative work, i.e. the energetic error normalized by the ideally constant amount of potential energy. First this normalization is presented followed by the implications. Then it will be explained why this design principle is not completely correct.

F.1.1.1 Normalized Energy Error

Recall from chapter 4 the error in the stored potential energy due to a finite object stiffness and position errors. The actual stored amount of work was normalized with the ideally constant amount of work and written as function of the normalized spring extension.

Recall Eq. (4.9) for the actual stored energy:

$$V' = \frac{1}{2} \left(\frac{\kappa k_M (e - s_M)^2}{\kappa + 1} - k_M s_M^2 + 2C \right) \quad (\text{F.1})$$

This actual stored energy was normalized by the constant $C = 1/2 k_M s_{M,max}^2$ and written as function of the normalized stroke: $\bar{s}_M = s_M / s_{M,max}$ and normalized error: $\bar{e} = e / s_{M,max}$. This yields:

$$\bar{V}' = \frac{V'}{\frac{1}{2} k_M s_{M,max}^2} = 1 - \bar{s}_M^2 + \frac{\kappa (\bar{s}_M - \bar{e})^2}{\kappa + 1} \quad (\text{F.2})$$

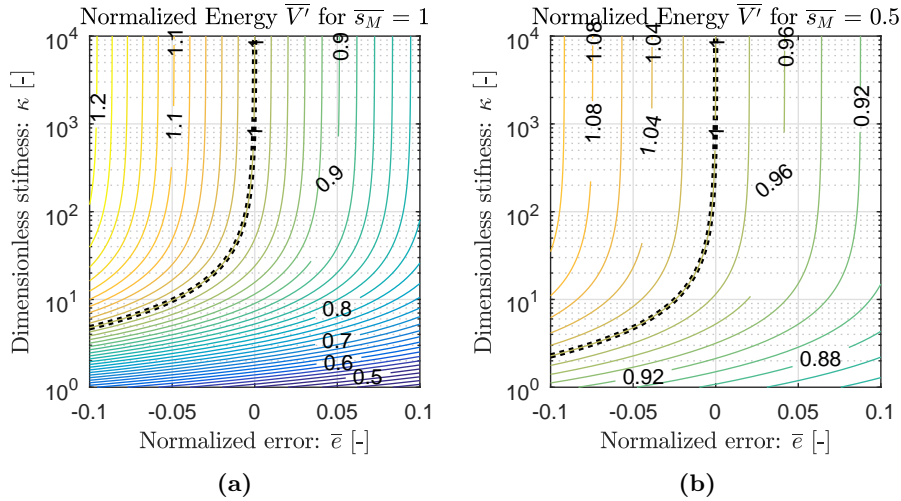


Figure F.1: Normalized Energy Error. The black dotted lines indicate the perfect balancing condition.

F.1.1.2 Implications

The effects on the normalized actual energy are visualized in Fig. F.1, this section discusses the implications.

First of all it should be noted that ideally $V' = C$ and hence ideally $\bar{V}' = 1$. This is indicated by the black dashed line in Fig. F.1. This ensures no energy needs to be supplied to the mechanism, which is accompanied with losses.

To minimize the deviation from this ideal condition the dimensionless stiffness κ should be maximized and the normalized error \bar{e} should be minimized. To maximize κ , the spring stiffness k_M needs to be minimized. Recall from chapter 4 that the balancing force and deviation also reduce for a small stiffness. This would lead to the conclusion that the stiffness of the main spring should be as small as possible.

F.1.1.3 Falsification

The problem of this analysis is that it neglects that the constant C is also dependent on the stiffness.

To achieve a targeted output force with a low stiffness, a large stroke is required, which increases the constant C . The required stroke equals: $s_{M,max} = F_{M,max}/k_M$, where F_M is the targeted output force. Substituting this in $C = 1/2k_M s_{M,max}^2$ results in:

$$C = \frac{F_{M,max}^2}{2k_M} \quad (\text{F.3})$$

So indeed, the constant amount of potential energy increases for a decreasing stiffness. This increase in stored energy dominates over the reduction in the relative error, so the absolute error increases. This absolute error is what matters in the end. This is the reason why in chapter 4 was concluded that to minimize the work, the spring stiffness should be maximized.

Based on this new design insight the spring stiffness was increased, but the time lacked to reevaluate the conceptual design.

F.1.2 Outdated Typology Selection

Unfortunately, the incompleteness in the analysis of the energy error was not discovered until the detailed design was nearly completed. This detailed design could still be adjusted, but the time lacked to re-evaluate the conceptual design that was based on this principle. For the sake of completeness the outdated selection is incorporated in this appendix.

This selection starts with an overview of the selection criteria. Then the different embodiment are compared, followed by a comparison.

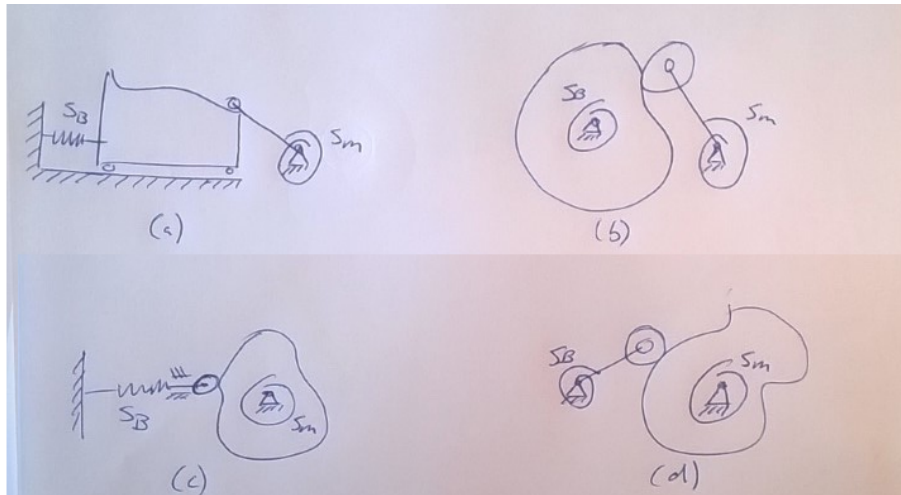


Figure F.2: Sketch of SBFA Embodiments. S_M denotes the main spring and S_B the balancing spring. **a:** Main spring at follower with translational buffer cam. **b:** Main spring at follower with rotational buffer Cam. **c:** Main spring at cam with translational buffer. **d:** Main spring at cam with rotational buffer.

F.1.2.1 Selection Criteria

For the comparison and selection of the balancer embodiment, the following criteria are identified:

1. *Energy Saving* A low energy consumption is the main goal of this thesis. The (falsified) design principle states that the relative energetic error reduces when the stiffness increases, hence the ability to implement a large stroke can be used as metric to compare the energy consumption.
2. *Compact* A compact balancer is likely to have a low mass and inertia, which enable a *lightweight* and *fast* design.

F.1.2.2 Description

Recall from chapter 4 that a statically balanced mechanism consist out of two springs with a special transmission between them. Moreover it was concluded that the input should attach to the main spring, which paves the way to a design in which the cam itself forms an in- or output.

The scope of cams considered is limited to planar cams, as they are easily produced using e.g. a laser cutter, wire EDM or a 3-axis milling machine. A concept using a spatial, cylindrical, cam is explored in appendix F.2. The geometry of this cam is quite complex, which impedes production and troubleshooting, which is unwanted for a first prototype.

Inspired on [45] and [64] the cam mechanism are categorized in rotational or translational cam and rotational or translational follower. The same assumption as in [45] is done that the type of springs is similar to the type of DoF, as this likely results in compact designs. For example a rotational cam is always connected to a rotational spring and a linear cam is always connected to a translation spring. Consequently to this assumption, the component to the main spring is always rotational, as this is a torsion spring. This component can be either a cam or a follower. The buffer is the opposite, but can be either rotational or translational. This leaves the four options which are discussed subsequently.

Main Spring at Follower with Translational Buffer Cam The balancer with a rotational follower connected to the main spring and a translational buffer cam is depicted in Fig. F.2a.

A drawback to the employment of a rotational follower connected to the main spring is that its rotation is limited to a maximum of 180° . Singularities will arise when this limit is exceeded, consequently the trajectory is no longer deterministic. This imposes a lower limit to the stiffness of the main spring, which is disadvantageous for the energetic performance.

This is explained in more detail for the example depicted in Fig. F.3a. This translating cam has a sinusoidal trajectory, which oscillates around the hinge of the follower. Now image the cam to move to the right, consequently the cam will rotate clockwise. This continues until the follower is upright, as depicted in Fig. F.3b. In this position, the follower can start to move in clockwise or counterclockwise direction. The trajectory of the follower is for this point not fully determined by the cam. This

has large consequences, as it might reverse the motion direction of the follower. The same holds for the lowest position, when the follower is rotated 180° further. These singular positions should be avoided, as the follower trajectory needs to be fully determined to ensure a reliable functioning, hence the rotation of the follower is limited to 180° .

Recall that the output needs to be concentric with the the cylindrical housing of the mechanism to enable it to float. Therefore the main spring needs also to be concentric, this means that the cam is positioned with an offset w.r.t. the main axis of the device, this comprises the compactness. Moreover it requires linear guides, which take more space than rotational bearings. . For instance, the smallest linear ball bearing of SKF, the LBBR 3 with an outer diameter of 7 mm and a length of 10 mm, is significantly larger than second smallest rotational ball bearing, the W6381/1 with an outer diameter of 3 mm and a width of 1 mm. The static load ratings of both bearings is approximately 50 N.

Main Spring at Follower with Rotational Buffer Cam The balancer with a rotational follower at the main spring and a rotational cam is depicted in Fig. F.2b. Also for this case the motion range of the follower is limited to a maximum of 180° to avoid singularities.

When an external cam is used, the pivot point has an offset w.r.t. the main axis, but an internal cam could be co-axially positioned, which likely results in a compact design.

Main Spring at Cam with Translational Buffer Follower Fig. F.2c shows a cam connected to the main spring and a translational follower to the buffer spring.

The cam can be designed for multiple revolutions, an example is shown in Fig. F.3c. Consequently, there is no inherent lower limit to the to the stiffness of the main spring, this improves the energetic performance.

A translating follower requires space in radial direction, and therefore it is likely to result in a mechanism with a large diameter.

Main Spring at Cam with Rotational Buffer Follower Fig. F.2d depicts a cam connected to the main spring, balanced by a rotational follower.

Again, the range of the cam is not limited by singularities, which enables a very compliant main spring. When the pivot points of the followers are positioned closely to the cam, this results in a compact design.

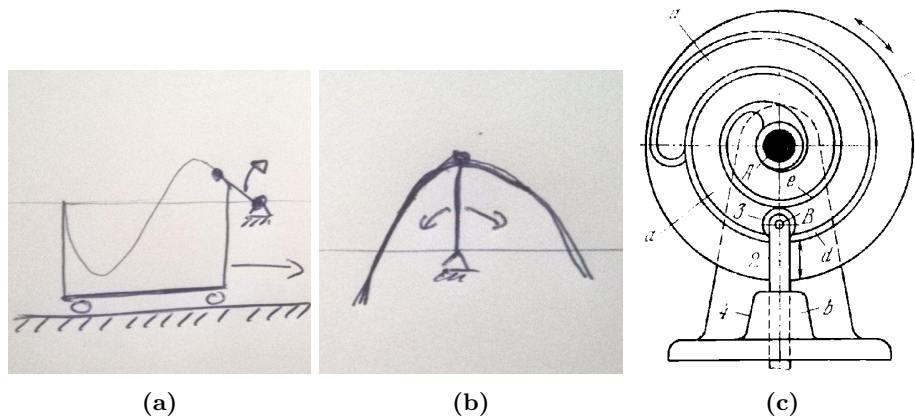


Figure F.3: **a:** Translational cam with sinusoidal profile. The follower moves clockwise when the cam moves to the right. **b:** Singular position of follower. In this position the follower can continue to rotate clockwise and counterclockwise. **c:** Example of a rotational cam with translating slider. This cam is designed to rotate multiple rotations.

F.1.2.3 Comparison

In Table F.1 the advantages and drawbacks of the four SBFA embodiments are tabulated. From this table follows that a rotational cam connected to the main spring combined with a rotational follower is the best solution, as it does not pose a limit to the stiffness of the main spring and allows for a compact design for a rotational mechanism.

Table F.1: Comparison of CAM mechanisms for SBFA

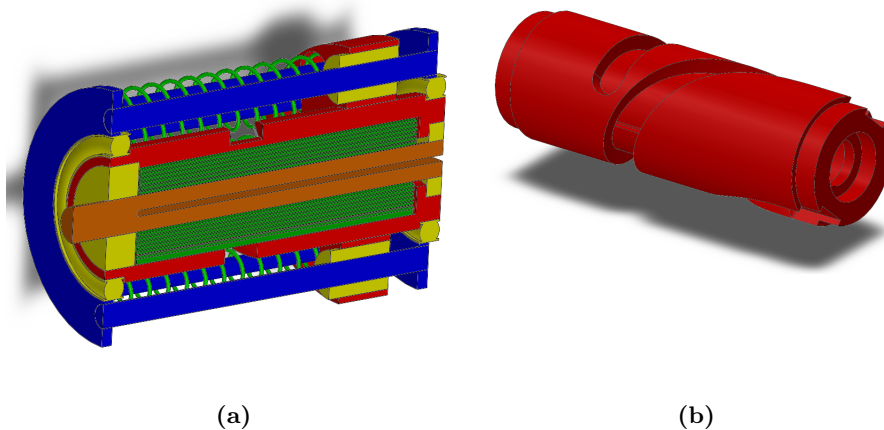
Criteria	Follower to Main Spring		Cam to Main Spring	
	Rot. Cam	Trans. Cam	Rot. Follower	Trans. Follower
1 Energy Saving	– Lower limit to main spring stiffness do to limited follower rotation $< 180^\circ$	– Lower limit to main spring stiffness do to limited follower rotation $< 180^\circ$	+ No lower limit to stiffness as cam rotation can be multiple revolutions	+ No lower limit to stiffness as cam rotation can be multiple revolutions
2 Compact	+ Compact when internal cam is used	– Cam with offset w.r.t. main axis. Linear guides are large.	+ Compact when When hinge close to cam	– Radial space required for follower motion.

F.2 SBFA with a cylindrical CAM

This section describes briefly an SBFA with spatial cam instead of a planar cam. In Fig. F.4 an SBFA is depicted with a cylindrical cam. The transmission is realized using a groove in the outer surface of the cam, that results in a translational motion of the follower when the cam rotates. Although this mechanism is quite compact it has some major drawbacks.

- The cam is a complex geometry and requires a multi-axis CNC-machine to produce. Modifications are rather cumbersome compared to a planar cam, where new cam could be simply lasercutted or milled with more conventional machinery. This makes it less suitable for a prototype.
- The main spring can be positioned inside the cam, but stock-springs are too large to do this. In Fig. F.4 a custom tension spring is used. The need for custom springs makes this principle also less suitable as prototype
- The mechanism requires translational guides to prevent rotation of the follower. Linear guides require a stiff frame and very precise manufacturing.

Because of these drawbacks this type of cam was considered as not feasible for a first prototype. It might be interesting to investigate the use of spatial cam for the development of follow-up mechanisms.

**Figure F.4:** Cylindrical SBFA

Appendix G

Additions to Chapter 8

G.1 Carriage Locking Mechanism

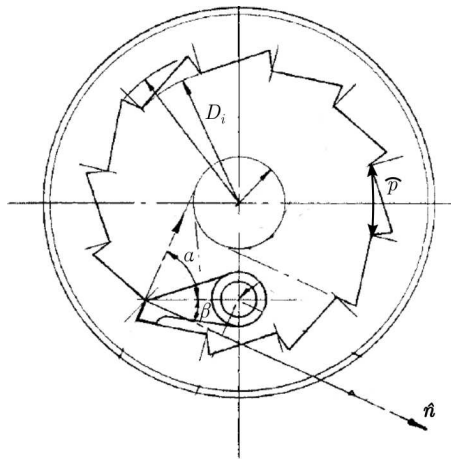


Figure G.1: Parameterization of the ratchet. Image taken from [61].

This section elaborates on the design of the ratchet as locking mechanism of the carriage. In Fig. G.1 a ratchet and its main parameters are depicted. \mathbf{n} is the normal vector of the main contact surface of the tooth. The angle β between this vector and the pivot should be larger than the friction angle to prevent jamming of the pawl. The advised value is $\beta = 30^\circ$.

The inner diameter of the ratchet was set to $D_i = 54$ mm to obtain a compact design. This compact design could be achieved by placing the components such that the either the radial or axial dimension was as small as possible. Ultimately a small axial dimension was selected as a larger diameter provides more space for the ratchet teeth, increasing the resolution.

The pitch p is the arc length between two tooth tips, measured over the circle they describe. Hence it relates to the internal diameter D_i and number of teeth Z according to:

$$p = \frac{\pi D_i}{Z} \quad (\text{G.1})$$

It was estimated¹ that the pitch should be at least 0.5 mm to ensure it is manufacturable using lasercutting. A smaller pitch might realized using more advanced machinery. The application of Eq. (G.1) yields in $Z = 339$ teeth, which was rounded of to a convenient $Z = 300$.

The required width w of the ratchet follows from [61]:

$$w = \frac{cT}{Z\sigma p^2} \quad (\text{G.2})$$

¹Jan van Frankenhuyzen, a research engineer, aided me to to determine this practical limit

Where σ is the maximum allowable stress, T the applied torque and c an empirical coefficient, which equals $c = 20$ for $Z > 20$. The ratchet has two pawls and engages on two teeth simultaneously. Together they have to withstand the maximum output torque, hence the torque to evaluate the strength equals half the maximum output torque. The ratchet is made from ASTM 304 stainless steel, with a yield strength of $\sigma_y = 230$ MPa. With a safety factor of 2 this results in a minimum width of 1.3 mm. Ultimately the width is set to $w = 2$ mm.

The design of the ratchet was evaluated using a FEA in SOLIDWORKS. The outer diameter of the ratchet is fixed. The carriage is able to rotate along its main axis and was loaded with a torque of 1.5 Nm in this rotational direction. The shafts of the pawls are suspended in the carriage using a “bearing connector” and the contact between the pawl and ratchet was set to “no penetration” without friction. The resulting Von Mises stress in the ring a pawl are depicted in Fig. G.2. Furthermore a radius of $r = 0.15$ mm was assumed for the corner of the tooth rooth, as in practice machining will always result in a radius in this corner.

Except for the peaks, the Von Mises stress is approximately half the yield strength. The occurring local stress peaks have a maximum of 204 MPa. This analysis confirms the satisfactory mechanical strength of the ratchet.

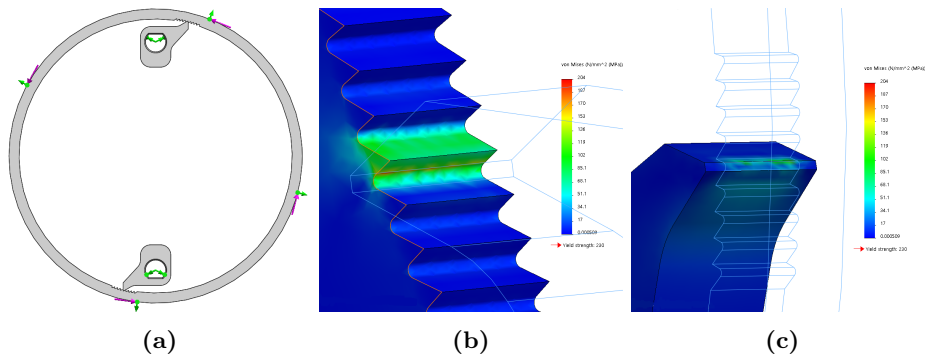


Figure G.2: Finite Element Analysis (FEA) of ratchet. **a:** Model. The motion of outer diameter of the ratchet and the holes of the pawls are constrained in all directions except for rotation about their axis. A torque of 1.4 Nm is applied on the outer diameter of the ratchet. **a:** Von Mises stress in the ratchet tooth. **b:** Von Mises stress in the pawl.

G.2 SBFA

G.2.1 Cam Geometry

The procedure to convert the desired trajectory in a cam geometry is inspired on by Tsay and Lin [64]. The global idea is the trajectory of the follower center P is first expressed in a global coordinate frame, as function of the spring extension ϕ_M . Then this global trajectory is converted to a trajectory in a *rotating* local frame². This local frame has the same origin, but its orientation is defined to be equal to the $|\phi_M$. As both the expression for the orientation and global trajectory are functions of ϕ_M , the trajectory in the local frame is described as function of ϕ_M . The actual cam geometry follows from can offset of the local trajectory to incorporate the radius of the follower. The resulting local cam-geometry in Cartesian coordinates is stated as [64]:

$$\hat{\mathbf{S}} = \begin{bmatrix} S_{\hat{x}} \\ S_{\hat{y}} \end{bmatrix} = \begin{bmatrix} a \cos \psi_M - \cos(\psi_B + \psi_M) \\ -a \sin \psi_M - b \sin(\psi_B + \psi_M) \end{bmatrix} - \hat{\mathbf{n}}r_b \quad (\text{G.3})$$

²In fact, Tsay and Lin do it in the opposite way: they define the cam geometry in the global frame and consider the coordinates of the follower in rotating local frame. Nevertheless for the static analysis that follows later on it is more convenient to regard the cam as the local geometry and ultimately it results in the same cam geometry.

Where ψ_B is defined as function of ϕ_M by Eq. (8.7), r_b is the radius of the bearing, a and b the dimensions depicted as in Fig. 8.7b and $\hat{\mathbf{n}}$ the unit normal vector in the local coordinate frame, expressed by:

$$\hat{\mathbf{n}} = \begin{bmatrix} n_{\hat{x}} \\ n_{\hat{y}} \end{bmatrix} = \begin{bmatrix} \frac{a \cos \psi_M - b \left(1 + \frac{\partial \psi_B}{\partial \psi_M}\right) \cos(\psi_B + \psi_M)}{\sqrt{a^2 - 2ab \left(1 + \frac{\partial \psi_B}{\partial \psi_M}\right) \cos \psi_B + b^2 \left(1 + \frac{\partial \psi_B}{\partial \psi_M}\right)^2}} \\ \frac{-a \sin \psi_M + b \left(1 + \frac{\partial \psi_B}{\partial \psi_M}\right) \cos(\psi_B + \psi_M)}{\sqrt{a^2 - 2ab \left(1 + \frac{\partial \psi_B}{\partial \psi_M}\right) \cos \psi_B + b^2 \left(1 + \frac{\partial \psi_B}{\partial \psi_M}\right)^2}} \end{bmatrix} \quad (\text{G.4})$$

G.2.2 Static Analysis

This subsection elaborates on the static analysis. The contact force depends both on the static equilibrium of the follower and the direction of the normal vector of the surface. Combining these two will result in an expression for the normal force.

The moment equilibrium of the cam follower yields:

$$F_y b \cos \psi_B + F_x b \sin \psi_B + T_B = 0 \quad (\text{G.5})$$

Where F_x and F_y are the components of the normal force F_N in the global frame. As the horizontal and vertical components of the contact force are proportional to the components of the normal vector of the cam surface in the global frame, they can be substituted by $F_x = -n_x F_N$ and $F_y = -n_y F_N$. The minus sign is introduced as the normal force is in opposite direction to the normal vector of the cam. The normal vector in the global coordinates is obtained using:

$$\mathbf{n} = \begin{bmatrix} n_x \\ n_y \end{bmatrix} = \mathbf{R}(\psi_M) \hat{\mathbf{n}} \quad (\text{G.6})$$

Where $\mathbf{R}(\psi_M)$ denotes the rotation matrix:

$$\mathbf{R}(\psi_M) = \begin{bmatrix} \cos \psi_M & -\sin \psi_M \\ \sin \psi_M & \cos \psi_M \end{bmatrix} \quad (\text{G.7})$$

This results in the following expression for the contact force:

$$F_N = \frac{T_B}{(n_y b \cos \psi_B + n_x b \sin \psi_B)} \quad (\text{G.8})$$

G.3 Differential

G.3.1 Derivation of Equilibrium Condition

Recall the kinematics for a general differential:

$$\dot{x}_u = a_1 \dot{x}_p + a_2 \dot{x}_f \quad (\text{G.9})$$

Where a_1 and a_2 are two constants defining the transmission ratio of one branch when the other is blocked. As the mechanism has two DoFs, the principle of virtual energy is applied twice, each time with one of the two DoFs treated if fixed. Fixing x_f yields:

$$\delta U|_{\delta x_f=0} \rightarrow F_u \frac{\partial x_u}{\partial x_p} \delta x_p + F_p \delta x_p \quad (\text{G.10})$$

$$F_u a_1 + F_p = 0 \quad (\text{G.11})$$

And constraining the other results in:

$$\delta U|_{\delta x_p=0} \rightarrow F_u \frac{\partial x_u}{\partial x_f} \delta x_f + F_f \delta x_f \quad (\text{G.12})$$

$$F_u a_2 + F_f = 0 \quad (\text{G.13})$$

Combining Eqs. (G.11) and (G.13) results in the following condition for static equilibrium of the differential:

$$F_u = \frac{-F_p}{a_1} = \frac{-F_f}{a_2} \quad (\text{G.14})$$

The very same relation is valid for moment equilibrium in case of a rotational differential.

G.3.2 Selection of Connection Permutation

This subsection verifies the selected connection permutation of the differential. To do so, first the equation for the kinematics of a planetary gear is introduced. Second, it will be explained how the performance of these permutations is evaluated, followed by an overview of the performance for all possibilities.

G.3.2.1 Planetary Gear Kinematics

First of all, the general equation of the planetary gear equals:

$$\omega_c(Z_r + Z_s) = \omega_r Z_r + \omega_s Z_s \quad (\text{G.15})$$

Where ω_s , ω_r and ω_c are the angular velocities of the sun gear, ring gear and carrier respectively. Z_s and Z_r are the numbers of teeth of the planet and sun.

G.3.2.2 Measure for Performance Evaluation

The differential is used to drive the sizing and forcing mode subsequently with one input. The analysis of the kinematics of these motions will result in criteria to the differential. The ability of the six permutations to satisfy these criteria is used to compare them.

The kinematics of the implemented differential are as follows: In the sizing mode the two inputs move simultaneously: $\dot{x}_f = \dot{x}_p$. In the forcing mode the carriage position is stationary: $\dot{x}_f = 0$. When these motions are combined with the differential kinematics of Eq. (G.9), this results in:

$$\dot{x}_u = \begin{cases} (a_1 + a_2)\dot{x}_p & \text{if } \dot{x}_f = \dot{x}_p \text{ (sizing)} \\ a_2\dot{x}_f & \text{if } \dot{x}_p = 0 \text{ (forcing)} \end{cases} \quad (\text{G.16})$$

The transfer ratios of sizing and forcing equal respectively $i_1 = \dot{x}_p/\dot{x}_u = a_1 + a_2$ and $i_2 = \dot{x}_f/\dot{x}_u = a_2$. The normalized ratio equals:

$$\iota = \frac{i_2}{i_1} = \frac{a_2}{a_1 + a_2} \quad (\text{G.17})$$

The value of ι is subjected to two constraints to ensure proper functioning:

- $\iota > 0$: The forcing and sizing have to move in the same direction, hence $\iota > 0$.
- $\iota > 1$: As described in chapter 3 the performance increases with ι . Hence, ι should be at least larger than 1, else the performance is reduced.

So by inspecting the value for ι the best permutation for the connection of the differential can be selected.

G.3.2.3 Performance Evaluation

The kinematics of the planetary gear, Eq. (G.15), can be combined with the general kinematics of the differential, Eq. (G.9) when it is specified which in- and output is connected to the ringgear, sungear or carrier. An example will be given for one permutation to explain this in detail, then an overview is presented for all six permutations.

For the example permutation, the carrier is the forcing output and the sun is the input. Consequently, the ring is the positioning output. This can be mathematically expressed as $\dot{x}_f = \omega_c$, $\dot{x}_u = \omega_s$ and $\dot{x}_p = \omega_r$. These values can be substituted in Eq. (G.15) and rearranged to:

$$\dot{x}_u = \underbrace{\frac{-Z_r}{Z_s}}_{a_1} \dot{x}_p + \underbrace{\frac{Z_r + Z_s}{Z_s}}_{a_2} \dot{x}_f \quad (\text{G.18})$$

which leads to the expressions for a_1 and a_2 . Substituting this in Eq. (G.17) results in the following expression for the normalized ratio:

$$\iota = \frac{Z_r + Z_s}{Z_s} \quad (\text{G.19})$$

The number of teeth Z_r and Z_s are *positive integers*, i.e. $Z_r \in \{1, 2, 3, \dots\}$ and $Z_s \in \{1, 2, 3, \dots\}$, thus $\iota > 1$. This means that both criteria are always satisfied. The procure of the example is repeated for every permutation. The resulting expressions for the normalized ratios are presented in Table G.1.

Table G.1: Possible Connections to Differential

Forcing Output	Input		
	Ring $\dot{x}_a = \omega_r$	Carrier $\dot{x}_a = \omega_c$	Sun $\dot{x}_a = \omega_s$
Ring $\dot{x}_f = \omega_r$	X	$\dot{x}_p = \omega_s$ $\iota = \frac{Z_r}{Z_r + Z_s}$ X $\iota < 1$	$\dot{x}_p = \omega_c$ $\iota = -\frac{Z_r}{Z_s}$ X $\iota < 0$
Carrier $\dot{x}_f = \omega_c$	$\dot{x}_p = \omega_s$ $\iota = \frac{Z_r + Z_s}{Z_r}$ ✓ $\iota > 1$	X	$\dot{x}_p = \omega_r$ $\iota = \frac{Z_r + Z_s}{Z_s}$ ✓ $\iota > 1$
Sun $\dot{x}_f = \omega_s$	$\dot{x}_p = \omega_c$ $\iota = -\frac{Z_s}{Z_r}$ X $\iota < 0$	$\dot{x}_p = \omega_r$ $\iota = \frac{Z_s}{Z_r + Z_s}$ X $\iota < 1$	X

From Table G.1 follows that only a feasible solution is achieved when the carrier is the forcing output. The ring gear has always more tooth, because the ring gear is always larger than the sun. Hence $Z_r > Z_s$. To obtain a compact design, the sun is preferred over the ring, because this results in the largest ratio for the same gear.

G.3.2.4 Ratio conversion

Typically the ratio of a gearbox is specified under the assumption that the sun is the input, the carrier the output and the ring is fixed, i.e. $\omega_r = 0$. The expression for specified gearbox ratio of the differential i_{Diff} follows from rewriting Eq. (G.15) to:

$$i_{Diff} = \frac{\omega_s}{\omega_c} = \frac{Z_r + Z_s}{Z_s} \quad (\text{G.20})$$

Comparing this equation with the normalized ratio ι for the selected permutation, as listed in Table G.1, results in the conclusion that these expressions are equal, so: $\iota = i_{Diff}$. The parameters a_1 and a_2 follow from Eqs. (G.18) and (G.20). From these equations it follows that a_2 equals i_{Diff} . The second term of Eq. (G.18) can be rearranged to $Z_r = (a_2 - 1)/Z_s$. Substitution of this expression in the first term of Eq. (G.18) yields the expression: $a_1 = 1 - a_2 = 1 - i_{Diff}$.

G.4 Threshold Mechanism

G.4.1 Spring Selection

The springs of the threshold mechanism should be able to store the required energy associated with the force-characteristic. The required extension to store this amount energy is bound to ensure it results in a practical value for the cam rotation. The same database as for the design of the SBFA is used, with the following constraints to the required extension of the inspected springs:

$$s_{reg} \leq s_{max} \quad (\text{G.21})$$

$$4^\circ \leq s_{reg} \leq 6^\circ \quad (\text{G.22})$$

Where

$$s_{reg} = \sqrt{\frac{2T_t \psi_{M,t}}{N_s k_s}} \quad (\text{G.23})$$

Spring TEVEMA TS101720 with a stiffness $k_s = 0.9099$ Nm/rad and a maximum extension of $s_{max} = 25^\circ$ (0.436 rad) is the smallest possible spring and therefore selected.

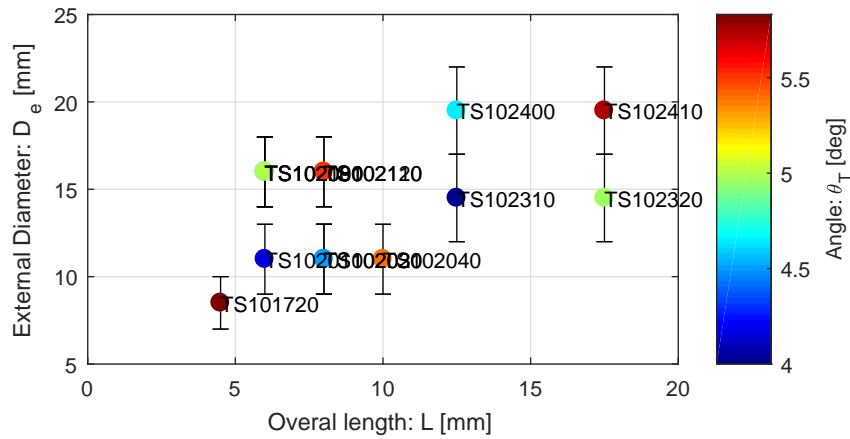


Figure G.3: Feasible springs for threshold mechanism

G.5 Tension Tool

Because the notch of the buffer cam was unreachable another way had to be found to set the pretension of the main springs. A custom tool, depicted in Fig. G.4, was designed for this purpose. It consists of a wrenchlike-body, lasercutted from a steel plate. Holes are added to insert two M3 socket cap screws, on which the vernier protractor can rest. The set screw can be used as reference for a repeatable setting and finetuning.



Figure G.4: Tension tool. This tool functions similar to a wrench. The set screw functions as adjustable reference.

Appendix H

Additions to Chapter 9

H.1 Forcing Data Set

Fig. H.1 depicts the portion of the complete dataset that is used to compute the force reduction. The colored curves indicate the used data and the grey curves indicate the complete dataset. The included data contains the data for an spring deflection larger than 8° but smaller than 99% of the maximum estimated output torque of that condition. As such, the data excludes sizing, switching and is corrected for the high high peaks that arise at the end of the motion range of the spring.

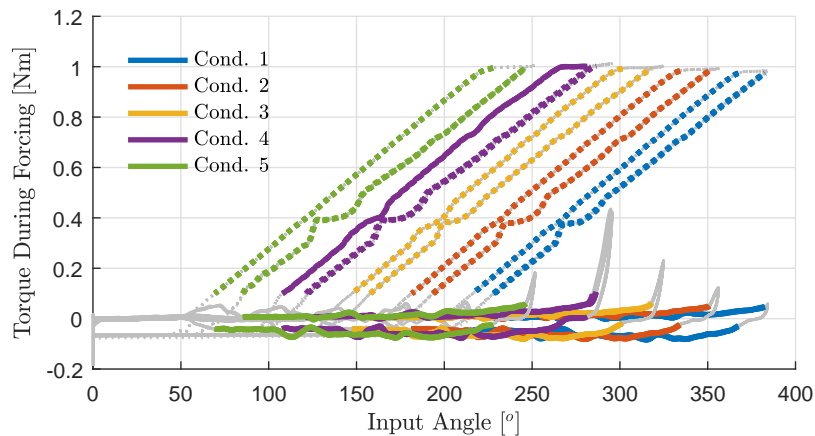


Figure H.1: Data used to compute the force reduction. The colored lines indicate the used data, the grey data represent the complete data set

H.2 Spring Extension versus Input Torque

In Fig. H.2 the input torque is plotted versus the spring extension. This plot shows a fairly consistent behavior, which suggest the ripples, especially those with a large amplitude, do not have a stochastic nature.

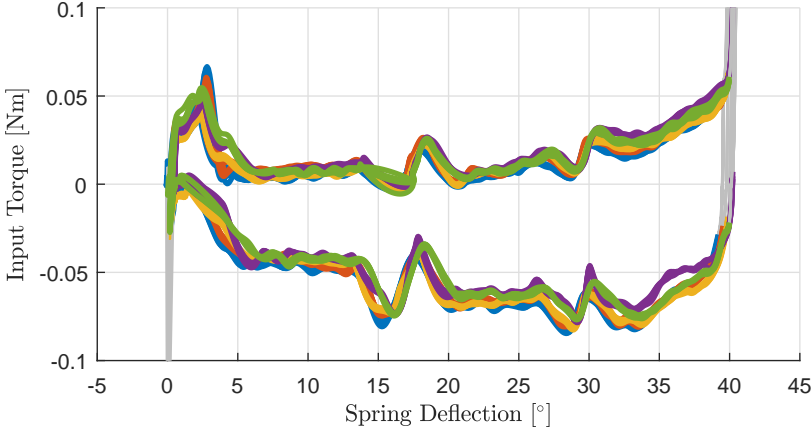


Figure H.2: Input torque versus spring extension.

Bibliography

- [1] A. Wolf, R. Steinmann, and H. Schunk, *Grippers in motion: the fascination of automated handling tasks*. Springer Science & Business Media, 2006.
- [2] I. F. on Robotics, “Executive summary world robotics 2016 industrial robots.” [urlhttp://www.ifr.org/industrial-robots/statistics/](http://www.ifr.org/industrial-robots/statistics/), 2016. [Online, accessed 16-06-2016].
- [3] cia.gov, “The world factbook: Population growth rate.” <https://www.cia.gov/Library/publications/the-world-factbook/fields/2002.html>, 2016. [Online, accessed 11-11-2016].
- [4] T. Laliberté and C. M. Gosselin, “Underactuation in space robotic hands,” in *International Symposium on Artificial Intelligence, Robotics and Automation in Space, Montréal, Canada*, pp. 18–21, 2001.
- [5] M. Guarnieri, I. Takao, E. F. Fukushima, and S. Hirose, “Helios viii search and rescue robot: Design of an adaptive gripper and system improvements,” in *2007 IEEE/RSJ International Conference on Intelligent Robots and Systems*, pp. 1775–1780, IEEE, 2007.
- [6] K. Khokar, R. Alqasemi, S. Sarkar, K. Reed, and R. Dubey, “A novel telerobotic method for human-in-the-loop assisted grasping based on intention recognition,” in *2014 IEEE International Conference on Robotics and Automation (ICRA)*, pp. 4762–4769, IEEE, 2014.
- [7] A. Bicchi and V. Kumar, “Robotic grasping and contact: A review,” in *ICRA*, pp. 348–353, Citeseer, 2000.
- [8] Y. Mei, Y.-H. Lu, Y. C. Hu, and C. G. Lee, “Deployment of mobile robots with energy and timing constraints,” *Robotics, IEEE Transactions on*, vol. 22, no. 3, pp. 507–522, 2006.
- [9] G. Mathijssen, B. Brackx, M. Van Damme, D. Lefeber, and B. Vanderborght, “Series-parallel elastic actuation (spea) with intermittent mechanism for reduced motor torque and increased efficiency,” in *2013 IEEE/RSJ International Conference on Intelligent Robots and Systems*, pp. 5841–5846, IEEE, 2013.
- [10] J. Kruit and J. Cool, “Body-powered hand prosthesis with low operating power for children,” *Journal of medical engineering & technology*, vol. 13, no. 1-2, pp. 129–133, 1989.
- [11] J. J. Neven, “Key concepts towards an energy efficient and versatile robotic gripper: A literature suvey,” 2016.
- [12] robotiq.com, “Adaptive robot gripper 2-finger (85 & 140) instruction manual.” <http://robotiq.com/products/adaptive-robot-gripper/universal-robots-bundle/>, 2015. [Online, Accessed 16-06-2016].
- [13] G. J. Monkman, S. Hesse, R. Steinmann, and H. Schunk, *Robot grippers*. John Wiley & Sons, 2007.
- [14] A. Morecki and J. Knapczyk, *Basics of robotics: theory and components of manipulators and robots*, vol. 402. Springer, 2014.
- [15] G. Fantoni, M. Santochi, G. Dini, K. Tracht, B. Scholz-Reiter, J. Fleischer, T. K. Lien, G. Seliger, G. Reinhart, J. Franke, *et al.*, “Grasping devices and methods in automated production processes,” *CIRP Annals-Manufacturing Technology*, vol. 63, no. 2, pp. 679–701, 2014.

- [16] C. Blanes, M. Mellado, C. Ortiz, and A. Valera, “Review. technologies for robot grippers in pick and place operations for fresh fruits and vegetables,” *Spanish Journal of Agricultural Research*, vol. 9, no. 4, pp. 1130–1141, 2011.
- [17] G. A. Kragten, *Underactuated hands: fundamentals, performance analysis and design*. PhD thesis, Delft University of Technology, 2011.
- [18] D. S. Paul, “Self-locking friction based robotic gripper,” 1998. US Patent 5,746,464.
- [19] S. Kobayashi, “Clamp device for transferring construction material,” 1994. US Patent 5,280,982.
- [20] M. Plooij, M. Wisse, and H. Vallery, “Reducing the energy consumption of robots using the bidirectional clutched parallel elastic actuator,” *IEEE Transactions on Robotics*, 2016.
- [21] M. Controzzi, C. Cipriani, and M. C. Carrozza, “Miniaturized non-back-drivable mechanism for robotic applications,” *Mechanism and Machine Theory*, vol. 45, no. 10, pp. 1395–1406, 2010.
- [22] F. Montagnani, M. Controzzi, and C. Cipriani, “Non-back-drivable rotary mechanism with intrinsic compliance for robotic thumb abduction adduction,” *Advanced Robotics*, vol. 29, no. 8, pp. 561–571, 2015.
- [23] J. Herder, *Energy-free systems: theory, conception, and design of statically balanced spring mechanisms*. PhD thesis, TU Delft, Delft University of Technology, 2001.
- [24] M. Plooij, T. Van Der Hoeven, G. Dunning, and M. Wisse, “Statically balanced brakes,” *Precision Engineering*, vol. 43, pp. 468–478, 2016.
- [25] S. Westerman, “Design of a statically balanced mechanism using magnets and springs,” Master’s thesis, Delft University of Technology, 2015.
- [26] J. C. Cool, “Ontwerpen in de medische techniek,” 1989. [Lecture Notes].
- [27] M. Plooij, G. Mathijssen, P. Cherelle, D. Lefeber, and B. Vanderborght, “Lock your robot: A review of locking devices in robotics,” *Robotics & Automation Magazine, IEEE*, vol. 22, no. 1, pp. 106–117, 2015.
- [28] M. Plooij, W. Wolfslag, and M. Wisse, “Clutched elastic actuators,” *IEEE/ASME Transactions on Mechatronics*, 2017.
- [29] T. Takaki and T. Omata, “Load-sensitive continuously variable transmission for robot hands,” in *Robotics and Automation, 2004. Proceedings. ICRA’04. 2004 IEEE International Conference on*, vol. 4, pp. 3391–3396, IEEE, 2004.
- [30] B. Vanderborght, A. Albu-Schäffer, A. Bicchi, E. Burdet, D. G. Caldwell, R. Carloni, M. Catalano, O. Eiberger, W. Friedl, G. Ganesh, *et al.*, “Variable impedance actuators: A review,” *Robotics and autonomous systems*, vol. 61, no. 12, pp. 1601–1614, 2013.
- [31] M. A. Roa and R. Suárez, “Grasp quality measures: review and performance,” *Autonomous robots*, vol. 38, no. 1, pp. 65–88, 2015.
- [32] G. A. Kragten and J. L. Herder, “The ability of underactuated hands to grasp and hold objects,” *Mechanism and Machine Theory*, vol. 45, no. 3, pp. 408–425, 2010.
- [33] J. Braun, “Formulea handbook,” 2012.
- [34] J.-U. Chu, D.-H. Jung, and Y.-J. Lee, “Design and control of a multifunction myoelectric hand with new adaptive grasping and self-locking mechanisms,” in *Robotics and Automation, 2008. ICRA 2008. IEEE International Conference on*, pp. 743–748, IEEE, 2008.
- [35] G. Puchhammer, “Clutch module for prosthesis,” 2012. US Patent 8,257,446.
- [36] T. Takaki and T. Omata, “100g-100n finger joint with load-sensitive continuously variable transmission,” in *Proceedings 2006 IEEE International Conference on Robotics and Automation, 2006. ICRA 2006.*, pp. 976–981, IEEE, 2006.

- [37] R. F. Weir and J. W. Sensinger, “Design of artificial arms and hands for prosthetic applications,” in *Standard Handbook of Biomedical Engineering and Design*, McGraw Hill, New York, 2003.
- [38] L. Birglen and C. M. Gosselin, “Force analysis of connected differential mechanisms: application to grasping,” *The International Journal of Robotics Research*, vol. 25, no. 10, pp. 1033–1046, 2006.
- [39] S. Wolf, O. Eiberger, and G. Hirzinger, “The dlr fsj: Energy based design of a variable stiffness joint,” in *Robotics and Automation (ICRA), 2011 IEEE International Conference on*, pp. 5082–5089, IEEE, 2011.
- [40] A. Jafari, N. G. Tsagarakis, and D. G. Caldwell, “Awas-ii: A new actuator with adjustable stiffness based on the novel principle of adaptable pivot point and variable lever ratio,” in *Robotics and Automation (ICRA), 2011 IEEE International Conference on*, pp. 4638–4643, IEEE, 2011.
- [41] B.-S. Kim and J.-B. Song, “Design and control of a variable stiffness actuator based on adjustable moment arm,” *IEEE Transactions on Robotics*, vol. 28, no. 5, pp. 1145–1151, 2012.
- [42] L. C. Visser, R. Carloni, F. Klijnsstra, and S. Stramigioli, “A prototype of a novel energy efficient variable stiffness actuator,” in *2010 Annual International Conference of the IEEE Engineering in Medicine and Biology*, pp. 3703–3706, IEEE, 2010.
- [43] S. Hirose, M. Imazato, Y. Kudo, and Y. Umetani, “Internally-balanced magnet unit,” *Advanced robotics*, vol. 1, no. 3, pp. 225–242, 1986.
- [44] O. Gutfleisch, M. A. Willard, E. Brück, C. H. Chen, S. Sankar, and J. P. Liu, “Magnetic materials and devices for the 21st century: stronger, lighter, and more energy efficient,” *Advanced materials*, vol. 23, no. 7, pp. 821–842, 2011.
- [45] T. Hoeven van der, “Statically balanced singular-friction locking,” Master’s thesis, Delft University of Technology, 2015.
- [46] L. F. Van der Spaa, “Reducing energy consumption in robotics.” Literature Survey, Delft University of Technology, 2016.
- [47] M. V. Liarokapis, B. Calli, A. J. Spiers, and A. M. Dollar, “Unplanned, model-free, single grasp object classification with underactuated hands and force sensors,” in *Intelligent Robots and Systems (IROS), 2015 IEEE/RSJ International Conference on*, pp. 5073–5080, IEEE, 2015.
- [48] L. Birglen, T. Laliberté, and C. M. Gosselin, *Underactuated robotic hands*, vol. 40. Springer, 2007.
- [49] W. Matek, D. Muhs, and H. Wittel, *Roloff/Matek machine-onderdelen: normering, berekening, vormgeving*. Academic Service, 2000.
- [50] P. Breedveld, J. Herder, and T. Tomiyama, “Teaching creativity in mechanical design,” in *4th World Conference on Design Research (IASDR2011), Delft, The Netherlands, Oct*, 2011.
- [51] Vosse, “Plugles robot arm: Energy recuperation using spring mechanisms,” Master’s thesis, Delft University of Technology, 2016.
- [52] NSK, “Miniature Ball Bearings,” 2011. [Catalog E126h].
- [53] SKF, “Linear motion standard range,” 2012. [Catalog].
- [54] en.wikipedia.org, “Freewheel.” en.wikipedia.org/wiki/Freewheel, 2017. [Online, accessed 26-06-2017].
- [55] G. Mathijssen, R. Furnémont, T. Verstraten, C. Espinoza, S. Beckers, D. Lefeber, and B. Vanderborght, “Study on electric energy consumed in intermittent series-parallel elastic actuators (ispea),” *Bioinspiration & Biomimetics*, vol. 12, no. 3, p. 036008, 2017.
- [56] matexgears.com, “Planetary Gears.” <http://www.matexgears.com/planetary-gears.html>, 2017. [Online, accessed 07-06-2017].
- [57] onviollc.com, “Cycloidal speed reducers.” <http://www.onviollc.com/products/cycloidal-speed-reducers.asp>, 2017. [Online, accessed 07-06-2017].

- [58] sumitomodrive.com, “Fine cyclo series.” www.sumitomodrive.com/uploads/product/files/file-2669.pdf, 2017. [Online, accessed 07-06-2017].
- [59] J. W. Sensinger and J. H. Lipsey, “Cycloid vs. harmonic drives for use in high ratio, single stage robotic transmissions,” in *Robotics and Automation (ICRA), 2012 IEEE International Conference on*, pp. 4130–4135, IEEE, 2012.
- [60] ”harmonicdrive.net”, “Miniature gear units.” <http://www.harmonicdrive.net/products/>, 2017. [Online, Accessed 07-06-2017].
- [61] R. A. Walsh and R. A. Walsh, *Handbook of machining and metalworking calculations*. McGraw-Hill New York, 2001.
- [62] tevema-industrial-springs.com, “Tevema Technical Springs.” http://www.tevema-industrial-springs.com/catalogue_en.html, 2017. [Online, accessed 19-06-2017].
- [63] tevema-industrial-springs.com, “The Spring Catalogue 13.” <http://www.lesjoforsab.com/technical-information/catalogues.asp>, 2017. [Online, accessed 19-06-2017].
- [64] D. Tsay and B. Lin, “Profile determination of planar and spatial cams with cylindrical roller-followers,” *Proceedings of the Institution of Mechanical Engineers, Part C: Journal of Mechanical Engineering Science*, vol. 210, no. 6, pp. 565–574, 1996.
- [65] maedler.nl, “Spur Gears, Steel, Module 0.5.” maedler.nl/product/1643/1618/1034/1076/stirnzahnraeder-aus-stahl-modul-05, 2017. [Online, accessed 14-08-2017].
- [66] F. Freudenstein and E. Maki, “The creation of mechanisms according to kinematic structure and function,” *Environment and Planning B: Planning and Design*, vol. 6, no. 4, pp. 375–391, 1979.
- [67] P. Kuppens, *Automated Robot Design With Artificial Evolution*. TU Delft, Delft University of Technology, 2016.
- [68] J. G. Ayats, U. Diego-Ayala, J. M. Canela, F. Fenollosa, and J. Vivancos, “Hypergraphs for the analysis of complex mechanisms comprising planetary gear trains and other variable or fixed transmissions,” *Mechanism and machine theory*, vol. 51, pp. 217–229, 2012.
- [69] mathworld.wolfram.com, “Hypergraph.” <http://mathworld.wolfram.com/Hypergraph.html>, 2016. [Online, accessed 01-11-2016].
- [70] A. Bretto, “Hypergraph theory,” *An introduction. Mathematical Engineering. Cham: Springer*, 2013.
- [71] N. J. A. Sloane, “The on-line encyclopedia of integer sequences: A005142.” <http://oeis.org/A005142>, 2013. [Online, accessed 01-11-2016].